Davide Manuel
Ribero Morgado

Sensores de toque para electrónica automóvel impressa em 3D: análise, síntese, e aspectos de compatibilidade electromagnética

Touch sensors for 3D-printed automobile electronics: analysis, synthesis, and electromagnetic compatibility issues

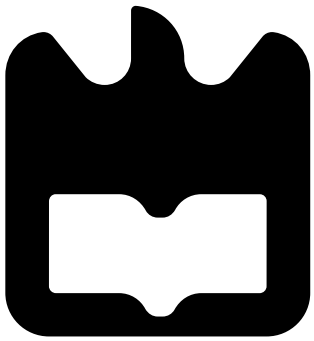

Davide Manuel
Ribero Morgado

Sensores de toque para electrónica automóvel impressa em 3D: análise, síntese, e aspectos de compatibilidade electromagnética

Touch sensors for 3D-printed automobile electronics: analysis, synthesis, and electromagnetic compatibility issues

Dissertação apresentada à Universidade de Aveiro para cumprimento dos requesitos necessários à obtenção do grau de Mestre em Engenharia Eletrónica e Telecomunicações, realizada sob a orientação científica do Doutor Stanislav Maslovski (orientador), Investigador Principal do Departamento de Eletrónica, Telecomunicações e Informática da Universidade de Aveiro e do Doutor Pedro Fonseca (co-orientador), Professor Auxiliar do Departamento de Eletrónica, Telecomunicações e Informática da Universidade de Aveiro.

Esta Dissertação de Mestrado insere-se no Projeto Additive Manufacturing for Smart Plastics (AM4SP) - POCI-01-0247-FEDER-070521 co-financiado por fundos do Portugal 2020 do Fundo Europeu de Desenvolvimento Regional e com a participação da empresa promotora Simoldes Plásticos e a Universidade de Aveiro.

o júri / the jury

presidente / president

Professor Doutor Telmo Reis Cunha
Professor Associado da Universidade de Aveiro

vogais / examiners committee

Professor Doutor Telmo Rui Carvalhinho Cunha Fernandes
Professor Adjunto do Instituto Politécnico de Leiria

Doutor Stanislav Maslovski
Investigador Principal em Regime Laboral da Universidade de Aveiro

agradecimentos / acknowledgements

Os meus sinceros agradecimentos,

Primeiramente à minha namorada por ser o meu pilar em todos os momentos e por me apoiar incondicionalmente em toda esta fase.

À minha família, principalmente aos meus pais e irmã pela confiança e apoio.

Aos meus amigos pela camaradagem ao longo destes bons anos.

Um especial agradecimento ao meu orientador e co-orientador, Stanislav Maslovski e Pedro Fonseca, pela disponilidade, ajuda e confiança durante a elaboração desta dissertação.

Ao NBicla da Associação Acádemica da Universidade de Aveiro e ao IEEE UA SB por terem sido a minha segunda casa, nos bons e nos maus momentos e por me ajudarem a desenvolver as minhas capacidades.

Ao SAC da secção portuguesa do IEEE Portugal e ao SAC da região 8 do IEEE pelos conselhos e pelas oportunidades que me proporcionaram.

Ao Instituto de Telecomunicações pela cedência de espaços e equipamentos para realizar a dissertação.

À Universidade de Aveiro, por me acolher e me proporcionar momentos de aprendizagem e evolução ao longo deste 5 árduos, mas gratificantes anos.

A todos os que cruzaram e marcaram o meu percurso,

Muito obrigado!

Palavras Chave

Estrutura Interdigital, Elétrodos, Frequência de ressonância, Sensores de toque, Aplicações automóvel, Manufatura Aditiva

Resumo

A Manufatura Aditiva tem vindo a desenvolver-se cada vez mais, proporcionando inúmeras vantagens à indústria. Dentro delas a utilização de um material com propriedades condutoras e aliado a técnicas de impressão 3D, permite desenvolver novos dispositivos embutidos/incorporados numa peça de plástico.

Uma das indústrias que mais se pode aplicar métodos de Manufatura Aditiva é a indústria automóvel. A eletrificação dos automóveis, os carros conetados, condução autónoma, a sensorização dos equipamentos e o conforto são alguns dos desafios que esta indústria enfrenta. Assim, a inovação faz-se no sentido de desenvolvimento de produtos para responder aos desafios apresentados, sempre com o foco no utilizador.

Assim, esta Dissertação de Mestrado tem como objetivo estudar, explorar e expandir estes conceitos e aplicá-los ao desenvolvimento de um sensor de toque, além de perceber quais os problemas de compatibilidade e interferências eletromagnéticas num ambiente automóvel, mais concretamente numa porta inteligente para um carro.

O trabalho iniciou-se com o estudo dos métodos de Manufatura Aditiva, tipos de medidas para um sensor de toque, design, compatibilidade e interferência eletromagnética destes sensores. Desenvolveram-se ferramentas para auxílio dos cálculos de capacitância, indutância e frequência de ressonância. Também se elaborou um script para obtenção dos parâmetros das frequências de ressonância nas gamas desejadas.

Estas ferramentas possibilitaram o desenvolvimento de uma macro para criar as estruturas 3D num simulador e, assim, poder simular os parâmetros obtidos. Com as simulações alcançaram-se duas estruturas nas frequências desejadas e com as estruturas 3D criadas passámos à medição experimental, produzindo uma Printed Circuit Board (PCB) para cada estrutura.

Assim, com estes processos, concluiu-se que as nossas medições experimentais permitem validar as ferramentas desenvolvidas, assim como todo o estudo e teoria desenvolvida.

Keywords Interdigitated Electrodes (IDE), electrodes, resonant frequency, optimization, touch sensors, automotive applications, Additive Manufacturing (AM).

Abstract

The Additive Manufacturing has been developing more and more, providing numerous advantages to the industry. Among such advantages is the use of materials with conductive properties combined with 3D printing techniques, which enables development of new devices embedded in plastic elements.

One of the industries where Additive Manufacturing methods can be applied most successfully is the automotive industry. The electrification of cars, connected cars, autonomous driving, equipment enriched with sensors for better comfort are some of the challenges that this industry faces. Thus, innovation is made in the sense of developing new products to meet the presented challenges, always focusing on the user.

Thus, this Master Thesis aims to study, explore and expand these concepts and apply them to the development of a touch sensor, as well as to understand what are the problems of compatibility and electromagnetic interference that can be encountered in automotive environment, specifically, in a smart door for a car.

This work begins with the study of Additive Manufacturing methods, the types of measurements for a touch sensor, the sensor designs, and the electromagnetic compatibility and interference issues relevant for such sensors. Useful tools are developed to calculate the sensor capacitance, inductance and resonant frequency. Also, a script is developed to obtain the structural parameters for the resonant frequencies in desired ranges.

These tools made it possible to develop a macro to automate creation of 3D structures in CST Studio Suite and thus to be able to simulate such structures for a large set of obtained parameters. Based on the simulations, we designed two sensor structures operating at the desired frequencies and, with the 3D structures ready, moved on to the experimental measurements, producing a PCB prototype for each structure.

Thus, by completing these procedures it was concluded that the experimental measurements allowed us to test the developed tools and models and to validate the entire study.

Contents

List of Figures

List of Tables

Acronyms

HMI Human-To-Machine Interface

EMC ElectroMagnetic Compatibility

EMI ElectroMagnetic Interference

PCB Printed Circuit Board

AM Additive Manufacturing

AM4SP Additive Manufacturing for Smart Plastics

UX User eXperience

STL STereoLithography

DDS Drug Delivery Systems

R2R Reel-to-Reel

PDMS Polydimethylsiloxane

DUT Device Under Test

RH Relative Humidity

IDE Interdigitated Electrodes

PP Parallel plate

ASTM American Society for Testing and Materials

PE Printed Electronics

MCU MicroController Unit

HBM Human Body Model

RF Radio Frequency

ISM Industrial, Scientific and Medical applications

IC Integrated Circuits

ESD Electrostatic Discharge

EFT Electrical Fast Transient

MATLAB MATrix LABoratory®

PCT Partial Capacitance Technique

IT Institute of Telecommunications

SVP Sensitivity Variation Parameter

GMD Geometric Mean Distance

AMSD Arithmetic Mean Square Distance

AMD Arithmetic Mean Distance

VNA Vector Network Analyzer

FDS Frequency Domain Solver

MLS MultiLayer Solver

PEC Perfect Electric Conductor

Para ti minha estrelinha!

Chapter 1

Introduction

This chapter presents a contextualization and motivation for the work undertaken. It consists of an introduction to the topic, a consideration of the reasons for exploring it, a listing of the objectives of the work, and a description of the structure of the dissertation.

1.1 Context

On September 27, 1998 history was made by Henry Ford with the first Ford Model T [26]. The automobile industry has been revolutionized with mass customization. The mass customization helps to maintain the production efficiency and gives economic advantages for the customers [27]. Today, there are many industries and companies that use mass production to produce different types of cars. Cars that will meet different needs of users, comfort, speed, eco-friendliness, among others. But the real question is: what does a Tesla Model Y, a Peugeot 106, or a hydrogen car have in common? The cheaper cars do not have the same technologies, the same comfort, the same aerodynamics, or the same performance, but the interior structures are very similar and this does not correspond to the price difference between these cars. Despite the differences, all these cars have similar glass elevators, similar panels, and similar screens. But why?

The source of the problem and the solution to the problem are hidden in the first lines when talking about manufacturing. The problem and the solution is manufacturing!

Traditional manufacturing produces components with high precision and low complexity, where the material can be removed by drilling, grinding, or machining techniques or cast in molds. The advantages of traditional manufacturing offers are: low cost for large volume production [28], studied, known and standardized materials list, and fast large scale production. However, it has some disadvantages such as: a single process for all operations, it is necessary to have different machines for each operation, the limitation in terms of complex geometries, the market time to design and build a new structure is considerably high, amongst others.

The problems that exist in traditional manufacturing processes can be solved or improved with AM, in the case of 3D printing technologies because AM has a high level of complexity that can result in more complete and customized structures [29]. AM is the "process of joining materials to make objects from 3D model data, usually layer upon layer, as opposed to the subtractive manufacturing methodologies." according to ASTM Standard F2792-12a [6].

The AM has numerous advantages over traditional manufacturing, such as reducing time and market costs, accelerating prototyping, making companies more efficient and competitive

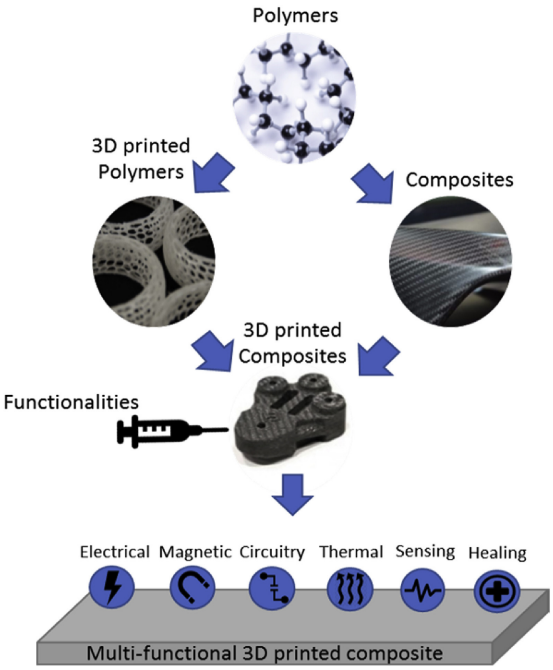

Figure 1.1: Illustration of multifunctional AM concept starting from polymers and finished with 3D printed composites. Source: [1].

---

in innovation, enabling low-cost mass customization, amongst others [30].

Since its inception, 3D printing technologies have evolved for a long time and have had a significant impact on the commercial and industrial sectors. This is because with this technology industry and businesses can save a lot of time to create prototypes (rapid prototyping). Additionally, 3D printing offers numerous other advantages such as reduced use of materials, minimized waste, ease of access, and flexible design process to print more complex designs and structures as compared to the traditional manufacturing processes [31]. An example of what is possible to create with 3D printing, a multifunctional concept, is shown in the Figure 1.1.

The 3D printing and AM have been evolving rapidly and in parallel. One can take advantage of both technologies separately, but it is better to combine these two technologies to get the most out of them. Figure 1.2 depicts how these two technologies have evolved very quickly and shows how the curves continue to evolve together.

In the automotive industry, 3D printing technologies have helped and are helping today to manufacture new cars and support old cars (Automotive Aftermarket). 3D printing can also enable new tools and processes needed for the digitization of the automotive industry. With Industry 4.0 and digitization, industry and companies need to adapt quickly to keep up with the market. The automotive industry is no different, it also needs to adapt to this new environment. Car electrification, connected cars, autonomous driving, equipment detection and comfort are some of the challenges this industry is facing. Thus, innovation is made towards product development to meet the challenges presented, always focusing on the user. As a result, interest in concepts such as the Human-To-Machine Interface (HMI) and User eXperience (UX) has been highlighted in this industry and, together with 3D printing or other techniques, it is possible to create parts of the car that are much more difficult to create with

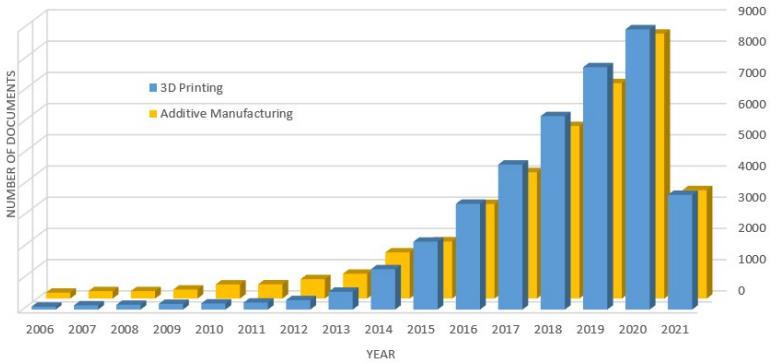

Figure 1.2: Illustration of roles between 3D Printing and Additive Manufacturing provided by Scopus [2] on May 16th, 2021.

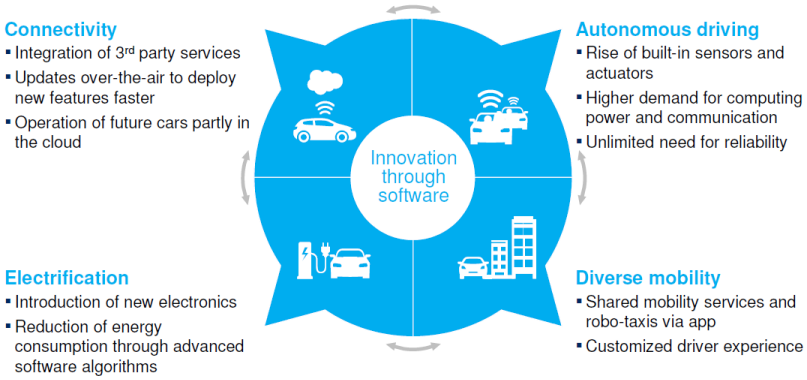

Figure 1.3: Key for automotive electronics innovation. Source: [3, 4].

---

traditional manufacturing processes and it is also possible to incorporate smart electronics into these two concepts (HMI and UX).

With these four concepts it is possible to build new ways of conceiving, designing, producing and driving the car. The Figure 1.3 shows in detail each concept.

To improve the concepts of HMI and UX it is necessary to understand, explore and study the AM methods, simulate and measure many structures and develop prototypes to answer questions such as:

- How can existing structures be customized and improved?
- What is the best design for these structures?
- How do these not interfere with other technologies in a car?

The study of electrical, magnetic, and thermal characterization is necessary when active components such as near-field communication devices, contactless battery chargers, powerful LEDs, and/or haptic feedback controllers are placed in close proximity to touch sensors, receiver antennas, and low-power electronic circuits.

1.2 Scope and Motivation

To improve the technology inside a car to give more comfort, more safety and more customization it is necessary to delve deeper into these technologies, 3D printing/techniques, AM and materials. This study and knowledge is a crucial part of taking the technology further.

The dissertation is integrated in the AM4SP project. AM4SP is a joint research project by Simoldes Plásticos, a TIER1 manufacturer that produces plastic components for automotive manufacturers, and the University of Aveiro. The project aims to create innovative solutions for automotive plastic components, namely for door panels, based on the AM technology. This will allow the creation of customized components, where the electric circuits will also be built by AM processes, creating new forms of user interaction. AM4SP thus consists of the development of a door panel with the integration of custom and disruptive components, using AM technologies, and their integration in an injected part [32].

The motivation for this master thesis comes mainly from a love of 3D printing and modeling coupled with the electrical concepts and programming. It is focused on:

- characterization of components in terms of electrical and magnetic characteristics;
- structure creation, simulation, and prototyping in order to be able to investigate whether the touch method is feasible;
- developing structures that can be integrated using AM.

These goals are intertwined with the preferences for choosing this dissertation.

1.3 Work objectives

The main objective of this Master Thesis is to create and study touch sensors, and understand the problems of ElectroMagnetic Compatibility (EMC) and ElectroMagnetic Interference (EMI) combined with AM, in addition to studying the impact of these aspects on automotive electronics. To this end, several intermediate objectives must be achieved:

1. Conducting a literature review on 3D printed electronics, sensors and actuators;
2. Learn how to work with the electromagnetic simulation software, CST Microwave Studio and estimate key EMC parameters for a few designs of 3D-printed HMI devices;
3. Implementation of the device with parameters obtained earlier in the EMC simulation tool;
4. Performing measurements of different parameters in a laboratory;
5. Make tools to automate the process of calculating the parameters, and tool to create different structures that vary with the parameters obtained;
6. Develop the structures and prototype PCBs;
7. Investigate possible methods for detecting touch on sensors that can be applied to AM.

Objective 1 is important to understand the theoretical part and can be the beginning of the dissertation.

Objective 2 allows to learn how to identify the key parameters, how they can be changed and how to parametrize the structure under study in a way that it can help with the development of the project. Thus this can be a crucial step.

Objective 3 allows to merge the theoretical and design objectives 1 and 2 with the simulation task.

Objective 4 is to investigate the reliability of tools that will automate the process of calculation, simulation, design and printing of these sensors.

Objective 5, 6 and 7 is to create structures, simulate, prototype, and print them in order to be able to investigate whether the printing method is feasible for these structures.

1.4 Methodology

The process of structuring and approaching the problem started by investigating the possible methods to be used. Besides the theoretical investigations, most of the practical implementations of the work contained in this dissertation are based on the use of software tools. As such, for the programming, MATLAB® [33] was used as the main tool for determining the initial parameters for the simulations in CST Studio Suite [34]. The CST Studio Suite was used to simulate the structures with the parameters provided by MATLAB® script to design the sensors and obtain results estimating EMC, EMI, the Scattering Parameters (S-parameters), and mainly to validate the parameters provided by the MATLAB® script.

In MATLAB® a function was created to calculate the capacitance. Another function was created to obtain the inductance, that was given in [18]. With the values of capacitance and inductance it was possible to obtain the resonant frequency. Also, a script was created that performed many calculation of the capacitance and the inductance to obtain the resonant frequency specified by the user. With this script it was possible to obtain the parameters and geometries for the specified resonant frequencies. A macro was created in CST Studio Suite to generate new structures for each set of new parameters provided by the MATLAB script.

In order to verify and demonstrate the proposed sensor concept during the thesis, the experimental values were measured. To measure the values, a set of PCBs was developed, generated from structures made in the CST Studio Suite.

The settings used for the measurements, the code for MATLAB®, the CST Studio Suite macro, and the experimental tests are presented and described in more detail further in the text of this thesis.

1.5 Dissertation structure

This dissertation is divided into 7 chapters detailed below:

Chapter 1 - *Introduction*: contextualization of the topic and scope of this document, the motivation, the work objectives, and the methodologies for this research. It briefly describes how the document is organized and the contributions associated with this research.

Chapter 2 - *State of the Art*: introduces the main technologies for printing electronics with and without direct substrate contact, physical and chemical capacitive sensors, types of materials, inks and substrates, types of measurements on touch sensors, sensor geometries

and design, electromagnetic compatibility and interference, problems and concerns, and radio frequency spectrum.

Chapter 3 - *Calculations*: introduces the analytical models and implementations to obtain the values of the capacitance, the inductance, and the resonant frequency. It also provides an explanation of the script that runs for many parameters, and saves them when the resonant frequency is reached. An analysis and discussion of the experienced problems, the methods used to solve the problems, and the achieved results is presented.

Chapter 4 - *Simulations*: this chapter allows to run different simulations using the results obtained in the Calculations. To arrive at the simulations the previous process was explained, namely the construction of a parameterized macro file, and the materials and methods used to simulate. An analysis and discussion of the chosen processes, the tried problems, the methods used to solve the problems, and the achieved results are also described.

Chapter 5 - *Experimental Measurements*: is relevant for measuring the experimental values of the created structures, and validating the performed calculations and simulations. It also shows the results and gives a detailed analysis of the obtained measurements.

Chapter 6 - *Conclusions*: aims to give the conclusions about the developed work, the main results, the limitations, and the future work.

Chapter 7 - *Appendices*: describes in more detail the auxiliary equations, tables and scripts developed.

Chapter 2

State of the Art

This chapter aims to detail the fundamentals of this work by conducting a thorough and extensive review of the current state of the art of various topics necessary for our work, giving some ideas about the approaches that are followed and why.

This chapter is organized as follows. Section 2.1 contains analysis of the new methods to make Printed Electronics (PE), divided in subsection with the focus to introduce in more detail the Non Contact technologies, Contact technologies, and some examples of physical and chemical capacitive sensors. Section 2.2 introduces an overview of types of materials, inks and substrates categorized by utility in each process of AM. Section 2.3 details types of measurements on touch sensors with Capacitive structures, Inductive structures and resonant circuits. It also provides different techniques for structures used to measure the values of the capacitance, inductance or resonant frequency. The Section 2.4 details the types of geometries in Capacitive structures and the parameters and techniques to design a better capacitive touch sensor. Section 2.5 has the focus to explain the EMC and EMI problems and concerns, as well as to give an overview of Radio Frequency (RF) spectrum and the problems related with interferences in the spectrum. Lastly, Section 2.6 provides an overview of the State of the Art.

2.1 Printed Electronics

To make electronic devices there are two ways to do it, by Conventional Electronics or by using PE techniques. The PE has different characteristics compared to the old methods of making electronics. These differences are briefly shown in Figure 2.1.

Both methods go through the same steps to obtain the final PCB circuit design and do PCB prototyping, but these steps had to be replaced with new and different methods to print electronics. These new methods can be divided into different technology categories, such as the following:

- Gravure Printing;
- Flexographic Printing;
- Screen Printing;
- Offset Printing;

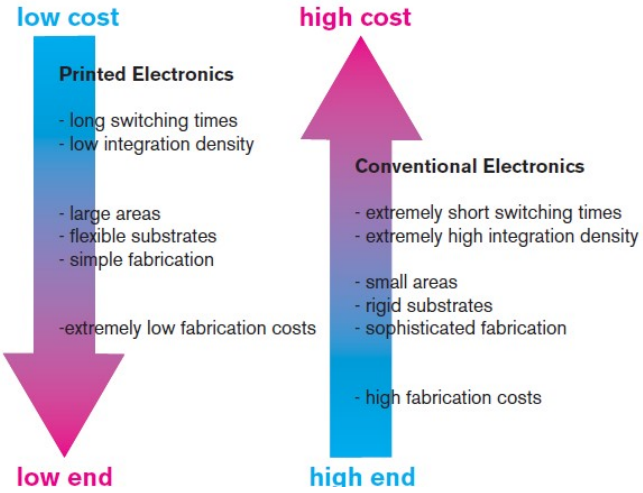

Figure 2.1: Comparison between Conventional Electronics and Printed Electronics [5].

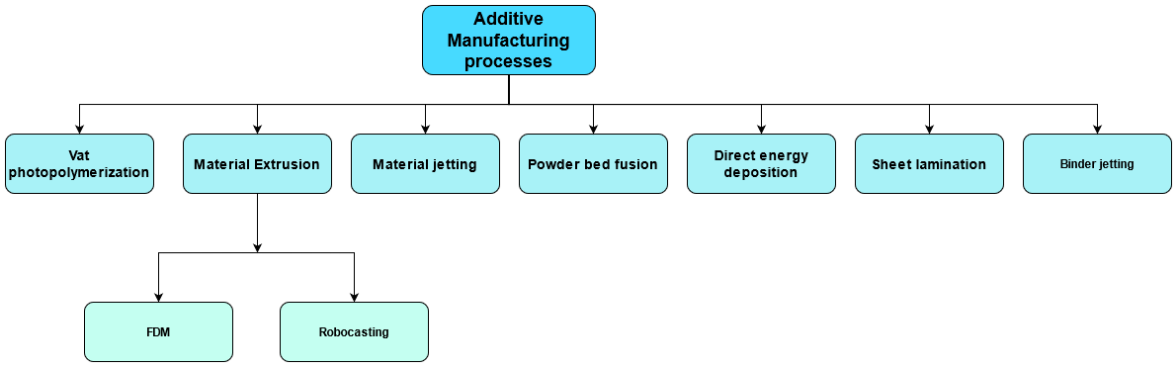

Figure 2.2: Additive manufacturing technologies summarized in a tree diagram according to ASTM Standard F2792-12a [6].

- Inkjet printing.

Each category and technique has advantages in different situations and each has unique process, parameters and performances, such as resolution, homogeneity, speed, ink, thickness and substrate properties [35, 36]. It is also important to note that there are different types of substrates and functional inks to these printed electronics processes. The Figure 2.2 shows an overview of technologies and techniques of AM accordingly to the ASTM Standard F2792-12a [6].

These technologies can be organized into categories, depending on whether there is no direct contact between the deposited material and the substrate (Non-Contact technologies) and whether the printing equipment contacts the substrate (Contact Technologies).

2.1.1 Non-Contact Technologies

Starting with non-contact technologies, these are technologies that, as the name implies, have no direct contact beyond the deposited material and the substrate. They are characterized with the advantage of decreasing contamination of the deposited material, and deterio-

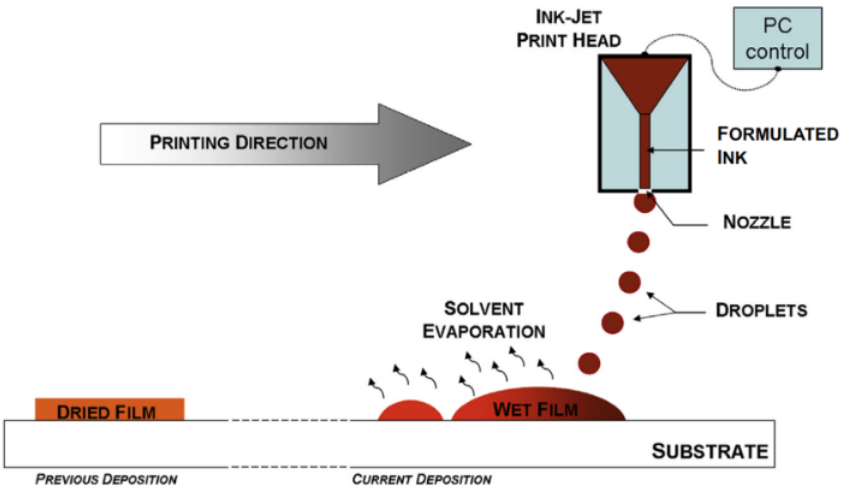

Figure 2.3: Illustration of the inkjet printing process, showing the basic components and the drops that fall from the nozzle onto the substrate. Source: [7].

---

ration of the substrate, and increasing the accuracy of layer alignment. Another advantage is that such methods do not need a physical mask to define the desired layout, you only need a digital file to achieve the desired layout. The last advantage allows to simplify the process of switching and customization without any extra cost and a lot of time to change. One disadvantage is the large-scale process [36]. In what follows the main non contact technologies are discussed.

Inkjet Printing

Inkjet printing is a technology that makes ink droplets fall onto the substrate from above. These droplets can be proteins, fluids, powders, minerals, nanoparticles, and conductive polymers, [37] amongst other materials. This technology can be applied to almost any substrate, from rigid to flexible, and from smooth to rough surfaces. They also have low raw material consumption, are environmentally friendly, and have many different applications like production of transducers, transistors, structural polymers, and ceramics. A disadvantage is the low process speed, and a possibility to have blockage in the nozzle due to clogging or drying of solvents, and limited use for large scale production [36]. The process that starts with drawing the model to be printed in a CAD software, is saved as an STereoLithography (STL) file or in other formats such as OBJ, FBX, COLLADA, among others. After loading the file to the 3D printer, the printer deposits droplets to the substrate accordingly to the coordinates and points in the 3D file. Figure 2.3 shows the process of printing.

Slot-Die

Slot Die is a technology that deposits a thin film of the solution, typically in the range of 5 to 30 µm, which is applied homogeneously across the substrate surface with minimal waste and low operating cost. The advantages are the high manufacturing yield and high uniformity of the obtained films, however, they are difficult to pattern, which reduces their applications and their use in complex structures [36]. It can be used to produce energy harvesting, energy storage, and smart materials. Figure 2.4 shows the process of printing.

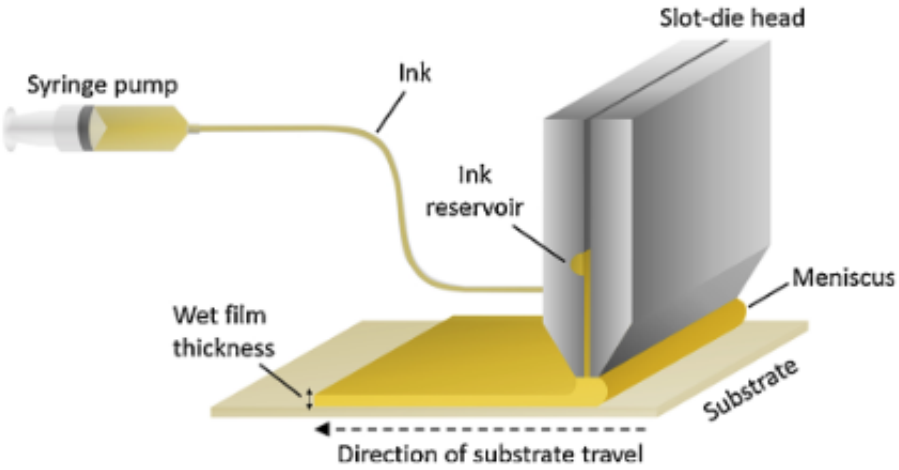

Figure 2.4: Illustration of the Slot Die process, showing the basic components and the thin film deposition. Source: [8].

Spray Deposition

Spray deposition is usually done in liquid form through a gas stream. The bulk material is divided into droplets, commonly known as an atomization process, to be subsequently transported to the substrate in a mixture of gas and a stream of droplets [36]. There are two ways to achieve atomization: one when mixing with air flow, with the name air-assisted atomization, and another when doing it with the kinetic energy, with the name ultrasonic atomization. The advantages are the high deposition efficiency and rate, and the main problems are due to the plastic deformation process, which leads to loss of ductility of the coating [38].

Laser Direct Writing

Laser Direct Writing is a process when laser processes the materials without any physical contact between the tool and the substrate. There are three types of Laser Direct Writing techniques:

- Laser direct-writing subtraction technique;
- Laser direct-writing addition technique;
- Laser direct-writing modification process.

They offer a higher resolution manufacturing and high deposition of biomaterials. However, this method requires very sophisticated equipment at high cost and is not able to create 3D patterns [36].

2.1.2 Contact Technologies

After the Non-Contact technologies, there are the contact technologies, where the printing equipment makes contact with the substrate.

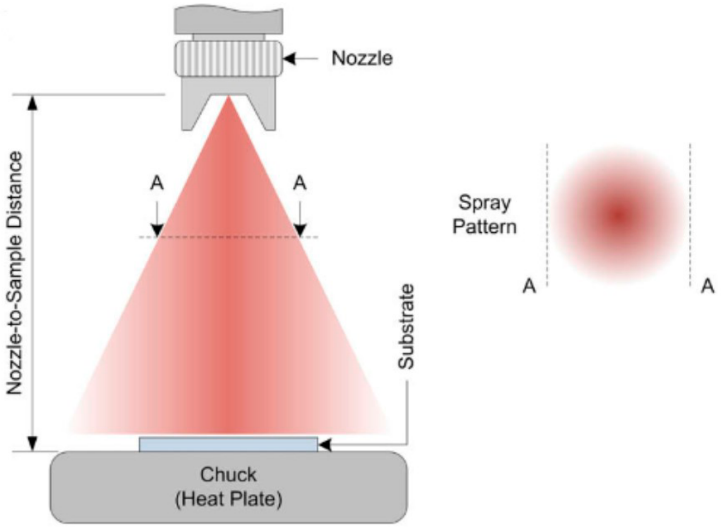

Figure 2.5: Illustration of Spray deposition, showing the basic components and the resulting spray pattern. Adapted from [9].

Screen Printing

Screen printing consists of using a screen mesh in direct contact with a substrate that distributes the paste and fills in the mesh [36]. It can be applied in the Reel-to-Reel (R2R) system or in a planar process. Screen printing is best suited for mass customization of Drug Delivery Systems (DDS) relying on a conventional regulatory strategy [10]. The advantages are that manufacturing is continuous, increasing production speed, and it is simple to produce thick patterns in shorter times. However, the system is more expensive, is difficult to clean, wastes materials (solutions, pastes and screens), and has lower resolution when compared to other techniques [36]. Figure 2.6 shows the process of screen printing.

Flexography

Flexography is a R2R technique of direct printing by transferring ink from an embossed cylinder onto a substrate [36] [39]. The patterns are on separate plates and those are attached on a plate cylinder [39]. Figure 2.7 shows the flexography process and the basic components: the cylinders with a substrate, patterns, and the anilox rollers to supply ink. It is considered to be a high-throughput method that allows mass production at higher print speeds [39]. However, it has limitations in image size and resolution due to patterns with excess ink compression between the substrate and the printing plate roller.

Gravure

Gravure is the reverse process of the Flexography, where the printed image is the negative [36]. Also as Flexography is considered a high throughput method allowing mass production at higher printing speeds [39]. It produces high quality patterns with high speed of fabrication (up to 0.1 m/s) [36]. In this process there exist only two rolls: the anilox roll to supply the ink and an impression cylinder to compress the substrate.

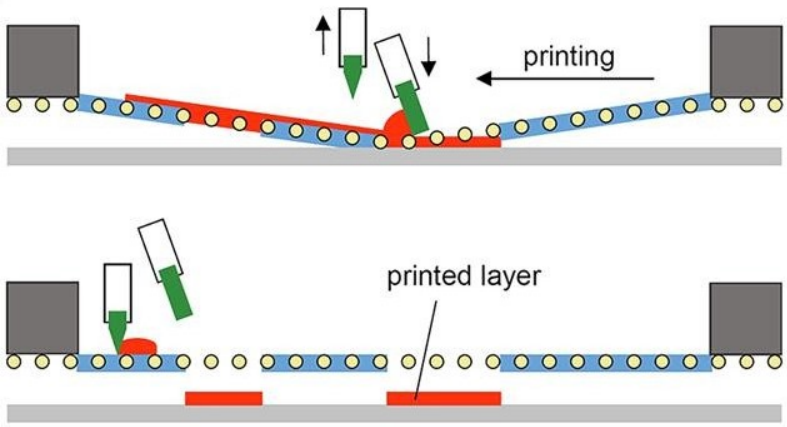

Figure 2.6: Illustration of the Screen Printing process, starting with the distribution of paste on the screen to fill open areas and then printing on the substrate [10].

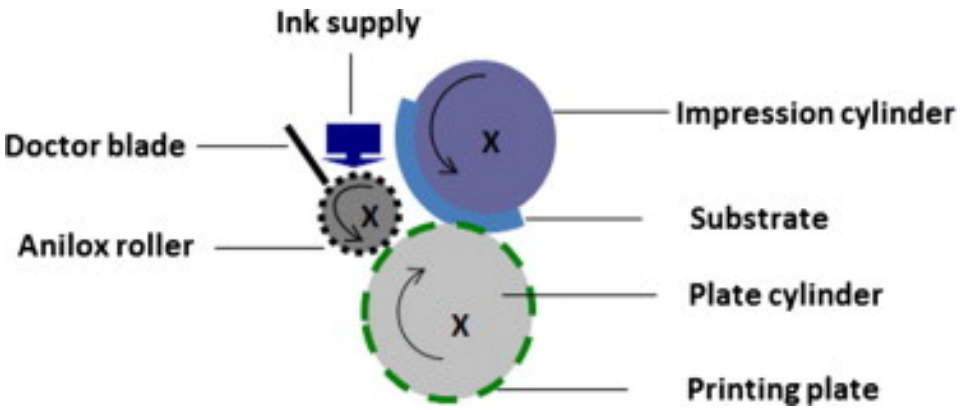

Figure 2.7: Illustration of the Flexography printing process and the basic components [11].

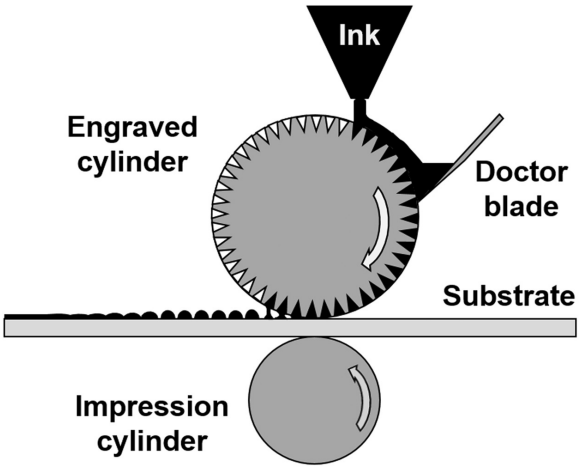

Figure 2.8: Illustration of Gravure printing process and the basic components [12].

Printing process overview					
Parameters / printing process	Inkjet	Screen	Flexography	Offset	Gravure
Typ. lateral resolution [μm]	> 50	> 100	> 30	> 20	> 20
Typ. layer thickness [μm]	0.3–20	3–25	0.5–8	0.5–2	0.1–5
Typ. viscosity of ink [Pas]	0.001–0.04	1–100	0.05–0.5	30–100	0.01–0.2
Typ. max. printing speed [m/s]	0.5	1	8	15	15

Table 2.1: Typical parameters of printing process. Source: [19, 20, 21].

2.1.3 Overview of Printing Process

An overview of the printing process can be seen from the data collected in on the Table 2.1.

2.1.4 Physical Capacitive Sensors

Parameters such as acceleration, force, and pressure, temperature, stiffness, density, thickness among others can be measured by physical sensors that can quantify variations of these physical properties on the Device Under Test (DUT) [36]. In what follows, some examples of the physical capacitive sensors used nowadays and sensors that can be printed or made using AM are shown.

Force and Pressure Sensors

As the name says these sensors are used to measure force and pressure. There exist different types of pressure sensors:

- Pressure sensors based on strain gauge [40, 41, 42];
- Capacitive pressure sensors [43, 44];
- Piezoresistive pressure sensors [45];

For the capacitive pressure sensors, the capacitive structure is employed due to its small dimensions and high spatial resolution. The material normally used to make these sensors is Polydimethylsiloxane (PDMS). When the PDMS thickness increases the sensitivity of sensor decreases [36].

Accelerometers

Accelerometers are another example of physical sensors. They are used in everyday's automotive applications and technologies, such as in smartphones, tablet computers, and smart bands. They are used to measure the acceleration of moving objects along reference axes used [36].

Strain Sensors

Strain sensors are used to transduce tensile or compressive stresses to electrical signals [22]. They are generally designed as resistive sensors, but there are some cases where they are capacitive [36].

2.1.5 Chemical Capacitive Sensors

Capacitive Chemical Sensors are used in monitoring devices for electrolytes, metabolites, heavy metals, and gases [36]. The following paragraph illustrates an example of a currently used capacitive chemical sensor that can be printed or made by using AM.

Relative Humidity Detectors

The most common chemical capacitive sensors in literature are Relative Humidity (RH) detectors. The most sensitive geometry for these sensors is with the serpentine electrodes, followed by spiral and IDE. The lowest sensitivity geometry is the meandered one [36]. The mentioned geometries are shown in Figure 2.17. To select the best layout it is necessary to understand the characteristics of our application to choose an appropriate layout, in other words, each layout is good for and depends on each final application. Some fabrication techniques such as laser writing, have shown a more linear response, on the other hand, inkjet printing has lower losses and higher sensitivity [36].

2.2 Types of materials, Inks and Substrates

This section presents the state of the art on the types of materials and substrates. There are many techniques for printing each material. Each material has different properties that translate into sensors with different characteristics suitable for different situations. It is possible to print organic and inorganic materials (metallic or non-metallic). To select which material to use, it is important to take into consideration some parameters such as flexibility, cost, and electrical performance. The latter is the most important parameter.

Inks can also be used to produce reliable droplets and conductive patterns, but it is important to know their physical and chemical properties. With inks it is possible to achieve a low-cost and simplified printing process. Nanoparticle inks comprise particles of metal or semiconductor oxides mixed with the desired solvent. The nanoparticles commonly used in inkjet printing are copper (Cu), silver (Ag), gold (Au), and nickel (Ni), but the most commonly used are Ag nanoparticles due to higher conductivity and lower price. Conductive polymers can also be used on flexible polymer substrates to facilitate electrical patterning and be useful due to good mechanical stability and adhesion to plastic substrates [46, 35]. The materials according to the seven categories with ASTM Standard F2792-12a ISO/ASTM2013 and their limitations and advantages are illustrated in the table 2.2.

The substrates available in IT-Aveiro that can be used for prototyping are shown in Table 7.1 in Appendix 7.1.

Printing process overview			
Process	Materials	Advantages	Disadvantages
Binder jetting	Gypsum Ceramics Stainless steel	Low cost Colorful printing No support structure	Low strength Post-processing Low mechanical properties
Material extrusion	Glass Ceramics Thermoplastics	Low cost Simple usage Multi material	Rough surface Low resolution Poor part strength
Directed energy deposition	Metals Titanium Cobalt chrome	High speed High durability Suitable to repair parts	Post-processing Poor surface finish Limited material use
Material jetting	Plastic Polyethylene Polypropylene	Low waste High accuracy Colorful printing	High cost Support structure Low mechanical properties
Sheet lamination	Paper Plastic Some metals	Low cost High speed Colorful printing	Post-processing Poor resolution Design limitations
Powder bed fusion	Titanium Aluminum Stainless steel	Low cost Multi material No support structure	Low speed Size limitation High power usage
Vat photopolymerization	Resin Plastic Polymer	High speed Great precision High resolution	Fragility of parts Support structure Limited material use

Table 2.2: Additive manufacturing process according [6], relevant materials and specifications. Adapted from [22].

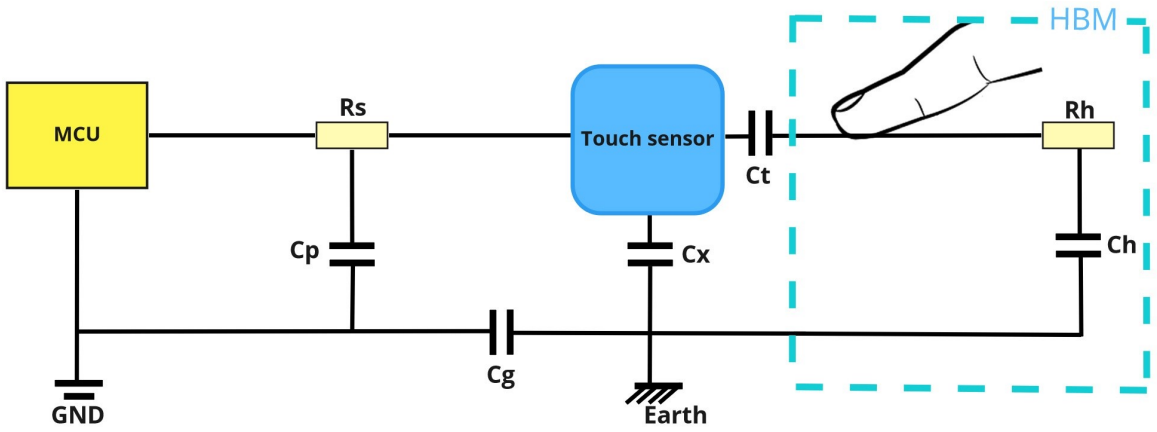

Figure 2.9: Self capacitance model without and with touch contact. Adapted from [13].

2.3 Types of Measurements for Touch Sensors

This section presents techniques and types of measurements for touch sensors. The process of using touch sensors is very complex because it requires making many decisions. It depends on the material type, the electrical and mechanical requirements, and the form of user interface. Before choosing a design it is important to introduce the methods to measuring changes of capacitance in capacitive structures: **Self Capacitance Measurement** or **Mutual Capacitance Measurement**, and the methods to measure the **resonance frequency in resonant circuits**.

2.3.1 Capacitive Structures

Capacitive structures use electrodes, one or more, to create an electric field and measure changes in it.

Self Capacitance Measurements

Touch sensors that use self capacitance measurement have a single electrode to measure the apparent capacitance between the electrode and the ground. [13, 47]. Figure 2.9 shows the circuit of the self capacitance sensor. The capacitance is obtained by the combination of the parasitic capacitance (C_p), touch sensor, and the ground return capacitance (G_g). These form the model circuit used for calibration and also as a reference to detect the capacitance change.

The circuit with touch contact is shown in the same figure in a block with the name Human Body Model (HBM). When human contact is applied the touch Capacitance (C_t) forms a series connection with HBM, and the capacitances C_h and C_g. The apparent capacitance is increased when the HBM is introduced due to the parallel path formed between them. In terms of produced electric field the self capacitance sensor induces electric field around it and can be used to interact on both sides (unless ground shielding is utilized) [47].

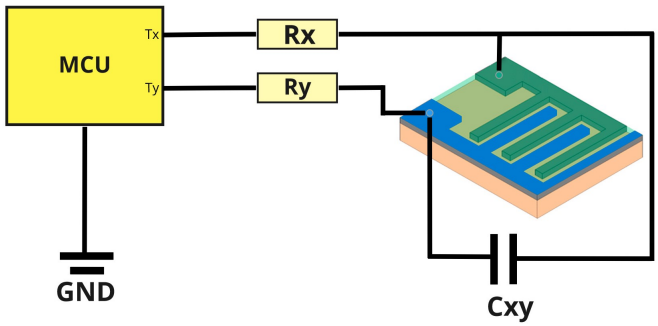

Figure 2.10: Mutual capacitance model without touch contact. Adapted from [13].

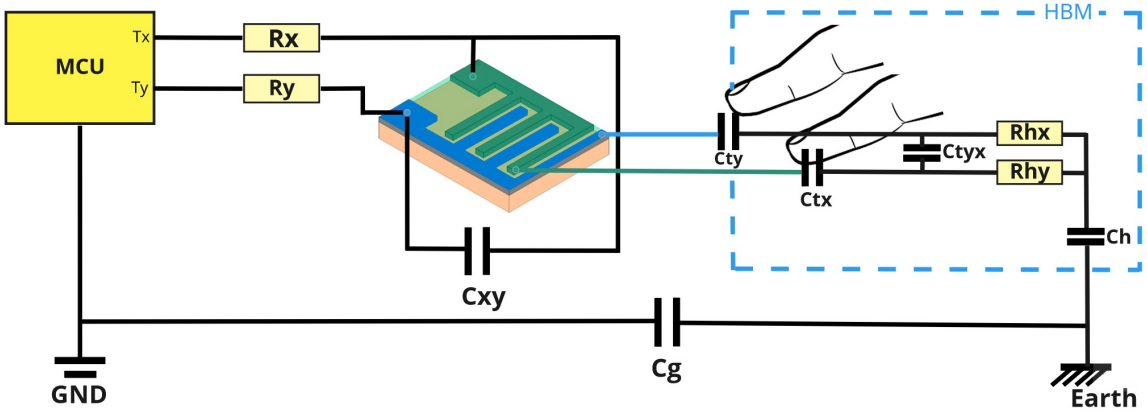

Figure 2.11: Mutual capacitance model with touch contact. Adapted from [13].

Mutual Capacitance Measurements

The Mutual Capacitance measurement also measures the change in capacitance like self capacitance, but here the second electrode of a capacitor is used instead of being grounded. Such sensors use two pair of electrodes for each node (in the Figures 2.10,2.11 as illustrated in blue and green colors for each pair of the electrodes). The sensor is formed by this pair of electrodes placed together in a form of interdigitated geometry to optimize the length of parallel conductors [13]. It uses two pins of a MicroController Unit (MCU) instead of just one pin as in the self capacitance case.

When human contact is applied over the sensor, the user can interact with the electric field between the electrode T_y and the electrode T_x, and the mutual capacitance between those T_y and T_x electrodes changes. This happens because the user interactions disturb the electric field distribution between the two electrodes.

Partial Capacitance Technique

A useful technique for calculating capacitance is the Partial Capacitance Technique (PCT) followed from the paper [15]. To understand this method, it is important to consider some structures to obtain formulas for the total capacitance. Situation with an equivalent capacitive structure of the IDE circuit with N electrodes in a layer is illustrated in Figure 2.12.

With the Figure 2.12 it is possible to reach the following conclusions:

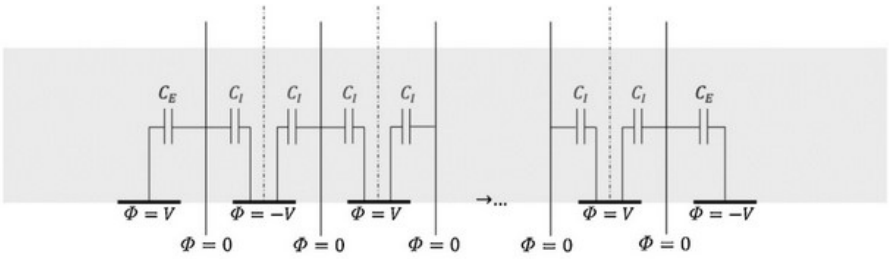

Figure 2.12: Equivalent circuit of IDE geometry in one layer. Source: [14].

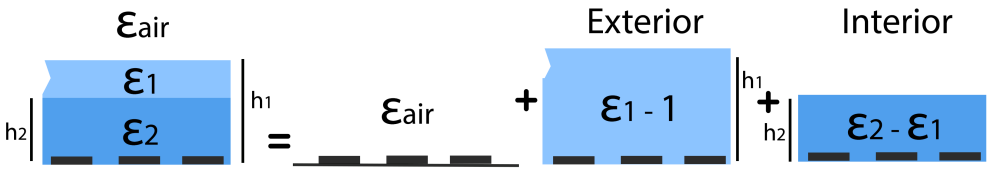

Figure 2.13: Split layers with PCT. Adapted from: [15].

- The voltage on the electrodes is switching between the positive and negative voltages;
- The capacitance C_I formed between each electrode and the neighbor electrode is half of the capacitance of an internal electrode relatively to the ground;
- C_E is the exterior capacitance.

The Figure 2.12 has a single layer, however the PCT method splits the layers and calculates the capacitance for each new layer as illustrated in the Figure 2.13.

2.3.2 Inductive Structures

Self Inductance

Analogous to the capacitance the inductance also have the self and mutual inductive components. Self inductance is a property of a coil that occurs when the magnetic field of a coil opposes any change in the coil current. Self induced electromotive force as expressed in terms of the magnetic field is given by the following equation 2.1:

$$\mathcal{E}_L = -N\frac{d\Phi_B}{dt} = -N\frac{d}{dt}\oint\oint B\,dA \tag{2.1}$$

And the relation of self induced electromotive force with the inductance is:

$$\mathcal{E}_L = -L\frac{di}{dt} \tag{2.2}$$

Combining the equations 2.1, 2.2 it is possible to obtain the inductance 2.3:

$$L = \frac{N\Phi_B}{i} \tag{2.3}$$

Mutual Inductance

The mutual inductance occurs when two coils are placed near each other and the mutual inductance M between the two coils (C_1 and C_2) can be expressed from the Neumann's formula [48] using the following equation 2.4:

$$M = \frac{\mu_0}{4\pi} \oint_k \oint_l \frac{dl \cdot dk}{|r - r'|} \tag{2.4}$$

Mean Distance Method

The method that calculates the average distance helps to calculate the inductance. This method considers each side of the coil as a single conductor consisting of N parallel conductor segments. This method depends on the three types of average distance [18, 49]:

- Geometric Mean Distance (GMD);
- Arithmetic Mean Square Distance (AMSD);
- Arithmetic Mean Distance (AMD).

Empirical Formulas

There exist different approaches to calculate and obtain the values of the inductance. Some of empirical formulas are:

- Greenhouse, used to calculate the inductance of spiral inductors [50];
- Nagaoka's, used to calculate the inductance of a solenoidal coil, which can be used to calculate the self and mutual inductances [51];
- Lorenz's, used for calculate the inductance of coaxial solenoids [51].

According to [52] the inductance for a single layer spiral inductor, as named "Greenhouse formula", is given by Eq. 2.5:

$$L = \frac{1.27\mu_0 n^2 d_{avg}}{2} [\ln \frac{2.07}{\varphi} + 0.18\varphi + 0.13\varphi^2] \tag{2.5}$$

Another way to obtain the inductance is with Nagaoka's formula [53] given by:

$$L = \frac{4\pi^2 N^2 r^2}{l} Kl \tag{2.6}$$

where l is the coil length and Kl is the Nagaoka's coefficient given by:

$$Kl = \frac{4}{3\pi k'} \left[\frac{k'^2}{k^2} (K(k) - E(k)) + E(k) - k \right] \tag{2.7}$$

Lorenz's formula [51] is applied to calculate the inductance of a solenoidal current. The formula is:

$$L = \frac{32\pi N^2 r^3}{3l^2} \left[\frac{2k^2 - 1}{k^3} E(k) + \frac{1 - k^2}{k^3} K(k) - 1 \right] \tag{2.8}$$

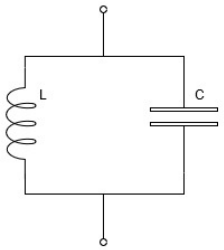

Figure 2.14: LC Circuit equivalent model.

---

where $K(k)$ and $E(k)$ are the complete elliptic integrals of the first and second kind, respectively, of the modulus k. The k is:

$$k = \sqrt{\frac{4r^2}{4r^2 + l^2}} \tag{2.9}$$

where r is the radius, l the length, and N the number of loops.

2.3.3 Resonant Circuits

Another method for making touch sensors is with resonant circuits. These circuits have such name because the sensors resonate at a certain frequency. These circuits can use inductive and capacitive structures presented earlier to form an LC circuit.

The LC circuit can have different forms of the inductor and capacitor structures. For example, the capacitor can be of spiral, serpentine, and other shapes. The equivalent circuit is shown in Figure 2.14.

The angular resonant frequency of the LC circuit in radians per second is given by Eq. 2.10:

$$\omega = \sqrt{\frac{1}{LC}} \tag{2.10}$$

where L is the inductance, and C is the capacitance. Alternatively, the resonant frequency in Hertz in given by the formula 2.11

$$f = \frac{1}{2\pi\sqrt{LC}} \tag{2.11}$$

To better understand the inductive part and the capacitive part, the following subsections focus on each separately.

2.3.4 Measurements Overview

Figure 2.15 shows the overview of self capacitance and figure 2.16 shows the overview of mutual capacitance.

These methods have some advantages and some constraints. The self capacitance method is characterized with a longer range of sensing and higher capacitance change when a finger is applied. However, these sensors are very sensitive to the surrounding environment [54]. On the other hand, the Mutual Capacitance method is improved, over another method, by the fact that the capacitance only changes when the finger approaches the sensor without

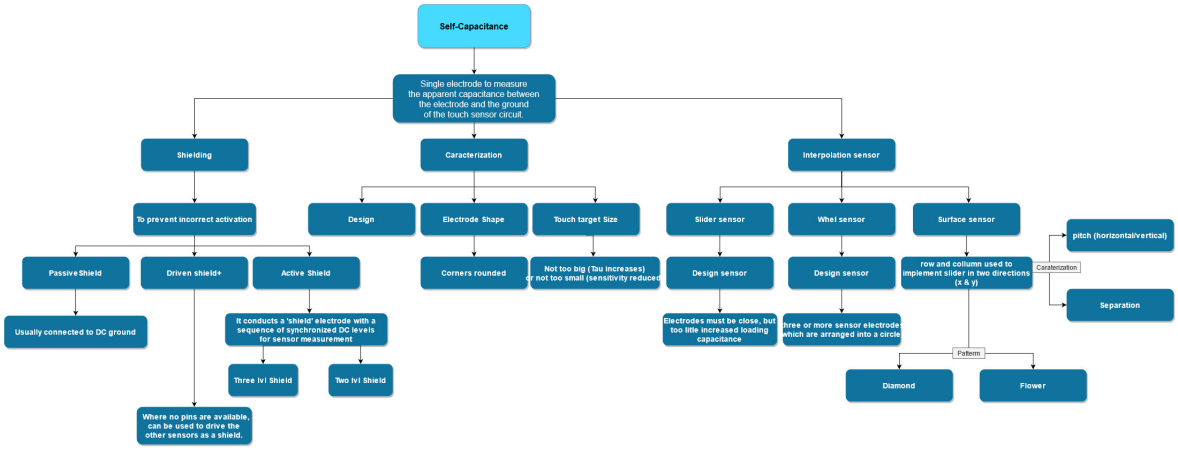

Figure 2.15: Overview of self capacitance characteristics and geometries for the design of a touch sensor.

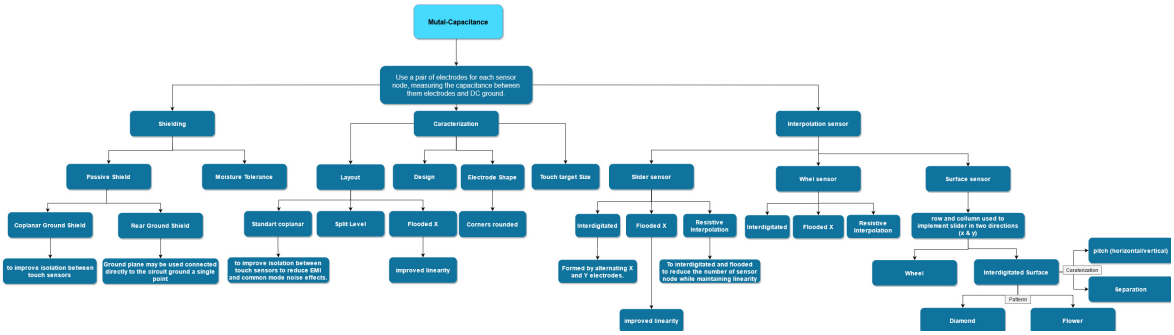

Figure 2.16: Overview of mutual capacitance characteristics and geometries for the design of a touch sensor.

physical contact. However, this method of capacitive sensor realization has high sensitivity to noise, humidity, and temperature [54]. This then makes it difficult to use this sensor in some applications.

For automotive applications there are some necessary constraints to keep in mind when designing sensors like these, such as [47]:

- A broad temperature range;
- A broad humidity range;
- Contamination by drivers, passengers, and the environment;
- The lifetime of the vehicle;
- As cars have more and more sensors it is necessary to install them more easily.

To minimize these problems it is necessary and crucial to choose a design and arrangement of electrodes to have excellent results in terms of frequency range and other parameters.

2.4 Designing a Capacitive Touch Sensor

After choosing the type of measurement it is very crucial to choose the characteristics and geometry of the sensor to minimize risk and get the best possible results. The following characteristics are important to optimize the geometries to fit the chosen application and the desired requirements. Some of the characteristics to be optimized are [13]:

- Strongest touch delta;
- Best noise tolerance;
- Best water rejection;
- Minimum sensor capacitance;
- Minimum power consumption;
- Minimum touch latency.

The way to optimize these characteristics is to choose the best electrode geometries, tactile target size, electrode separation, and shielding presented below.

2.4.1 Electrode geometries in Capacitive Structures

The electrodes can be organized and placed in different forms to form different geometries of the capacitive structures. The shape, place and arrangement of the electrodes will influence the sensitivity of the sensor, which can be used to facilitate the sensor design and optimisation. The Figure 2.17 shows the geometries: square-spiral, interdigitated, concentric ring, rectangular, and square, in single electrode.

With Figure 2.17 it is possible to conclude about the sensitivity between the sensors and geometries. The interdigitated geometry and the concentric ring have a good and uniform sensitivity. From the figure it is possible to see the Sensitivity Variation Parameter (SVP).

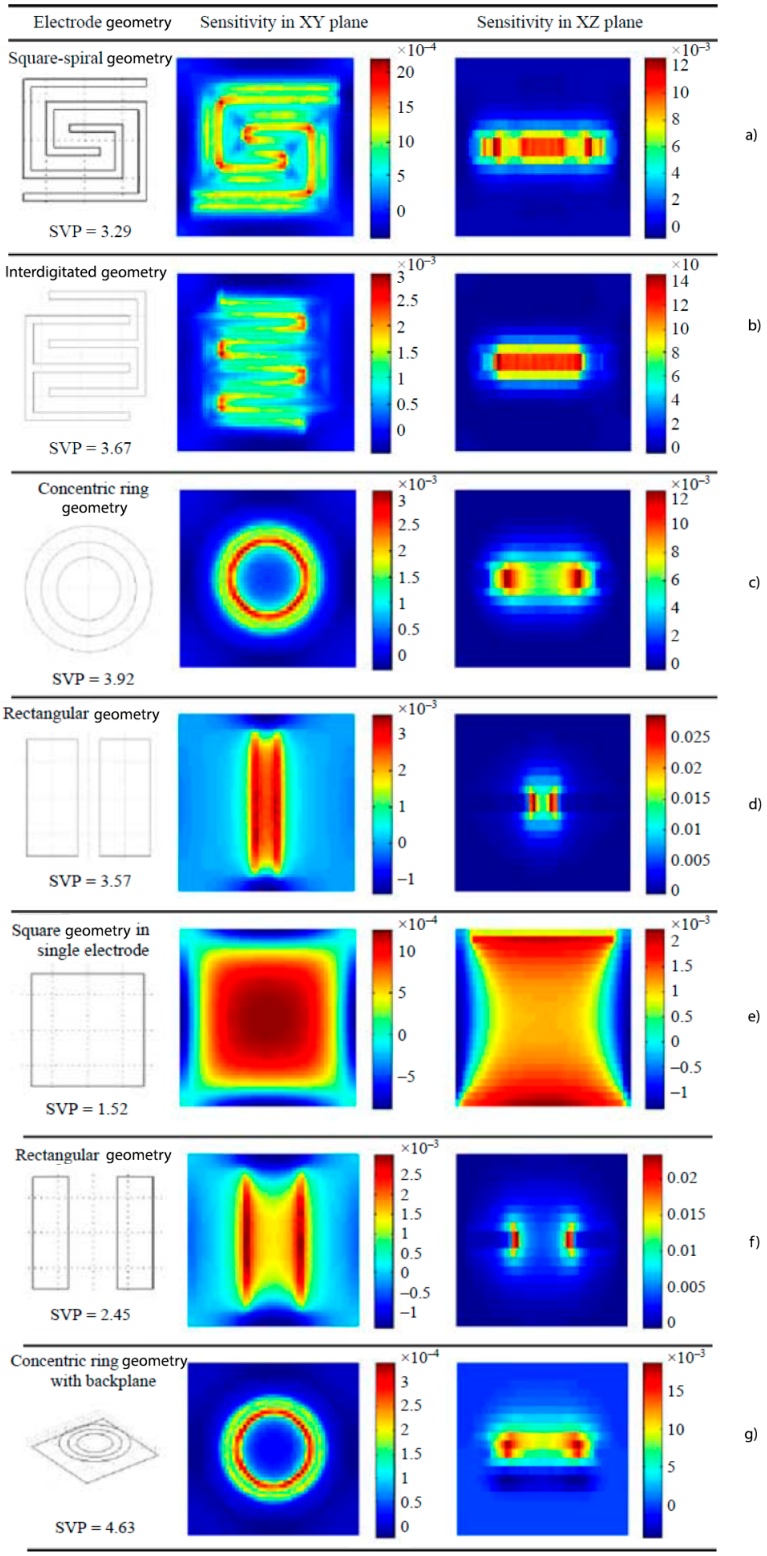

Figure 2.17: Illustration of electrodes geometries and their sensitivity. Adapted from [16].

This parameter shows how homogeneous the sensitivity distribution is. This is a parameter that is defined as follows [55]:

$$SVP = \frac{S_{\epsilon,dev}}{S_{\epsilon,avg}} \tag{2.12}$$

where $S_{\epsilon,avg}$ is the mean value given by:

$$S_{\epsilon,avg} = \frac{1}{M}\sum_{j=1}^{M} S_{\epsilon,j} \tag{2.13}$$

and $S_{\epsilon,dev}$ is the standard deviation given by:

$$S_{\epsilon,dev} = \left(\frac{1}{M}\sum_{j=1}^{M}(S_{\epsilon,j} - S_{\epsilon,avg})^2\right)^{1/2} \tag{2.14}$$

where $S_{\epsilon,j}$ is the relative capacitance given by:

$$S_{\epsilon,j} = (\frac{(C_{\epsilon,j} - C_0)/C_0}{\beta_j}) \tag{2.15}$$

With $j = 1, 2, ..., M$ elements (dimensionless), C_0 is the capacitance when all elements are in free space (or air), and $C_{\epsilon,j}$ is the capacitance when the j element has a dielectric with relative permittivity ϵ.

If the SVP is smaller the sensor will be more homogeneous. Among the geometries presented, the square with a single electrode, is the geometry that has the smallest value of SVP, followed by the rectangular geometry, whose electrodes are placed closer together.

The geometries most used for capacitive sensing are IDE and Parallel plate (PP). The PP has a simple geometry and it is easy to modify and perform the calculations [56]. The IDE geometry is a very popular solution for printed sensors because of their planar capacitance geometry, which means the electrodes of the sensor form a coplanar line (strip of thin metallic film on the surface of dielectric with two ground electrodes adjacent and parallel to the strip [57]) [36, 16].

2.4.2 Touch Sensor Design

Electrode layouts

The first characteristic is the electrode layouts. There are two standard coplanar layouts shown in Figure 2.18 made in the interdigitated geometry. With this geometry, the length of the electrodes is maximized and the separation of the electrodes increases, and thus the capacitance of the sensor decreases. It is important to note that by increasing the distance between the X and Y electrodes, the capacitance will decrease and the length of the electrodes will also decrease. To emphasize, this geometry is usually implemented in a single layer PCB but can be split between two layers [13].

Another possibility is a flooded X layout. This layout has a solid area denominated by X and one geometry of electrodes (Y) on top as illustrated in Figure 2.19. With this layout, the X area shields the Y electrodes from the circuit noise. However, it needs a thicker touch cover and this implies that sensors suffer from low sensitivity. Flooded X sensors are typically used when the touch cover is thinner than the substrate [13].

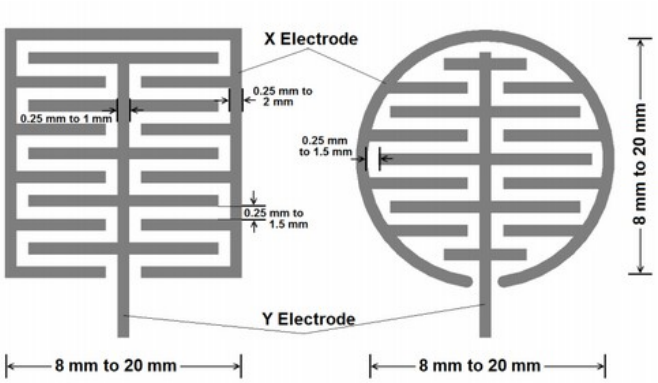

Figure 2.18: Illustration of the standard coplanar layouts. Source: [13].

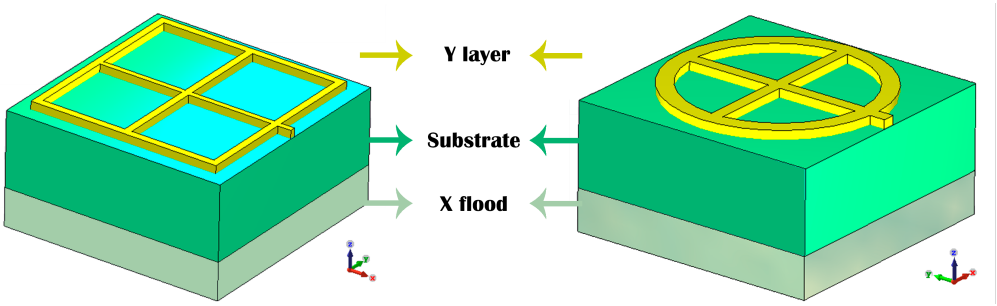

Figure 2.19: Illustration of Flooded X layouts. Figure is not to scale.

Touch Target Size

This subsection and the next two will focus on connecting sensors to form a slider, wheel, and surface sensors. If the size of the sensor is larger than the users fingertip, the sensitivity is not affected, and the user can place a touch anywhere. However, a rather large sensor can create a negative effect — hand shadow — when the fingertip approaches the sensor, which can cause the proximity effect due to the coupling to the sensor[13].

Electrode Separation

The separation of the electrodes must be sufficient not to cause an unintended change in capacitance in other neighboring electrodes. This separation will affect the SVP, illustrated in Figure 2.17. In this Figure it is possible to see the geometries d) and f), which have different separations between the two electrodes. If this separation increases the distribution will be more uniform.

Sensor Designs

This subsection will focus on the connection between sensors to form a slider, wheel, and surface sensors. The sensors can be divided into groups:

- Zero-dimensional sensors: represent a single point of contact. Typical implementation is a key;

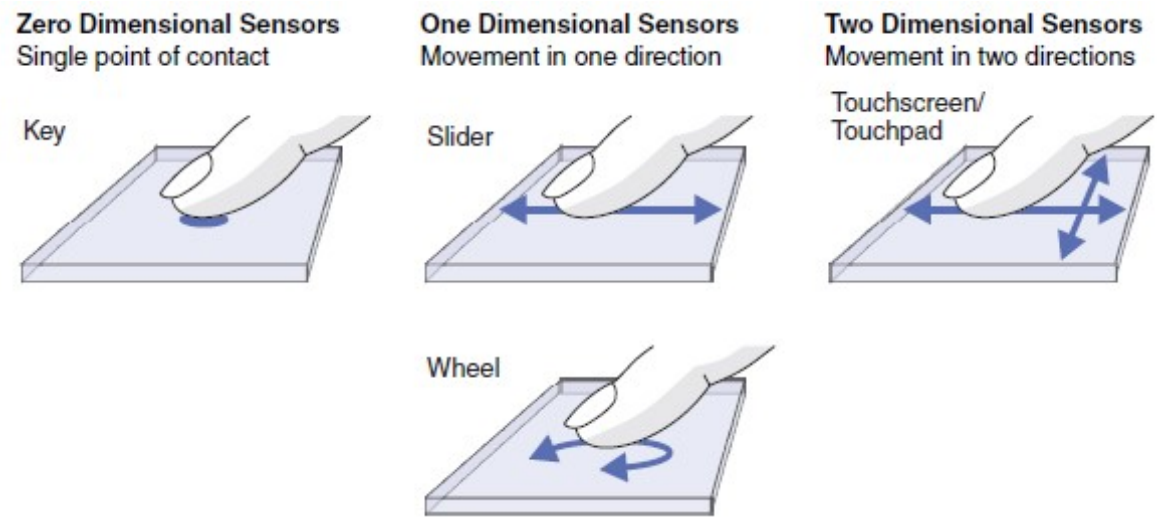

Figure 2.20: Illustration of sensors divided in categories (zero, one, and two dimensions). Source: [17].

- One-dimensional sensors: allow the detection of linear motion or a finger touch according to an axis. Typical implementations are sliders or wheels;

- Two-dimensional sensors: allow the motion detection or a finger touch according to two axes. Typical implementations are touch screens or touchpads.

These categories can be seen in Figure 2.20.

The sensor is composed of two or more sensors together. The difference between them is the arrangement of the X and Y electrodes placed in separate parts of the PCB layer. The geometry arrangement can be divided into interdigitated, flooded and resistive interpolation X to form the three sensors (selector, wheel and surface).

Interdigitated sensors can be used to determine the position of touch contact using spatial interpolation between the sensors. They can use X and Y electrodes on the same layer or separate them into different layers, where X is located in the furthest layer from the top surface. With interdigitated geometry the strongest touch delta is achieved.

Flooded X is used to improve the linearity of X electrodes because these are located on a separate layer. Also it can use spatial interpolation without complex routing around Y.

Resistive interpolation is applied to the interdigitated or flooded X layout to reduce the number of sensor node measurements. It has the advantages that it maintains linearity due to the resistive interpolation. It is used in sensors such as sliders and wheels.

Surface sensors are a little different. They can use interdigitated sliders extended to two dimensions to form the interdigitated surface, and also can use flooded X layouts [13].

Shielding

Shielding is very relevant for touch sensors. It aims at protecting the sensor against incorrect activation caused by EMI, external noise, or in the case when it is touched in parts that are not to be touch sensitive. Mutual capacitance can be isolated with the passive shield.

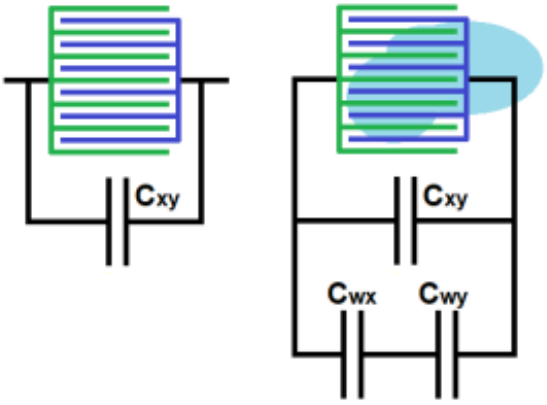

Figure 2.21: Illustration of moisture droplets and coupling created. Source: [13].

Passive shield is usually connected to the DC ground. There exist two types of passive shields to apply to the mutual capacitance sensors:

- Rear ground shield is used to prevent touch or EMI occuring from behind;
- Coplanar ground shield to provide better isolation of touch sensors.

The rear ground shield directly connects the ground plane to the circuit ground at a single point. It can be used to shield an electrode on the back to prevent false detection or to prevent interference from the power driver circuitry or switching signals. However it can reduce the sensitivity of the touch sensors significantly, and this must be taken into consideration [13].

The coplanar ground shield is implemented to reduce EMI, improve isolation between the touch sensors and reduce common mode noise effects [13].

The **moisture droplets** may be used to isolate the sensor node to not cause any accidental touch detection. With this solution, the droplets increase the X-Y coupling (form a capacitance between the water and X electrode denominated as C_{wx} and other capacitance between the water and Y electrode denominated as C_{wy}). Figure 2.21 shown the coupling formed when applied the moisture droplets [13]. Can be used in applications such as: E-locks, car access keypads, thermostats, amongst others. Common applications include exterior/interior security panels, E-locks, thermostats, and car access keypads. Whether moisture tolerance is feasible depends on the mechanical design and the environment [47].

2.5 Electromagnetic Compatibility and Electromagnetic Interference Problems and Concerns

According to the [58] Electromagnetic Compatibility EMC means "the ability of equipment to function satisfactorily in its electromagnetic environment without introducing intolerable electromagnetic disturbances to their equipment in that environment" or in other words "It's the capacity of the systems to operate in an electromagnetic environment with a defined margin of safety and design levels or performance without suffering or causing degradation as a result of electromagnetic interference" [59].

According to the [60] Electromagnetic Interference EMI is "a disturbance that affects an electrical circuit due to either electromagnetic conduction or electromagnetic radiation emitted from an external source".

The sources that cause EMI can be categorized into (adapted from [60]):

- Incidental interference: the device cannot distinguish the desired signal due to another strong signal (this raises questions when designing the circuit and in circuit shielding requirements);
- External noise: noise provided from external sources (electromagnetic or electrical sources);
- Intermodulation distortion: occurs when two or more signals are passed through a non-linear system;
- Spurious Emissions: signals that are outside of the prescribed frequency band of a transceiver;
- Adjacent Channel Interference: caused by receiving a strong signal at a frequency close to the selected signal;
- Environmental Interference: caused by environmental radiation that can interfere with operation and effectiveness of electronic systems;
- Band Congestion: Overcrowding of frequency bands, transmitter and receiver design can cause significant interference to devices operating on nearby or shared frequencies;
- Intentional Interference (Jamming): intentional emission of energy to cause noise or interference in others devices (for example, to prevent people and vehicles from being tracked in a limited area).

The effects of EMI can be categorize into [60]:

- Disruptive effects: happen when a transient enters the equipment by inductive coupling (either over data or power lines);
- Dissipative effects: due to the materials used to manufacture the Integrated Circuits (IC) they can withstand a repeated number of power surges, however, in the long run, such surges will eventually degrade the components and may result in an inoperative device;
- Destructive effects: conditions with high energy levels that cause the equipment to fail immediately.

Inside an automobile the EMC effects and stresses are related to Electrostatic Discharge (ESD), Electrical Fast Transient (EFT), surge or automotive transient [61]. The ESD is an abrupt transferring of electrostatic charge between bodies that have different potentials when brought in direct contact. A good example of ESD is HBM which transfers electrostatic charge from the human body via a series resistor to an object. The EFT is applied across the electrical lines and I/O ports of a car, due to the very fast burst of pulses generated by commutated circuits. The surge transient is caused by commutation or lightning transients. The surge pulse energy can have high energy levels that can be three or four times higher than the EFT or ESD [61].

Other interference can be caused by radio frequencies presented in the next subsection.

Available frequencies		
Frequencies (MHz)	Application	Ref.
40,66 - 40,7	ISM	32*
433,05 - 434,79	ISM	43*
28 - 29,7	AM	29*
144 - 145,8	AM	35*
430 – 432	AM	43*
430 - 435	AM	43*
438 - 440	AM	43*
1240 – 1300	AM	49*

* The page number corresponds to reference [23].

Table 2.3: Overview of the radio frequency spectrum of frequencies that do not require a license in order not to pollute the spectrum. Frequency sources of [23].

2.5.1 Radio Frequency Spectrum Overview

Regarding the EMC and EMI it is important to take into consideration the available RF spectrum in order not to interfere and pollute it, and it is also necessary to choose the frequencies that do not need a license in order not to have any problems with regulatory authorities. According to the [23] table for RF spectrum in Portugal, and recurring to [62] the frequencies that are available without a license are frequencies for Industrial, Scientific and Medical applications (ISM), and frequencies for amateur (AM).
Table 2.3 are shown the frequencies available for ISM and AM that can be used on the calculation, simulation, and practical part of this dissertation.

2.6 Final Remarks

In this chapter, an overview of the state of the art related to AM technologies, the techniques that can be used in touch sensors, and the concepts concerning EMC and EMI applied to such sensors have been presented.

The Printed Electronics section gives an overview of additive manufacturing technologies, their advantages, disadvantages, and under what circumstances they can be used. Inkjet printing is a process that has good lateral resolution, about $50\mu m$, and good layer resolution, about $0.3 - 20\mu m$, despite the low speeds it achieves. This process can be used because it can achieve good results and the machine to print on is more affordable than others.

The section on Types of Measurements in Touch Sensors gives some methods for measuring values, capacitance changes, or resonant frequency changes, in touch sensors. Self and mutual capacitance methods can be used to measure the capacitance and the change in capacitance when a finger is placed. Using resonant circuits it is possible to detect the resonant frequency and the changes in it when a finger is placed. The latter method is better because it does not depend only on the capacitance coupling, like self and mutual capacitance methods, but it depends also on the interplay of the capacitance and the inductance.

The section on Designing a Capacitive Touch Sensor provides the types of capacitive structures and some designs and fixes needed to realize a better capacitive touch sensor, with

the strongest touch delta, better noise tolerance, and so on. The geometry with IDE can be beneficial in order to optimize the length of parallel electrodes.

Electromagnetic Compatibility and Electromagnetic Interference Problems and Concerns is a section devoted to introducing these concepts to illustrate the sources and effects EMC and EMI. It also provides an overview of the radio spectrum and the frequencies that do not require a license not to interfere with the radio spectrum.

Chapter 3

Calculations

This chapter aims to explain the methods used in calculations and their implementation to obtain an analytical model for a touch sensor, with the knowledge of what already exists today. It also illustrates the results from the obtained calculations, as well as their analysis and discussion.

3.1 Analytical Models

In this section, the models presented in the State of the Art chapter are explained in more detail to obtain the analytical model for capacitive and inductive structures.

3.1.1 Analytical Models - Capacitive structure

As demonstrated in the State of the Art chapter, there are different approaches to electrode placement: spiral, serpentine, interdigitated, amongst others. However, the geometry that we followed was IDE, in order to optimize the length between the parallel electrodes, and due to their good sensitivity.

The other approach adopted to calculate the analytical model was PCT, due to its simplicity when compared to other approaches, and the good results that this approach can achieve.

Beginning by explaining the process of obtaining the analytic capability model. The process followed was explored in [15]. To begin, it is important to understand Figure 2.12. Using the electric network analysis to evaluate the equivalent circuit it is possible to reach some conclusions:

- The C_I of one electrode and the neighboring electrode are connected in series. According to the equation for calculating series capacitors 3.1, since the C_I between the electrodes are equal, we get the $C_I/2$;

- The situation when the interior capacitor and exterior capacitor are in series is obtained by 3.1, and is given by $(C_I C_E)/(C_I + C_E)$;

$$C_{eq} = \frac{C_1 C_2}{C_1 + C_2} = C_1/2(if C_1 = C_2) \tag{3.1}$$

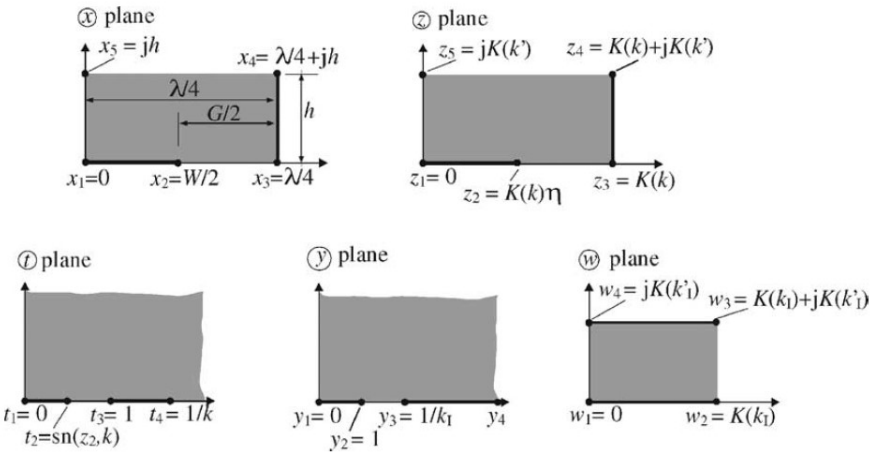

Figure 3.1: Transformations used to calculate $C_{Interior}$. The solid lines are the fixed equipotential lines and their transformations, and the gray regions are the dielectrics. Source: [15].

The equation for the total capacitance in an array of N electrodes, is given by 3.2:

$$C = (N-3)\frac{C_I}{2} + 2\frac{C_I C_E}{C_I + C_E} \tag{3.2}$$

For this equation to work properly, the number of electrodes must be greater than 3.

From the Figure 2.13 formula 3.3 can be obtained, which consists of summing each partial capacitance layer to obtain the total capacitance of the upper half plane.

$$C_{total-Upper} = C_{h\,\inf} + (\epsilon_1 - 1)C_{h1} + (\epsilon_2 - \epsilon_1)C_{h2} \tag{3.3}$$

Where ϵ_1 and ϵ_2 are the relative dielectric constants that correspond to layer 1 and layer 2, ϵ_{air} is the relative dielectric constant of air, Ch is the geometric capacitance, which depends on the height h (the subindex $h1$ corresponds to the height of layer 1, the $h2$ corresponds to the height of layer 2, and h_{inf} corresponds to an infinite air layer).

Interior Capacitance

The next process is to obtain the formula to calculate the half capacitance between the interior and the ground potential. The conformal mapping technique is used to transform the existing area into a rectangular area with known dimensions, Figure 3.1. The transformation shown in Figure 3.1 must conform with the equation 3.4, given by:

$$4r = \frac{K(k')}{K(k)} \tag{3.4}$$

Where r is:

$$r = \frac{h}{\lambda} \tag{3.5}$$

The $K(k')$ is the elliptic integral of the first kind with modulus k, and k' is the complementary modulus.

$$k = \left(\frac{v2(0,q)}{v3(0,q)}\right)^2 \tag{3.6}$$

$$k' = \sqrt{1 - k^2} \tag{3.7}$$

Where $v2$ and $v3$ are the Jacobi theta functions,[63, 64], where q is:

$$q = \exp\left(-\pi \frac{K(k')}{K(k)}\right) = \exp(-4\pi r) \tag{3.8}$$

In this part it is necessary to do 3 transformations using figure 3.1. Firstly, we transform the plane x into the plane z with the formula 3.9, and secondly, we transform the rectangle of the plane z into the plane t with the formula 3.10.

$$z = \frac{4K(k)}{\lambda} x \tag{3.9}$$

$$t = \mathrm{sn}(z, k) \tag{3.10}$$

Where $sn(z, k)$ is the Jacobi elliptic function [63, 64] of modulus k.

The last transformation occurs in the transformation of the first quadrant of the t plane into the first quadrant of the y plane, obtaining the following equation 3.11:

$$y = \frac{t}{t_2} \sqrt{\frac{t_4^2 - t_2^2}{t_4^2 - t^2}} \tag{3.11}$$

where the variables t_2 and t_4 are shown in Figure 3.1.

With these transformations the dimensions of the w plane are now known and it is possible to calculate the capacitance of the interior electrodes in the x plane directly 3.12:

$$C_I = \epsilon_0 \epsilon_r L \frac{K(k_I)}{K(k_I')} \tag{3.12}$$

External Capacitance

The following transformations and formulas are needed to obtain the external capacitance of the electrodes. Starting with the map transformations for $C_{Exterior}$ shown in Figure 3.2, starting with the x plane. This has the right side extended to the semi-infinite strip. To map this semi-infinite strip to the t plane it is necessary to use the following equation 3.13:

$$t = \cosh \frac{\pi}{2h} x \tag{3.13}$$

The t plane is then mapped into the y plane using the following equation 3.14:

$$y = t \sqrt{\frac{t_4^2 - 1}{t_4^2 - t^2}} \tag{3.14}$$

To transform the y plane into the w plane we need to use the Schwarz-Christoffel transformation [65]. It will map the quadrant y plane into the rectangle in w plane.

$$w = \int_0^y \frac{dw'}{\sqrt{(1 - w'^2)(1 - k_E w'^2)}} \tag{3.15}$$

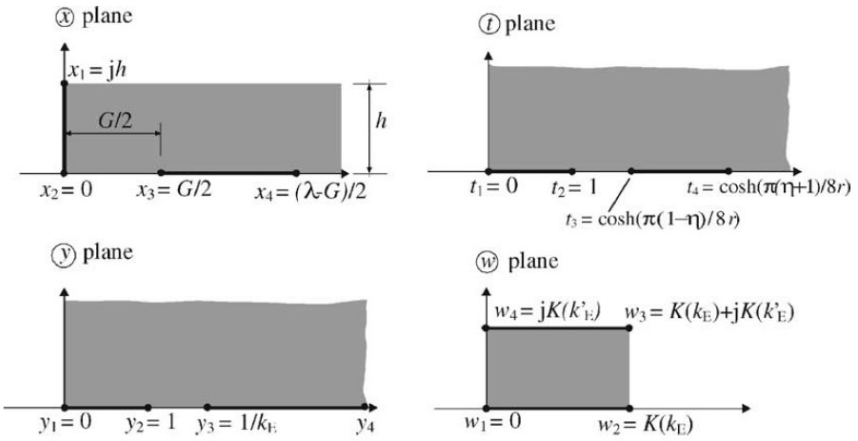

Figure 3.2: Transformations used to calculate $C_{Exterior}$. The solid lines are the fixed equipotential lines and their transformations, and the gray regions are the dielectrics. Source: [15].

---

where k_E is given by the following equation 3.16:

$$k_E = \frac{1}{t_3}\sqrt{\frac{t_4^2 - t_3^2}{t_4^2 - 1}} \tag{3.16}$$

With these equations 3.13, 3.15, and 3.16 it is possible to map a semi-infinite strip (x plane) to a rectangular region (w plane). Using the dimensions of the w plane it is possible to obtain the exterior capacitance ($C_{Exterior}$) over the x plane using the following equation 3.17:

$$C_{Exterior} = \epsilon_0 \epsilon_r L \frac{K(k_E)}{K(k'_E)} \tag{3.17}$$

Looking at equation 3.3, what follows are the boundary cases for the infinite height layer. The infinite height layers correspond to $h \to \infty$, and consequently $r \to \infty$ (3.5). Thus, it is possible to calculate the limits of k_I and k_E as the thickness tends to infinity (∞).

$$\lim_{h\to\infty} k_I = K_{I\infty} = \sin\frac{\pi}{2}\eta \tag{3.18}$$

Total capacitance

With all the above equations it is possible to calculate the total interior capacitance ($C_{Interior}$):

$$C_{Interior} = C_{I_{air}} + C_{I_1} + C_{I_2} = \epsilon_0 L \left(\frac{K(k_{I\infty})}{K(k'_{I\infty})} + (\epsilon_1 - 1)\frac{K(k_{I_1})}{K(k'_{I_1})} + \epsilon_2 \frac{K(k_{I_2})}{K(k'_{I_2})} \right) \tag{3.19}$$

and the total exterior capacitance ($C_{Exterior}$):

$$C_{Exterior} = C_{E_{air}} + C_{E_1} + C_{E_2} = \epsilon_0 L \left(\frac{K(k_{E\infty})}{K(k'_{E\infty})} + (\epsilon_1 - 1)\frac{K(k_{E_1})}{K(k'_{E_1})} + \epsilon_2 \frac{K(k_{E_2})}{K(k'_{E_2})} \right) \tag{3.20}$$

where E_1 and E_2 correspond to layer 1 and layer 2, respectively.

	Interior electrodes	Exterior electrodes
Finite layer	$C_{\mathrm{I}} = \varepsilon_0 \varepsilon_{\mathrm{r}} \dfrac{K(k_{\mathrm{I}})}{K(k'_{\mathrm{I}})}$	$C_{\mathrm{E}} = \varepsilon_0 \varepsilon_{\mathrm{r}} \dfrac{K(k_{\mathrm{E}})}{K(k'_{\mathrm{E}})}$
	$k'_{\mathrm{I}} = \sqrt{1 - k_{\mathrm{I}}^2}$	$k'_{\mathrm{E}} = \sqrt{1 - k_{\mathrm{E}}^2}$
	$k_{\mathrm{I}} = t_2 \sqrt{\dfrac{t_4^2 - 1}{t_4^2 - t_2^2}}$	$k_{\mathrm{E}} = \dfrac{1}{t_3} \sqrt{\dfrac{t_4^2 - t_3^2}{t_4^2 - 1}}$
	$t_2 = \mathrm{sn}(K(k)\eta, k)$	$t_3 = \cos h \left(\dfrac{\pi(1-\eta)}{8r} \right)$
	$t_4 = \dfrac{1}{k}$	$t_4 = \cos h \left(\dfrac{\pi\,(\eta+1)}{8r} \right)$
	$k = \left(\dfrac{v_2(0,q)}{v_3(0,q)} \right)^2$	
	$q = \exp(-4\pi r)$	
Infinite layer	$C_I = \varepsilon_0 \varepsilon_{\mathrm{r}} \dfrac{K(k_{\mathrm{I}\infty})}{K(k'_{\mathrm{I}\infty})}$	$C_{\mathrm{E}} = \varepsilon_0 \varepsilon_{\mathrm{r}} \dfrac{K(k_{\mathrm{E}\infty})}{K(k'_{\mathrm{E}\infty})}$
	$k_{\mathrm{I}\infty} = \sin \left(\dfrac{\pi}{2} \eta \right)$	$k_{\mathrm{E}\infty} = \dfrac{2\sqrt{\eta}}{1+\eta}$

Figure 3.3: Equations detailed to calculate $C_{Interior}$ and $C_{exterior}$ for finite and infinite layers. Source: [15].

Finally, the total capacitance for IDE geometry is given by the following equation 3.2:

$$C_{IDC} = (N-3)\frac{C_{Interior}}{2} + 2\frac{C_{Interior}C_{Exterior}}{C_{Interior} + C_{Exterior}} \tag{3.21}$$

Equations overview

Figure 3.3 summarizes the main equations categorized by finite and infinite layers, and interior and exterior electrodes.

3.1.2 Analytical Models - Inductive structure

As demonstrated in the State of the Art chapter, there are different approaches to calculate the inductance. The selected method was to calculate the inductance using the Mean Distance Method. The equations were followed from [18].

Starting by introducing the equations to calculate the three types of distance used to obtain the Inductance. The equation to obtain GMD is 3.22:

$$L_{gmd} = \frac{\mu n^2 d_{avg} c_1}{2} \left[\ln \frac{c_2}{\rho} + c_3 \rho + c_4 \rho^2 \right] \tag{3.22}$$

where the $c1$ and $c2$ are the coefficients for different geometries, presented on 3.1:

Available coefficients				
Layout	c_1	c_2	c_3	c_4
Square	1.09	2.23	0.00	0.17
Hexagonal	1.09	2.23	0.00	0.17
Octagonal	1.07	2.29	0.00	0.19
Circle	1.00	2.46	0.00	0.20

Table 3.1: Coefficients (c_1, c_2, c_3, and c_4) for different layouts. Source: [24].

The formula to obtain AMSD is 3.23:

$$AMSD_L^2 = \frac{1}{N^2}\sum_{i=1}^{N}\sum_{j=1}^{N}\frac{1}{A^2}\int_{A_i}\int_{A_j}\delta_{i,j}^2\,dA_j\,dA_i \tag{3.23}$$

where $\delta_{i,j}$ is the distance between one integration point located in the rectangle A_i, and the other outside the rectangle A_j. The sum can be distributed into two parts for different cases (when the two integration points are in the same rectangle or different ones). The result is given by the equation 3.24:

$$AMSD_L^2 = \frac{1}{N^2}\left[N\cdot AMSD_1^2 + 2\sum_{k=1}^{N-1}(N-k)AMSD_2^2(kw)\right] \tag{3.24}$$

The formula to obtain AMD is 3.25:

$$AMD_L^2 = \frac{1}{N^2}\sum_{i=1}^{N}\sum_{j=1}^{N}\frac{1}{A^2}\int_{A_i}\int_{A_j}\delta_{i,j}^2\,dA_j\,dA_i \tag{3.25}$$

Similarly, the equation 3.23 of AMD can be distributed into two parts resulting in the following equation 3.26:

$$AMD_L^2 = \frac{1}{N^2}\left[N\cdot AMD_1 + 2\sum_{k=1}^{N-1}(N-k)AMD_2^2(kw)\right] \tag{3.26}$$

The auxiliary equations to obtain the $AMSD_1$, $AMSD_1$, AMD_1, and AMD_2 are in Appendix, section 7.2.2.

According to the method of mean distances, and the equations 3.22, 3.23, 3.25 it is possible to obtain the partial self inductances given by the following equation 3.27:

$$L_x = \frac{\mu_0 x}{2\pi}\left[\log\left(\sqrt{x^2+AMSD_L^2}+x\right) - \log(GMD_L) - \sqrt{1+\left(\frac{AMSD_L^2}{x}\right)^2} + \frac{AMD_L}{x}\right] \tag{3.27}$$

where μ_0 is the magnetic permeability of vacuum ($\mu_0 = 4\pi\cdot 10^{-7}$), x is $x = a, b$ used to obtain the partial self inductance of La and Lb of the length sides a and b [18].

After obtaining the partial self inductance it is necessary to calculate the mutual inductance. According to the method of mean distances and the equations 3.32, 3.31, and 3.30 it

is possible to obtain the partial mutual inductance, given by the equation 3.28:

$$M_x = \frac{\mu_0 x}{2\pi}\left[\log\left(\sqrt{x^2 + AMSD_{x'}^2} + x\right) - \log(GMD_{x'}) - \sqrt{1 + \left(\frac{AMSD_{x'}^2}{x}\right)^2} + \frac{AMD_L}{x'}\right] \tag{3.28}$$

Where:

- $x = a, b$;
- $x' = b, a$.

To obtain the equation for GMD of x':

$$\log GMD_{x'} = \frac{1}{N^2}\sum_{i=1}^{N}\sum_{j=N+1}^{2N}\frac{1}{A^2}\int_{A_i}\int_{A_j}\log\delta_{i,j}\,dA_j\,dA_i \tag{3.29}$$

The double sum is transformed into:

$$\log GMD_{x'} = \frac{1}{N^2}\left[\sum_{k=-(N-1)}^{N-1}(N-|k|)\log(GMD_2(x'+kw))\right] \tag{3.30}$$

where for each value of k are $(N-|k|)$ pairs of rectangles of mutual displacement $x'+kw$, and x' is b, a. To obtain the equation AMSD of x':

$$AMSD_{x'}^2 = \frac{1}{N^2}\left[\sum_{k=-(N-1)}^{N-1}(N-|k|)(x'+kw)^2\right] \tag{3.31}$$

and to obtain the equation AMD of x':

$$AMD_{x'} = \frac{1}{N^2}\left[\sum_{k=-(N-1)}^{N-1}(N-|k|)(x'+kw)\right] \tag{3.32}$$

Using the equations 3.28, and 3.27 it is possible to obtain the final equation in order to obtain the total inductance of a single turn coil 3.33:

$$L = 2N^2[L_a + L_b - (M_a + M_b)] \tag{3.33}$$

where N^2 is to take into account the number of turns.

3.1.3 Analytical Models - Structure overview

The final analytical models are formed by considering two important structures: a capacitor and an inductor.

Figure 3.4 shows the parameters used to obtain the Capacitance. where the parameters are:

- W is the width of the electrodes;

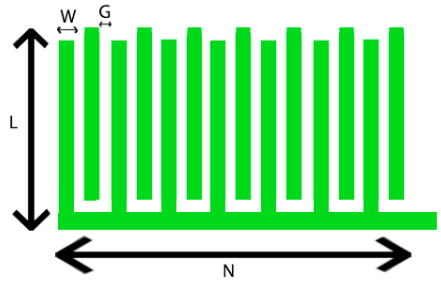

Figure 3.4: Parameters and dimensions to obtain the Capacitance.

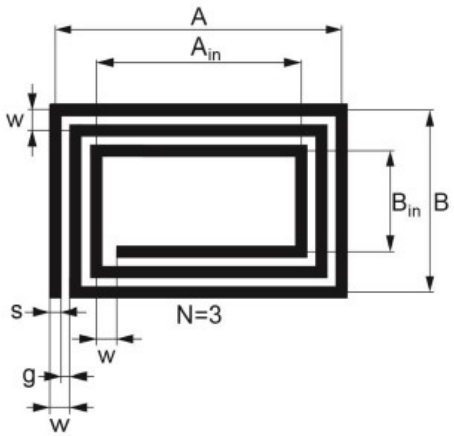

Figure 3.5: Parameters and dimensions of the planar spiral coil. Source: [18].

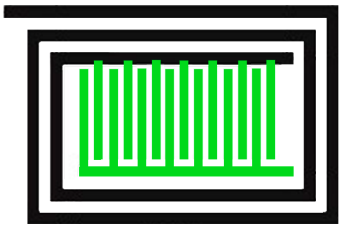

Figure 3.6: Illustration of 2D structure from analytical models.

- G is the gap between two electrodes;
- N is the number of electrodes;
- L is the length of each electrode.

Figure 3.5 shows the parameters used to obtain the inductance, where the parameters are:

- A is the length of the longer loop, from the middle of the conductors;
- A_{in} is the length of the shorter loop, from the middle of the conductors;
- B is the width of the longer loop, from the middle of the conductors;
- B_{in} is the width of the shorter loop, from the middle of the conductors;
- w is the winding distance ($w = s + g$);
- s is the conductor width;
- g is the gap between the conductors;
- N is the number of loops (in this case the loops are 3).

Figure 3.6 shows an example of a 2D geometry of the final structure, with the capacitive structure (shown in green) interconnected with the inductive structure (shown in black).

The following section provides information on implementing capacitive, and inductive structures in MATLAB®.

3.2 Implementations

The purpose of this section is to explain the procedures that we followed to implement the analytical models of the capacitive and inductive structures in MATLAB®.

We developed a function, shown in section 7.4, to make the capacitance calculations more flexible, and to automate many calculations. The function requires the input parameters listed below, and as the outputs it returns the electric characteristics. Thus, it will open up a wide range of possibilities to calculate any capacitance of any structure easily and quickly. The capacitance function inputs are:

- substrate height (h_s);
- electrode width (W_C);

- electrode gap (G_C);
- number of electrodes ($Nfingers$);
- relative permittivity 1 ($\varepsilon_{1,r}$);
- relative permittivity of the substrate ($\varepsilon_{s,r}$);
- length of the electrodes (L);
- Option parameter;

The relative permittivity 1 can be the relative permittivity of the finger, which is used to calculate the capacitance when a finger is placed on the sensor, or the relative permittivity of the air to calculate the capacitance without a finger. We implemented option parameters to select which scenario we want to use accordingly to this list:

- Option parameter 0 - scenario without finger and without the protective layer;
- Option parameter 1 - scenario with finger placed on the protective layer;
- Option parameter 2 - scenario with finger and without the protective layer;
- Option parameter 3 - scenario just with protective layer.

The capacitance function outputs are:

- the capacitance (C);
- the metallization (η) provided by $\eta = \frac{2W_C}{\lambda}$ (with $\lambda = 2(W_C + G_C)$);
- r give by equation 3.5.

The inductance calculations were also implemented as a function, and the code was taken from [18]. The inductance function inputs are:

- the number of loops (N);
- the length of the longest loop (A);
- the width of the longest loop (B);
- the winding distance (w);
- the conductor width (s);
- the height (h_s).

The output of the function is the inductance.

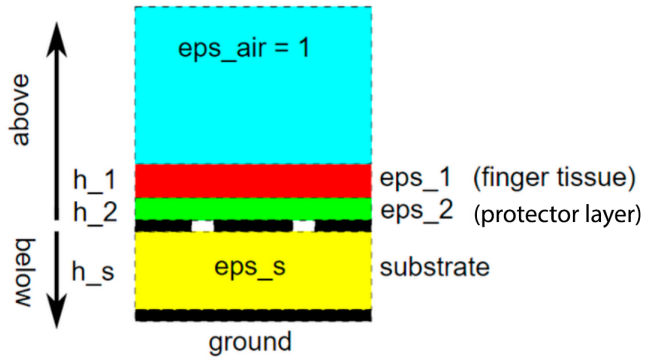

Figure 3.7: 2D side view with three layers.

3.2.1 Methods to adjust the Partial Capacitance Technique

After concluding the capacitance calculations for two layers, we implemented a three-layer method using the PCT for the cases when a finger is placed on the sensors. The three layers are:

- Substrate layer with a height of h_S and a relative permittivity of eps_s;
- Protective layer with a height of h_2 and a relative permittivity of eps_2;
- Finger layer with a height of h_1 and a relative permittivity of eps_1.

The protective layer is used to protect the sensors from corrosion and degradation over time, as well as electric problems. Figure 3.7 shows the 2D side view. The capacitance equation with these three layers is:

$$C = C_\infty + (\epsilon_1 - 1)C_{h1+h2} + (\epsilon_2 - \epsilon_1)C_{h2} + \epsilon_s C_{hs} \tag{3.34}$$

With this method we achieved some bad values of interior capacitance. Some parts of the interior capacitance equation had values close to 0. For this reason, we decided to implement another method. The new method consists of replacing the three layers by two layers, using the effective relative permittivity ($\epsilon_{effective}$) given by:

$$\epsilon_{effective} = \frac{h_1 + h_2}{(\frac{h_1}{\epsilon_{1_r}} + \frac{h_2}{\epsilon_{2_r}})} \tag{3.35}$$

As shown on Figure 3.8. With the second method the capacitance is given by the equation:

$$C = C_\infty + (\epsilon_{effective} - 1)C_{heffective} + \epsilon_s C_{hs} \tag{3.36}$$

where the thickness of the effective layer is given by $h_{effective} = h_1 + h_2$.

The results with three layers (method 1) and with two layers (method 2) are shown in Figure 3.9.

Figure 3.9 shows much lower values of interior and exterior capacitance in method 1 when compared to method 2. This is caused by the high value of relative permittivity of the human finger tissue above a layer with small permittivity. This is one of the problems of PCT,

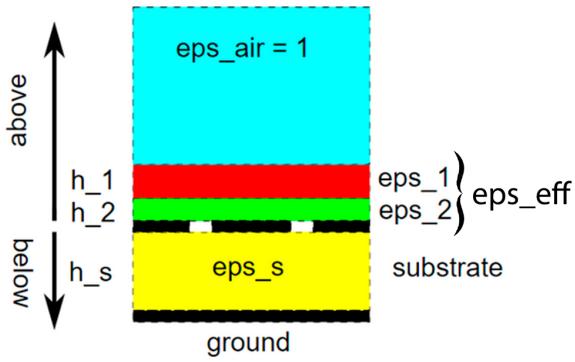

Figure 3.8: 2D side view with three layers divided in two by the effective relative permittivity.

Electrodes width and gap	Ci from method 1	Ci from method 2	Ce from method 1	Ce from method 2
0.0003	6.5787e-13	1.4768e-12	1.1068e-12	2.2231e-12
0.00031	6.5008e-13	1.4691e-12	1.1146e-12	2.216e-12
0.00032	6.4268e-13	1.4617e-12	1.1233e-12	2.2094e-12
0.00033	6.3564e-13	1.4548e-12	1.1327e-12	2.203e-12
0.00034	6.2894e-13	1.4482e-12	1.1428e-12	2.1971e-12
0.00035	6.2254e-13	1.4419e-12	1.1537e-12	2.1914e-12
0.00036	6.1643e-13	1.4359e-12	1.1652e-12	2.1859e-12
0.00037	6.1057e-13	1.4303e-12	1.1774e-12	2.1808e-12
0.00038	6.0494e-13	1.4249e-12	1.1903e-12	2.1759e-12
0.00039	5.9952e-13	1.4197e-12	1.2037e-12	2.1712e-12
0.0004	5.943e-13	1.4148e-12	1.2177e-12	2.1667e-12
0.00041	5.8924e-13	1.4101e-12	1.2323e-12	2.1624e-12
0.00042	5.8434e-13	1.4056e-12	1.2475e-12	2.1583e-12
0.00043	5.7957e-13	1.4013e-12	1.2632e-12	2.1543e-12
0.00044	5.7492e-13	1.3972e-12	1.2793e-12	2.1505e-12
0.00045	5.7037e-13	1.3932e-12	1.296e-12	2.1469e-12
0.00046	5.6592e-13	1.3894e-12	1.3132e-12	2.1434e-12
0.00047	5.6154e-13	1.3857e-12	1.3308e-12	2.14e-12
0.00048	5.5723e-13	1.3822e-12	1.3489e-12	2.1368e-12
0.00049	5.5297e-13	1.3789e-12	1.3674e-12	2.1336e-12

Figure 3.9: Comparison of $C_{interior}$ and $C_{exterior}$ in method 1 (three layers) and method 2 (two layers with effective relative permittivity) increasing the electrodes gaps and the widths.

which is only an approximate calculation technique. Therefore, we chose and implemented the effective layer method, replacing the protective layer and the finger layer by a single layer. As shown in the figure, the interior and exterior capacitance values of method 2 give better results from the physical point of view, which can help to solve the problem of PCT.

After obtaining the interior and exterior capacitance according to the equations 3.19, and 3.20, for the second method, we applied them to the total capacitance equation 3.2, in order to obtain the total capacitance according to the number of electrodes ($Nfingers$).

It is important to mention again that this three-layer method is used when a finger is placed on a sensor with a protective layer, using the the effective epsilon. If the finger is not considered, the epsilon corresponds to the layer we want, either the protective layer, or air, or just the finger.

3.2.2 Method to adjust the values when a finger is placed

A large capacitance difference was detected when we consider a finger placed on the sensor. However, in real sensors the finger does not cover the entire capacitive structure. To solve this problem, we implemented a factor that estimates how much a finger covers the capacitive structure. It is possible to take this additional factor into account by using the already calculated effective relative permittivity (regarding the method 2). Let $0 < fillingfactor \leq 1$ represent the relative area of the capacitive sensor that is touched with the finger. Then the following equation 3.37 can be used to calculate the effective permittivity of the material in proximity of the sensor, as a weighted average of the finger and air permittivities:

$$eps^*_{eff} = fillingfactor * eps_{eff} + (1 - fillingfactor) * 1; \tag{3.37}$$

The factor value was calculated considering the $8mm$ of contact diameter when touched, this value is referenced in [13]. Considering a size of $20mm$ per $20mm$ for capacitive sensor, the area is $400mm^2$. Considering the touch of the finger as a circle (with diameter $8mm$, and the radius $4mm$), the area is given by $A_{circle} = \pi r^2 = \pi 4^2 = 50.265mm^2$. Dividing the space fill by the total area, we obtained the value of the filling factor ($fillingfactor = \frac{50.265}{400} = 0.12566$).

3.2.3 Verify the capacitance values

To implement and verify the PCT methods and capacitance values from the capacitance function, five procedures were performed. The procedures were:

- Validate the values of the Jacobi theta functions;
- Compare the value of capacitance with the values of original papers;
- A plot was implemented to compare the capacitance values and the original papers, in order of metallization;
- A plot was developed to compare the capacitance values with the values of the original papers, as a function of metallization ratio to infinite air layer;
- A plot was developed to compare the capacitance values with the values of the original papers, as a function of metallization ratio to finite layer;
- A plot was developed to compare the capacitance values with the values of the original papers, as a function of ratio r to finite layer;

v2 analytical	v3 analytical	v2 add on	v3 add on
1.37061893287199e-51	1	1.37061893287199e-51	1
1.23244004162381e-37	1	1.23244004162381e-37	1
1.15982867525309e-29	1	1.15982867525309e-29	1
1.67417256964019e-24	1	1.67417256964019e-24	1
6.84517708824252e-21	1	6.84517708824252e-21	1
3.19754514382567e-18	1	3.19754514382567e-18	1
3.61597911034012e-16	1	3.61597911034012e-16	1
1.53741761418967e-14	1	1.53741761418967e-14	1
3.23594907508681e-13	1	3.23594907508681e-13	1
4.03994575829708e-12	1	4.03994575829708e-12	1
3.3856162342282e-11	1	3.38561623422819e-11	1

Figure 3.10: Results of comparison between Jacobi Theta analytical model and the MATLAB® add-on.

Second test		
Capacitance obtained	Capacitance of paper [15]	Capacitance of paper [67]
30.30476 pF	30.4 pF	27.4 pF

Table 3.2: Results of test with same parameters of original papers.

Jacobi Theta Functions

To calculate the Jacobi theta functions presented in the equations 3.6 we used a MATLAB® add-on [66]. However, to confirm the add-on results, we applied the analytical equations for $v2$ and $v3$ [63, 64] presented in Appendix, section 7.2.1. For the same parameters, the value of the width and gap of the electrodes, the results of Jacobi theta function are presented in Figure 3.10.

Capacitance value

The capacitance was calculated for the same parameters as in the original papers. The parameters were the following:

- Height of substrate : $2mm$;
- Width of electrodes : $200\mu m$;
- Gap of electrodes : $200\mu m$;
- Number of electrodes: 54;
- Relative permittivity of layer 1: 1.0006;
- Relative permittivity of substrate layer: 5.4;
- Length of electrodes: $20mm$;

. The results and the values of the original papers are presented in the table 3.2.

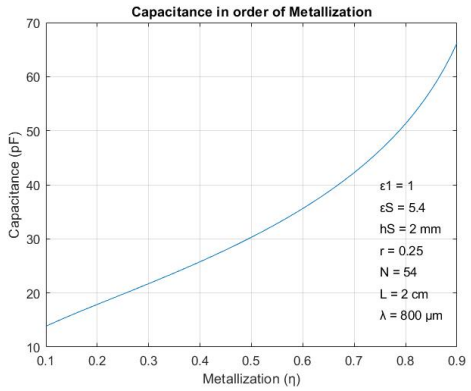

(a) Results obtained for the capacitance as a function of metallization ratio, infinite air layer.

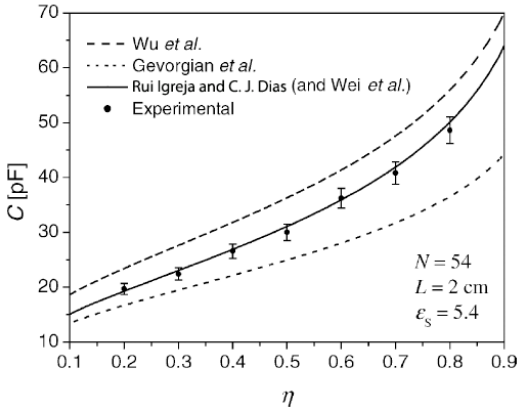

(b) Capacitance as a function of metallization ratio from the original articles, infinite air layer. Adapted: [15].

Figure 3.11: Comparison between the obtained results and the original articles.

Capacitance and metallization - infinite air layer

Several capacitance values were calculated as a function of metallization ratio (μ) for an infinite air layer ($\epsilon_1 = 1$) and then compared to the original articles. Figure 3.11 shows the results obtained.

Capacitance and metallization - finite layer

Several capacitance values were calculated as a function of metallization ratio (μ) for a finite layer above the electrodes ($\epsilon_1 = 3.15$) and then compared to the original articles. Figure 3.12 shows the results obtained.

Capacitance and ratio r - finite layer

Several capacitance values were calculated in order of ratio r (r) for a finite layer above the electrodes ($\epsilon_1 = 3.15$) and then compared to the original papers. Figure 3.13 shows the results obtained. The ratio r is the ratio between the height of the sensitive layer and the sensor wavelength, given in equation 3.5.

3.2.4 Script to obtain the desired frequencies

After implementing and verifying the PCT methods and capacitance values, using the outputs from the capacitance and inductance functions, it was possible to calculate the resonant frequency, applying the equation 2.11.

After having the functions to calculate the capacitance, inductance, and consequently the resonant frequencies, we developed a MATLAB® script to obtain the desired resonant frequencies 7.5. With the limits set for the initial parameters, the code performs all values up to that limit (for example, the minimum, and the maximum number of electrodes, the loops, amongst others). When the initial parameters change, a new resonant frequency is calculated. Once the resonant frequency is reached with a small margin (set at the beginning

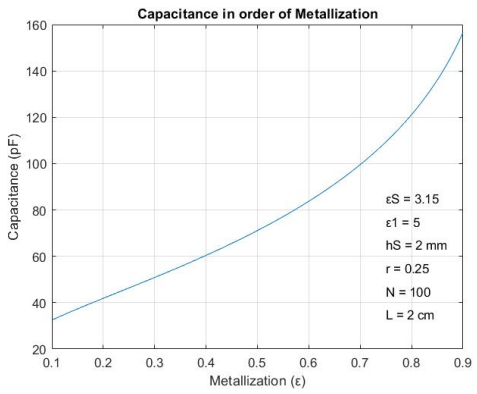

(a) Results obtained for Capacitance as a function of metallization ratio, finite layer.

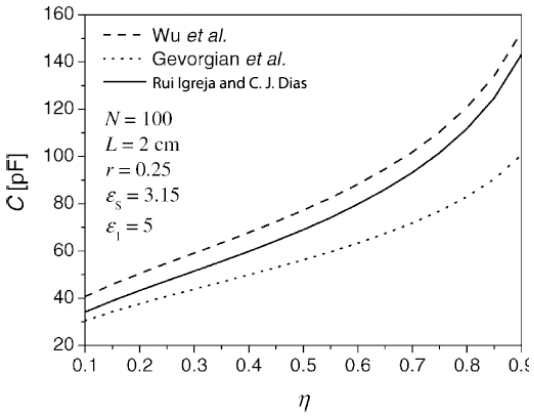

(b) Capacitance as a function metallization ratio from original papers. Adapted: [15].

Figure 3.12: Comparison between the obtained results and the original articles.

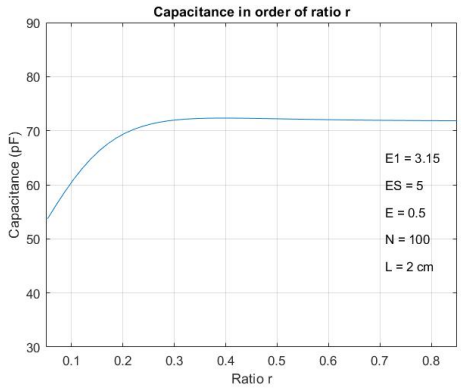

(a) Results obtained for Capacitance as a function of ratio r.

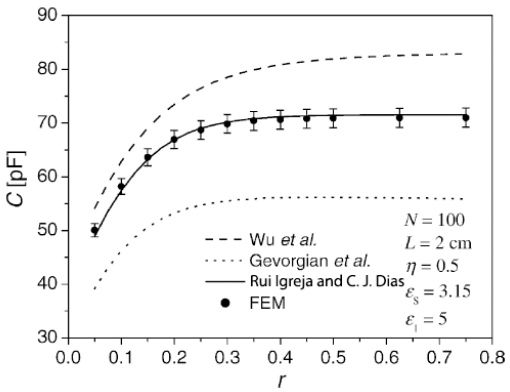

(b) Capacitance as a function of ratio r from original papers. Adapted: [15].

Figure 3.13: Comparison between the obtained results and the original articles.

of the script), the parameters are saved and the code continues to run until all parameters are covered. The changed parameters are: the number of loops ($Nloops$), the number of fingers ($Nfingers$), the capacitance width (W_C), and the relative permittivity of layer 1 ($\varepsilon_{1,r}$). Each parameter corresponds to a `for` cycle, allowing to repeat the same code for all changes to each parameter.

The inductor widths and gaps are calculated according to the remaining free space after the four variation parameters have been selected.

The size occupied so far is calculated through the space occupied by loops, widths and gaps of the inductor, and with the diameter of a track to obtain the space left for the gap between the electrodes. Thus, the calculated size can be divided by the number of electrodes, obtaining the size of each gap. If any width or gap is smaller than the minimum allowed by the PCB milling machine at IT-Aveiro, the parameters are considered invalid and the resonance frequency for these parameters is not even calculated. The minimum allowed for this machine is $0.2mm$, but we decided to use a minimum of $0.3mm$, in order not to approach the sizes too closely to the allowed minimum. The next step after obtaining the resonant frequencies on air, with $\varepsilon_{1,r}$ equal to 1, was to do the same procedure to calculate the resonant frequencies with a finger placed on the sensor, with relative permittivity $\varepsilon_{1,r} = 50$ (table with values in 7.2.3). The value of 50 corresponds to the relative permittivity value of the muscle. We chose this value because the human finger is made up of skin tissue, bone, and muscle. Muscle, and bone have the largest size compared to the skin tissue, therefore, the relative permittivity of muscle was selected.

It is important to note what frequencies we selected and used in MATLAB®. This selection was made according to the research conducted in table 2.3, and section 2.5.1. The range of frequencies per sensor were:

- First sensor with 28.00 to $29.70MHz$;
- Second sensor with 40.66 to $40.70MHz$;
- Third sensor with 144.00 to $145.80MHz$;

These frequencies were selected to increase the frequency range of the sensors and to study possible parasitic effects, and to not have closer frequencies that could result in inter-band electromagnetic interference problems, as seen in section 2.5.

With these procedures done it was possible to calculate the desired resonant frequencies, shown in the following sections.

3.3 Results

This section presents the parameters achieved in order to obtain the desired resonant frequency.

To achieve the results the parameters were:

- Relative permittivity of the protective layer (ϵ_1): 2.31 (paper layer);
- Height of the protective layer: $0.1mm$;
- Height of human finger layer: $30mm$;
- Relative permittivity of substrate layer: 3(Isola Astra);

Frequency	Freq. w/ finger and paper layer	Nloops	Nfingers	W_C	G_C	W_L	G_L
2.7754e+07	1.7781e+07	1.0000e+01	1.5000e+01	9.5000e-04	4.1400e-04	4.6000e-04	4.6000e-04
2.8210e+07	1.8074e+07	1.0000e+01	1.4000e+01	1.0500e-03	4.1143e-04	4.6000e-04	4.6000e-04
2.8150e+07	1.8033e+07	1.0000e+01	1.3000e+01	1.2000e-03	3.7385e-04	4.6000e-04	4.6000e-04
2.7650e+07	1.7706e+07	1.0000e+01	1.2000e+01	1.4000e-03	3.0500e-04	4.6000e-04	4.6000e-04

Figure 3.14: Results to achieve $28.00MHz$ with accuracy about $0.5MHz$ on Sensor 1.

Frequency	Freq. w/ finger and paper layer	Nloops	Nfingers	W_C	G_C	W_L	G_L
4.1144e+07	2.6351e+07	8.0000e+00	2.0000e+01	3.0000e-04	7.2875e-04	5.7500e-04	5.7500e-04
4.0407e+07	2.5874e+07	7.0000e+00	2.4000e+01	3.0000e-04	5.6071e-04	6.5714e-04	6.5714e-04
4.1065e+07	2.6303e+07	8.0000e+00	1.9000e+01	3.5000e-04	7.3289e-04	5.7500e-04	5.7500e-04
4.0262e+07	2.5779e+07	6.0000e+00	2.7000e+01	3.5000e-04	4.1914e-04	7.6667e-04	7.6667e-04
4.1036e+07	2.6275e+07	5.0000e+00	3.2000e+01	3.5000e-04	3.0375e-04	9.2000e-04	9.2000e-04
4.0572e+07	2.5996e+07	9.0000e+00	1.6000e+01	4.0000e-04	8.8194e-04	5.1111e-04	5.1111e-04
4.0992e+07	2.6247e+07	6.0000e+00	2.5000e+01	4.0000e-04	4.3067e-04	7.6667e-04	7.6667e-04
4.0587e+07	2.5988e+07	6.0000e+00	2.4000e+01	4.5000e-04	4.1528e-04	7.6667e-04	7.6667e-04
4.0310e+07	2.5826e+07	8.0000e+00	1.7000e+01	5.0000e-04	7.1029e-04	5.7500e-04	5.7500e-04
4.0374e+07	2.5853e+07	6.0000e+00	2.3000e+01	5.0000e-04	4.0290e-04	7.6667e-04	7.6667e-04
4.1091e+07	2.6330e+07	8.0000e+00	1.6000e+01	5.5000e-04	7.3594e-04	5.7500e-04	5.7500e-04
4.0349e+07	2.5838e+07	6.0000e+00	2.2000e+01	5.5000e-04	3.9394e-04	7.6667e-04	7.6667e-04
4.0617e+07	2.6019e+07	7.0000e+00	1.8000e+01	6.0000e-04	5.4762e-04	6.5714e-04	6.5714e-04
4.0517e+07	2.5947e+07	6.0000e+00	2.1000e+01	6.0000e-04	3.8889e-04	7.6667e-04	7.6667e-04
4.0935e+07	2.6233e+07	8.0000e+00	1.5000e+01	6.5000e-04	7.2167e-04	5.7500e-04	5.7500e-04
4.0887e+07	2.6186e+07	6.0000e+00	2.0000e+01	6.5000e-04	3.8833e-04	7.6667e-04	7.6667e-04
4.0473e+07	2.5938e+07	9.0000e+00	1.3000e+01	7.0000e-04	8.7778e-04	5.1111e-04	5.1111e-04
4.0750e+07	2.6101e+07	6.0000e+00	1.8000e+01	8.0000e-04	3.5370e-04	7.6667e-04	7.6667e-04
4.0455e+07	2.5919e+07	9.0000e+00	1.2000e+01	8.5000e-04	8.5926e-04	5.1111e-04	5.1111e-04
4.0895e+07	2.6206e+07	8.0000e+00	1.3000e+01	9.0000e-04	6.8269e-04	5.7500e-04	5.7500e-04
4.0355e+07	2.5849e+07	6.0000e+00	1.7000e+01	9.0000e-04	3.2157e-04	7.6667e-04	7.6667e-04
4.1100e+07	2.6314e+07	9.0000e+00	1.1000e+01	1.0000e-03	8.6465e-04	5.1111e-04	5.1111e-04
4.0734e+07	2.6100e+07	7.0000e+00	1.4000e+01	1.0000e-03	4.7551e-04	6.5714e-04	6.5714e-04
4.0236e+07	2.5761e+07	9.0000e+00	1.1000e+01	1.0500e-03	8.1465e-04	5.1111e-04	5.1111e-04
4.0211e+07	2.5759e+07	8.0000e+00	1.2000e+01	1.1000e-03	6.1458e-04	5.7500e-04	5.7500e-04
4.0665e+07	2.6052e+07	7.0000e+00	1.3000e+01	1.1500e-03	4.3901e-04	6.5714e-04	6.5714e-04
4.0856e+07	2.6122e+07	9.0000e+00	1.0000e+01	1.2500e-03	8.0111e-04	5.1111e-04	5.1111e-04
4.0270e+07	2.5778e+07	8.0000e+00	1.1000e+01	1.3000e-03	5.7045e-04	5.7500e-04	5.7500e-04

Figure 3.15: Results to achieve $40.66MHz$ with accuracy about $0.5MHz$ on Sensor 2.

- The thickness of substrate: $1.52mm$. We chose this value of thickness and relative permittivity from the table 7.1, Isola Astra with $1.52mm$.

- A filling factor of 0.12566, which corresponds to the estimated relative finger touch area above the capacitive structure.

The results are divided into three parts. The first part corresponds to the first values to obtain the frequencies 28, 40.66, and $144MHz$. The second and third parts result from new calculations, after seeing the results in the simulator. The second part is about the difference between the obtained and the desired resonant frequency at the third sensor. The second part discusses the interferences caused by the inductor in the first sensor.

3.3.1 Initial results

The initial results were obtained from the code (presented in section 7.5) that covered all parameter combinations and saved those that achieved the target resonant frequency with the desired accuracy. Figure 3.14 corresponds to the frequency of the first sensor, figure 3.15 corresponds to the frequency of the second sensor, and figure 3.16 corresponds to the frequency of the third sensor.

Frequency	Freq. w/ finger and paper layer	Nloops	Nfingers	W_C	G_C	W_L	G_L
1.4341e+08	8.8053e+07	6.0000e+00	5.0000e+00	5.0000e-04	3.6533e-03	7.6667e-04	7.6667e-04
1.4560e+08	9.0821e+07	5.0000e+00	6.0000e+00	5.0000e-04	2.9867e-03	9.2000e-04	9.2000e-04
1.4336e+08	9.1739e+07	3.0000e+00	1.1000e+01	5.0000e-04	1.4576e-03	1.5333e-03	1.5333e-03
1.4285e+08	8.9848e+07	4.0000e+00	7.0000e+00	8.0000e-04	2.2214e-03	1.1500e-03	1.1500e-03
1.4441e+08	9.1967e+07	3.0000e+00	9.0000e+00	9.0000e-04	1.4926e-03	1.5333e-03	1.5333e-03
1.4451e+08	8.7768e+07	5.0000e+00	5.0000e+00	1.2000e-03	2.9840e-03	9.2000e-04	9.2000e-04
1.4661e+08	9.2873e+07	3.0000e+00	8.0000e+00	1.2000e-03	1.4917e-03	1.5333e-03	1.5333e-03
1.4530e+08	9.0032e+07	4.0000e+00	6.0000e+00	1.3000e-03	2.2250e-03	1.1500e-03	1.1500e-03
1.4662e+08	9.3646e+07	2.0000e+00	1.0000e+01	1.6000e-03	6.3000e-04	2.3000e-03	2.3000e-03
1.4301e+08	8.9892e+07	3.0000e+00	7.0000e+00	1.8000e-03	1.2762e-03	1.5333e-03	1.5333e-03
1.4481e+08	8.7873e+07	4.0000e+00	5.0000e+00	2.3000e-03	1.9300e-03	1.1500e-03	1.1500e-03
1.4386e+08	9.1358e+07	2.0000e+00	8.0000e+00	2.4000e-03	3.8750e-04	2.3000e-03	2.3000e-03
1.4447e+08	8.9879e+07	3.0000e+00	6.0000e+00	2.5000e-03	1.0889e-03	1.5333e-03	1.5333e-03
1.4633e+08	9.0013e+07	3.0000e+00	5.0000e+00	3.5000e-03	8.0667e-04	1.5333e-03	1.5333e-03

Figure 3.16: Results to achieve 144.00MHz with accuracy about 2.0MHz on Sensor 3.

Frequency	Freq. w/ finger and paper layer	Nloops	Nfingers	W_C	G_C	W_L	G_L
1.6685e+08	1.0691e+08	2.0000e+00	1.7000e+01	3.0000e-04	1.0118e-03	2.3000e-03	2.3000e-03
1.6787e+08	1.0594e+08	4.0000e+00	7.0000e+00	3.5000e-04	2.6714e-03	1.1500e-03	1.1500e-03
1.6655e+08	1.0641e+08	3.0000e+00	1.0000e+01	3.5000e-04	1.8033e-03	1.5333e-03	1.5333e-03
1.6834e+08	1.0789e+08	2.0000e+00	1.6000e+01	3.5000e-04	1.0437e-03	2.3000e-03	2.3000e-03
1.6591e+08	1.0634e+08	2.0000e+00	1.5000e+01	4.5000e-04	1.0367e-03	2.3000e-03	2.3000e-03
1.6795e+08	1.0699e+08	3.0000e+00	9.0000e+00	5.0000e-04	1.8926e-03	1.5333e-03	1.5333e-03
1.6783e+08	1.0288e+08	5.0000e+00	5.0000e+00	5.5000e-04	3.6340e-03	9.2000e-04	9.2000e-04
1.6444e+08	1.0475e+08	3.0000e+00	9.0000e+00	5.5000e-04	1.8426e-03	1.5333e-03	1.5333e-03
1.6567e+08	1.0619e+08	2.0000e+00	1.4000e+01	5.5000e-04	1.0429e-03	2.3000e-03	2.3000e-03
1.6552e+08	1.0135e+08	5.0000e+00	5.0000e+00	6.0000e-04	3.5840e-03	9.2000e-04	9.2000e-04
1.6743e+08	1.0730e+08	2.0000e+00	1.3000e+01	6.5000e-04	1.0654e-03	2.3000e-03	2.3000e-03
1.6874e+08	1.0492e+08	4.0000e+00	6.0000e+00	7.0000e-04	2.8250e-03	1.1500e-03	1.1500e-03
1.6640e+08	1.0341e+08	4.0000e+00	6.0000e+00	7.5000e-04	2.7750e-03	1.1500e-03	1.1500e-03
1.6852e+08	1.0678e+08	3.0000e+00	8.0000e+00	7.5000e-04	1.9417e-03	1.5333e-03	1.5333e-03
1.6576e+08	1.0502e+08	3.0000e+00	8.0000e+00	8.0000e-04	1.8917e-03	1.5333e-03	1.5333e-03
1.6752e+08	1.0730e+08	2.0000e+00	1.2000e+01	8.0000e-04	1.0583e-03	2.3000e-03	2.3000e-03
1.6708e+08	1.0690e+08	2.0000e+00	1.1000e+01	1.0000e-03	1.0273e-03	2.3000e-03	2.3000e-03
1.6928e+08	1.0627e+08	3.0000e+00	7.0000e+00	1.1500e-03	1.9262e-03	1.5333e-03	1.5333e-03
1.6707e+08	1.0487e+08	3.0000e+00	7.0000e+00	1.2000e-03	1.8762e-03	1.5333e-03	1.5333e-03
1.6490e+08	1.0351e+08	3.0000e+00	7.0000e+00	1.2500e-03	1.8262e-03	1.5333e-03	1.5333e-03
1.6711e+08	1.0672e+08	2.0000e+00	1.0000e+01	1.2500e-03	9.8000e-04	2.3000e-03	2.3000e-03
1.6838e+08	1.0198e+08	4.0000e+00	5.0000e+00	1.5000e-03	2.7300e-03	1.1500e-03	1.1500e-03
1.6680e+08	1.0101e+08	4.0000e+00	5.0000e+00	1.5500e-03	2.6800e-03	1.1500e-03	1.1500e-03
1.6860e+08	1.0733e+08	2.0000e+00	9.0000e+00	1.5500e-03	9.2778e-04	2.3000e-03	2.3000e-03
1.6524e+08	1.0005e+08	4.0000e+00	5.0000e+00	1.6000e-03	2.6300e-03	1.1500e-03	1.1500e-03
1.6581e+08	1.0556e+08	2.0000e+00	9.0000e+00	1.6000e-03	8.7778e-04	2.3000e-03	2.3000e-03
1.6825e+08	1.0418e+08	3.0000e+00	6.0000e+00	1.8500e-03	1.7389e-03	1.5333e-03	1.5333e-03
1.6639e+08	1.0305e+08	3.0000e+00	6.0000e+00	1.9000e-03	1.6889e-03	1.5333e-03	1.5333e-03

Figure 3.17: Results to achieve 166.9MHz with accuracy of 2.0MHz on Sensor 3.

3.3.2 First approach results

The first approach results are obtained from the MATLAB® code after making the adjustments explained in more detail in Analysis and Discussion section. We adjusted the desired frequency for sensor 3 because with the initially obtained sensor parameters for the resonance at 144MHz, the simulator showed that we had not achieved this target frequency. For this reason we calculated the difference between the desired and the obtained value, adding this to the obtained result, which resulted in 166.9MHz. Figure 3.17 shows the result obtained.

3.3.3 Second approach results

The second approach results obtained from the MATLAB® code, after making the adjustments explained in more detail in Analysis and Discussion section, are shown in figure 3.18. Figure 3.18 corresponds to the frequency of the first sensor. We adjusted the parameters of sensor 1, with the objective of decreasing the parastic resonance effects in the first inductor that are close to the third sensor resonant frequency. The third sensor resonant frequency also was adjusted to correspond better to the values obtained with the simulator, because

Frequency	Freq. w/ finger and paper layer	Nloops	Nfingers	W_C	G_C	W_L	G_L
2.8325e+07	1.8166e+07	6.0000e+00	4.1000e+01	3.0000e-04	4.4024e-04	3.5000e-04	3.5000e-04
2.7757e+07	1.7802e+07	6.0000e+00	4.2000e+01	3.0000e-04	4.2262e-04	3.5000e-04	3.5000e-04
2.8019e+07	1.7970e+07	6.0000e+00	3.9000e+01	3.5000e-04	4.2821e-04	3.5000e-04	3.5000e-04
2.7912e+07	1.7902e+07	6.0000e+00	3.7000e+01	4.0000e-04	4.2027e-04	3.5000e-04	3.5000e-04
2.7997e+07	1.7958e+07	6.0000e+00	3.5000e+01	4.5000e-04	4.1714e-04	3.5000e-04	3.5000e-04
2.8276e+07	1.8138e+07	6.0000e+00	3.3000e+01	5.0000e-04	4.1970e-04	3.5000e-04	3.5000e-04
2.7891e+07	1.7892e+07	6.0000e+00	3.2000e+01	5.5000e-04	3.9844e-04	3.5000e-04	3.5000e-04
2.7588e+07	1.7699e+07	6.0000e+00	3.1000e+01	6.0000e-04	3.7903e-04	3.5000e-04	3.5000e-04
2.8340e+07	1.8184e+07	6.0000e+00	2.9000e+01	6.5000e-04	3.9655e-04	3.5000e-04	3.5000e-04
2.8257e+07	1.8132e+07	6.0000e+00	2.8000e+01	7.0000e-04	3.8393e-04	3.5000e-04	3.5000e-04
2.8262e+07	1.8137e+07	6.0000e+00	2.7000e+01	7.5000e-04	3.7407e-04	3.5000e-04	3.5000e-04
2.8358e+07	1.8200e+07	6.0000e+00	2.6000e+01	8.0000e-04	3.6731e-04	3.5000e-04	3.5000e-04
2.7809e+07	1.7851e+07	6.0000e+00	2.4000e+01	9.5000e-04	3.1458e-04	3.5000e-04	3.5000e-04
2.8238e+07	1.8128e+07	6.0000e+00	2.3000e+01	1.0000e-03	3.1957e-04	3.5000e-04	3.5000e-04

Figure 3.18: Results to achieved the $28.00MHz$ with accuracy about $0.5MHz$ on Sensor 1.

the simple LC circuit model for a sensor is not adequate at very high frequencies, because in reality all parts of the sensor have distributed LC parameters. A real inductor is made up of a series resistance, wire resistance, and a capacitor in parallel with the wire (forming a parasitic capacitance). The impedance of the inductor increases while the impedance of the parasitic capacitor decreases, when the frequency increases. When the impedance of the capacitor is less than the impedance of the inductor, the inductor behaves like a capacitor. Thus, the circuit will behave differently than expected the more the parasitic capacitance increases.

3.4 Analysis and Discussion

3.4.1 Jacobi theta function - Analysis

From **First Test** the values from the add-on [66] and the values from the analytical models 7.2.1 are almost the same. It is possible to conclude that one can use the add-on or the analytical model to calculate the Jacobi Theta function because both have good results.

3.4.2 Capacitance Comparison with original papers - Analysis

The value of capacitance achieved is quite close to Ref. [15].

From the procedure of calculating the capacitance as a function of metallization ratio for the cases of infinite air layer and finite layer the results on Figures 3.11a, 3.12a are practicality the same when compared with Ref. [15] in Figures 3.11b, and 3.12b. From the procedure of calculating the Capacitance as a function of ratio r with metallization (η) fixed to 0.5 is possible to observe that the curve of capacitance is very close as compared to Ref. [15] in Figure 3.13b. Here it is important to note that this reference does not define the specific values for the thickness of layer 1 that generates some variations in the capacitance value.

3.4.3 Results - Analysis

The achieved results are very relevant for the next section, and need more attention. In the figures it is possible to see the parameters used in the next section, Simulation. Comparing the resonant frequencies of initial results (3.14, 3.15, 3.16) with the first approach (Figure 3.17), and second approach (Figure 3.18) one can see a slight difference between them. This difference is more significant for sensor 3 (higher frequencies) and small for sensor 1 (lower frequencies). This is related with results of Simulation.

First approach - Analysis

The first approaches need some adjustment of the obtained frequency, in the case of sensor 3. The values of the resonant frequencies in the Simulation are lower. This is due to the resonant circuit model used, the simple LC oscillator model, because this model does not work so well when the frequency increases. For this reason we calculated the differences between the desired frequency and the frequency obtained in the simulator and added this value to the desired frequency in MATLAB®. Then we executed the script again and performed new simulations. Because of this, the final resonant frequency at sensor 3 is much higher ($166.9MHz$) when compared to the desired frequency ($144MHz$). This results were used to produce one simulation, and one PCB prototype.

Second approach - Analysis

The first approaches also needed an adjustment for sensor 1. This case in particular is quite different, because the frequency obtained in the simulation is the desired frequency, but the resonator has a problem with behaviour at higher frequencies. In simulation we detect that inductor itself was resonating (due to distributed parasitic capacitance) at frequencies very close to the resonant frequency of sensor 3. From this point we tried to execute the code to obtain an inductor with a smaller number of loops. Figure 3.18 shows these results. This can remove or decreases the parasitic effects and interferences that the first approach could cause in a real situation. For this reason, we simulated both approaches, and created two prototypes following from both approaches in order to study the possible effects and the interference that these approaches might cause.

3.4.4 Outcomes

From the obtained results it is possible to summarize the parameters that were used in the next Chapter. The initial results were used to create the initial structure in the next Chapter.

Using the values of sensor 1 and 2, from the initial results, and using the first approach (for sensor 3) it was possible to create a structure in the simulator, named structure 1, and with the second approach (for sensor 1), it was possible to make another structure in the simulator, as structure 2, with the objective to study the interferences caused by the inductor of sensor 1. The frequencies, and the parameters for both obtained structures are summarized in Table 3.4.

3.5 Final Remarks

The Calculations section introduces the first step in obtaining the desired frequencies. It starts with an explanation of the analytical models to obtain the theoretical equations that will be implemented in MATLAB®. To obtain the capacitance, the Partial Capacitance Technique (PCT) is used and for the inductance the Mean Distance Method is used. With the values of capacitance and the inductance it is easy to calculate the resonant frequency. To obtain the resonant frequency, the schemes, parameters and variables used to calculate the capacitance and inductance were explained. The process to obtain the parameters with the same resonant frequencies is also explained, as well as the obtained results, the definitions

Outcomes - initial structure	
Parameter	Structure with initial results
Sensors	S1 — S2 — S3
Frequency without finger $*^1$	28.32 — 40.734 — 142.85
Frequency with finger $*^1$	18.13 — 26.10 — 89.848
Number of electrodes	13 — 15 — 7
Width of capacitor $*^2$	1.2000 — 0.9000 — 0.8000
Gap of capacitor $*^2$	0.3785 — 0.4771 — 2.2114
Number of loops	10 — 7 — 4
Width of inductor $*^2$	0.4600 — 0.6571 — 1.1500
Gap of inductor $*^2$	0.4600 — 0.6571 — 1.1500

$*^1$ frequency in MHz.
$*^2$ in mm.

Table 3.3: Outcomes of Calculation chapter. The frequencies, and parameters of initial structure for each sensor (S1, S2 and S3.

Outcomes - overview		
Parameter	Structure 1	Structure 2
Sensors	S1 — S2 — S3	S1 — S2 — S3
Frequency without finger $*^1$	28.32 — 40.734 — 166.85	27.912 — 40.734 — 166.85
Frequency with finger $*^1$	18.13 — 26.10 — 106.91	17.90 — 26.10 — 106.91
Number of electrodes	25 — 14 — 17	37 — 14 — 17
Width of capacitor $*^2$	0.5000 — 1.0000 — 0.3000	0.4000 — 1.0000 — 0.3000
Gap of capacitor $*^2$	0.3230 — 0.4755 — 1.0118	0.4203 — 0.4755 — 1.0118
Number of loops	8 — 7 — 2	6 — 7 — 2
Width of inductor $*^2$	0.5750 — 0.6714 — 2.3000	0.3500 — 0.6714 — 2.3000
Gap of inductor $*^2$	0.5750 — 0.6714 — 2.3000	0.3500 — 0.6714 — 2.3000

$*^1$ frequency in MHz.
$*^2$ in mm.

Table 3.4: Outcomes of Calculation chapter. The frequencies, and parameters of structure 1 and 2 for each sensor.

of the problems, and the solution approaches that were followed. With the right parameters to obtain the desired resonant frequencies it is possible to test whether these are valid in the simulator. The simulation process will be explained in Chapter 4.

Chapter 4

Simulations

This chapter aims to explain the considered structures and their implementation to achieve a good simulation model for a touch sensor. It also illustrates the problems and solutions implemented during the simulation, and how the results of the MATLAB® code can influence the simulations, as well as the results of the simulations and their analysis and discussion. Each section of the chapter has been separated into: Macro Construction, Methods used to Simulate, and Simulations.

4.1 Implementations

4.1.1 3D Structure construction

Starting from explaining how a sensor array can be constructed for the three sensors. Figure 4.1 shows the 2D outline of a 3D model. The structure is formed by a sensor, where each sensor has a capacitor and an inductor that together will achieve a specific resonance frequency. The sensors are excited through the microstrip line coupled to the sensors through the mutual capacitance and the mutual inductance. To interrogate the sensors a VNA is used that sends a signal and measures the reflection from sensors. As an alternative to VNA for interrogating the sensors, there are two possible ways to do this: send a short voltage pulse on the microstrip line (such as a delta function pulse) and measure the reflected signal, or send signals at all 3 frequencies and measure the reflections at those frequencies. The sensors respond at the their own frequencies, more specifically the resonant frequency formed by the capacitor and the inductor. To improve the coupling between the microstrip line and the sensors the gaps between them and the width of the microstrip were changed. The gaps between the microstrip and the sensors have been reduced and the width of the microstrip increased to improve coupling. In the first case the reflected signal will have oscillations through at these three frequencies, without finger, and when the finger touches on sensors these oscillations will be dumped. The microstrip line also has the objective to transmit the signals at high speed to interrogate the sensors and to receive their response.

To simulate this implementation I used CST Studio Suite 2020 software [34] and created a macro with the Visual Basic for Applications script (VBA). I created the macro in order to create many sensor structures at once. Besides this, using a macro gives much more flexibility and automates the testing of parameters provided by MATLAB®. With this macro and the corresponding MATLAB® script, it opens up a wide range of possibilities to generate any sensor structures more easily and faster. Just change the initial parameters and the macro

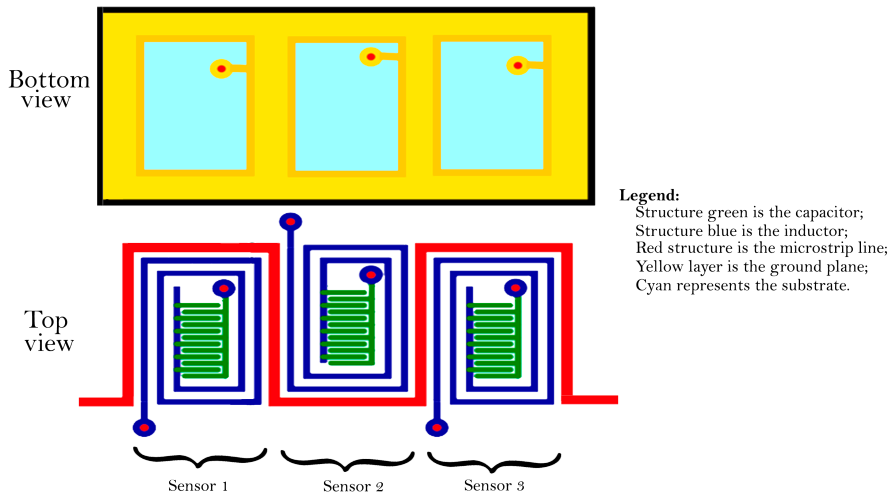

Figure 4.1: Outline of the overall structure and representation of the sensors.

---

will generate a new structure with new geometry. This implementation considers three main components of the structure: a ground plane, a microstrip line, and a sensor (formed by an inductor and a capacitor). Also it is possible to change the size of the sensors, the size of the vias (connecting the ground plane to the sensors), the number of sensors, the space from the board to the sensors, amongst others. The parameters that are not supplied by the MATLAB® script are the following:

- The width of the microstrip is: $2.5mm$;
- The outer diameter of vias is: $0.8mm$;
- The inner diameter of vias is: $0.4mm$;

These parameters cam be easily changed at the beginning of the macro file.

The microstrip width is relevant for giving the characteristic impedance of the microstrip line. Using the equations, included in section 7.3, the characteristic impedance value of the microstrip is 64.17Ω with the following characteristics:

- Relative Dielectric Constant (ϵ_r): 3 (ISOLA Astra referenced in the section 7.1);
- Track Width: $2.5mm$;
- Track Thickness: $0.035mm$ (ISOLA Astra cladding referenced in the section 7.1);
- Dielectric Thickness: $1.52mm$ (ISOLA Astra thickness referenced in the section 7.1).

4.1.2 Process and materials used to simulate

After concluding writing the macro, the next step was to simulate several structures with different geometrical parameters to obtain the S-parameters. These parameters are measured in terms of power (magnitude (dB)). The relation between the incident and the reflected power waves and the S-parameter matrix is [68]:

$$\begin{pmatrix} b1 \\ b2 \end{pmatrix} = \begin{pmatrix} S11 & S12 \\ S21 & S22 \end{pmatrix} \begin{pmatrix} a1 \\ a2 \end{pmatrix} \tag{4.1}$$

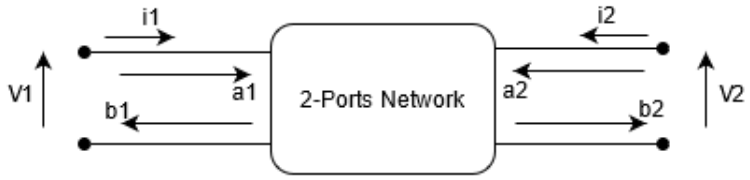

Figure 4.2: S-Parameters network of two-ports with incident and reflected waves.

Where $b1$, $b2$, $a1$, and $a2$ are the electric fields of the microwave signals. The Figure 4.2 shows the network with two-ports.

To stimulate the circuit we used two waveguide ports connected to each side of the microstrip line. These types of ports also allow for energy absorption and simulation of infinitely long waveguides or transmission lines.

The materials used in Simulation were:

- Copper (annealed) normal with relative permittivity of 1.0 and electric conductivity of $58MS/m$ (available on CST library material).
- Copper (annealed) Perfect Electric Conductor (PEC) (available on CST library material).
- The substrate Isola Astra with relative permittivity of 3.0 - reference in the section 7.1).

To simulate we used two methods. The FDS at first, based on the finite element method (FEM). The second method used was MLS, based on the method of moments (MOM) technique. With this method it was necessary to consider replacing the copper (annealed) normal to Copper (annealed) PEC with thickness equal to zero. We chose this due to the PEC having perfect conductivity even with zero thickness.

4.1.3 Process to Analysis the simulations

After each simulation we analyzed the obtained results. To do this, monitors were set at specific frequencies. To select them we looked at the S11 parameter plot, to see where the structure had high reflections. These points correspond to the sensor resonances. After selecting the monitors for the electric field (E-field) and magnetic field (H-field) at the desired frequencies, we continued with the simulation. The monitors are used with different types of fields or fields at various frequencies, and it is possible to see which part of the structure is excited at each monitored frequency.

After getting the simulations, and obtaining the desired resonant frequencies for each sensor we proceeded to the simulation with a protective layer (paper), and a finger placed on the sensor. The process was as follows:

1. Simulation with the protective layer - a layer was added above the sensor metallizations. For this layer we selected the characteristics of a thin PTFE layer, with relative permittivity of 2.31, and a thickness of $0.1mm$.
2. Simulation with protective layer and finger - a dielectric cylinder (with relative permittivity of 50) was added to simulate a finger with a diameter of $15mm$ and a height of $30mm$.

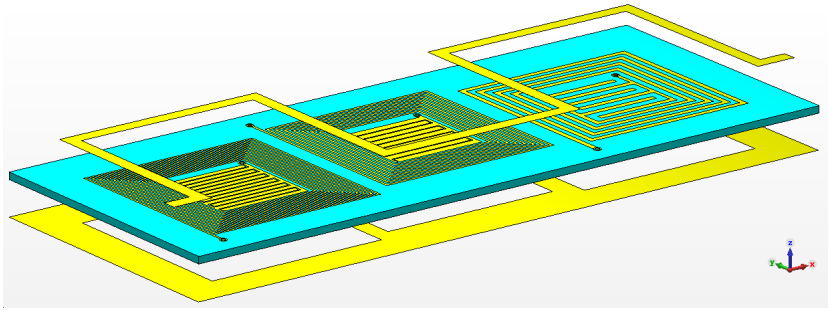

Figure 4.3: Structure obtained with macro file, separated in three main parts of final structure.

3. Simulation with finger - the final simulation was with a dielectric cylinder to simulate a finger and without the protective layer.

4.2 Results

The Results section shows the results obtained with the macro file and the simulations. This section is divided in:

1. Structure developed with macro file;
2. Simulations for a structure with initial parameters from MATLAB® with FDS;
3. Simulations for a structure with initial parameters from MATLAB® with MLS. Also the results of monitors are applied;
4. Simulations of structure 1 and the respective monitors;
5. Simulations of structure 2 and the respective monitors;
6. Simulation of Structure 2 using FDS;
7. Simulation with the protective layer;
8. Simulation with the protective layer and finger.

4.2.1 Structure developed with macro file

The first achieved result is the structure made using the macro file. The Figure 4.3 shows the structure separated into three main parts: ground plane (bottom), microstrip (top), and substrate, inductor and capacitor (middle). Figure 4.4 shows the results of macro file of top view and the figure 4.5 shows the bottom view.

4.2.2 Simulations of initial parameters with Frequency Domain Solver

The second result is for the FDS-simulated S-parameters for the structure with first set of parameters obtained with MATLAB® script, where the parameters are shown in table 3.3. Figure 4.6 shows the S-parameters obtained using FDS.

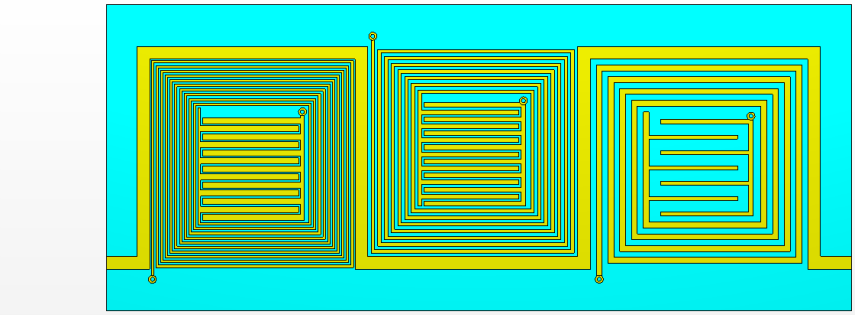

Figure 4.4: Top view of the structure obtained with macro file.

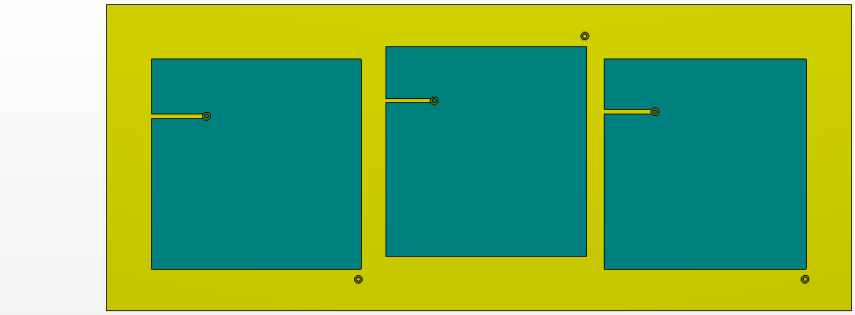

Figure 4.5: Bottom view of the structure obtained with macro file.

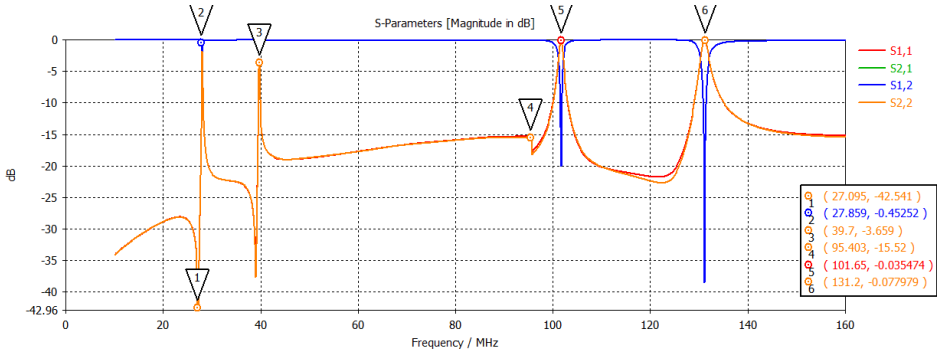

Figure 4.6: S-parameters obtained with the initial structural parameters with the FDS.

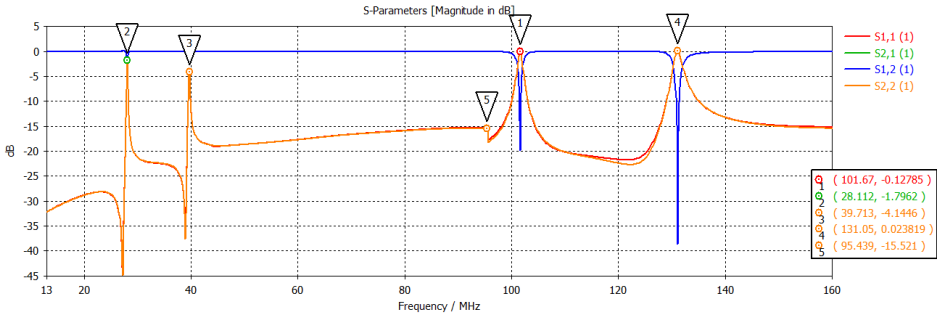

Figure 4.7: S-parameters obtained with the initial structural parameters with MLS.

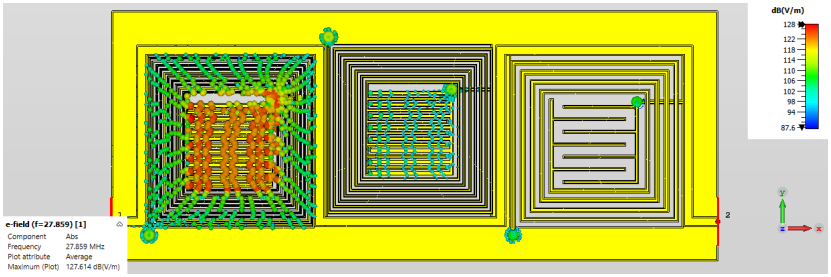

Figure 4.8: E-Field monitor applied in first simulation at $27.589MHz$.

4.2.3 Simulations of initial parameters with MultiLayer Solver

The third result was obtained with the same parameters as the second result, but in this case MLS was used to simulate. Figure 4.7 shows the S-parameters obtained. After calculating the S-parameters it was necessary to apply monitors at specific frequencies ($27.589MHz$, $39.7MHz$, 95.43, and 131.2). Figures 4.8, 4.9, 4.10, and 4.11 show the electric fields of the sensors at specific frequencies. The figures show snapshots of the magnitude and direction of the electric field vectors.

With the obtained results, more simulations were performed until the goal of reaching the three desired frequencies was achieved. As explained in the 3.4 section, the results for the third sensor did not reach the desired frequency, so it was necessary to calculate the frequency shift and add this difference to the MATLAB® script for the third sensor, obtain new sets of structural parameters for this sensor and simulate it in CST again. These process was repeated until we arrived at two different structures, structure 1 and structure 2.

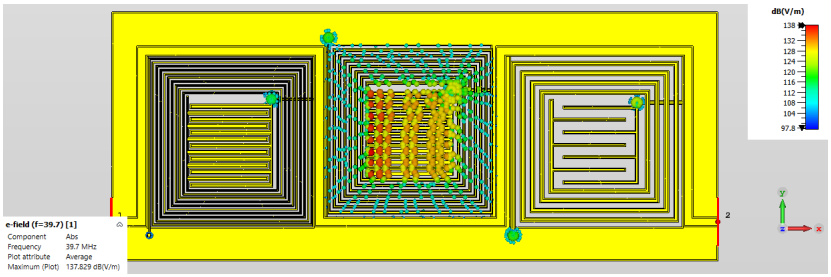

Figure 4.9: E-Field monitor applied in first simulation at $39.70MHz$.

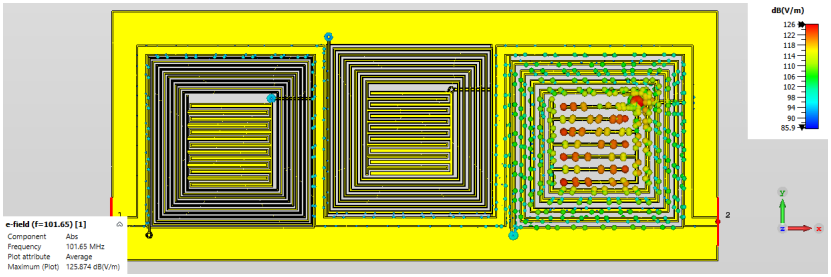

Figure 4.10: E-Field monitor applied in first simulation at $101.65MHz$.

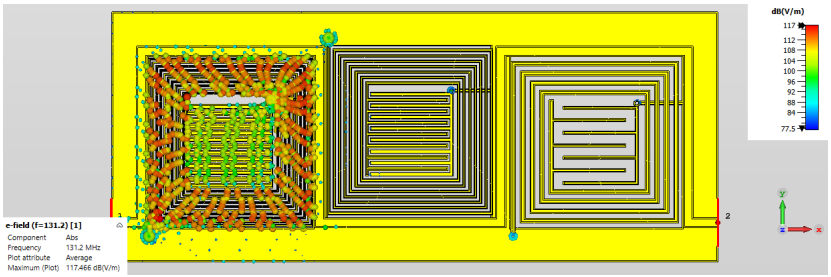

Figure 4.11: E-Field monitor applied in first simulation at $131.20MHz$.

4.2.4 Simulations of structure 1

The S-parameters of structure 1 are shown in Figure 4.12. The used parameters are shown in Table 3.4. where the monitors for this structure are shown in Figures 4.13, 4.14, 4.15, and 4.16.

4.2.5 Simulations of structure 2

The structure 2 has the S-parameters shown in Figure 4.17. where the monitors for this structure are shown in Figures 4.18, 4.19, 4.20, and 4.21.

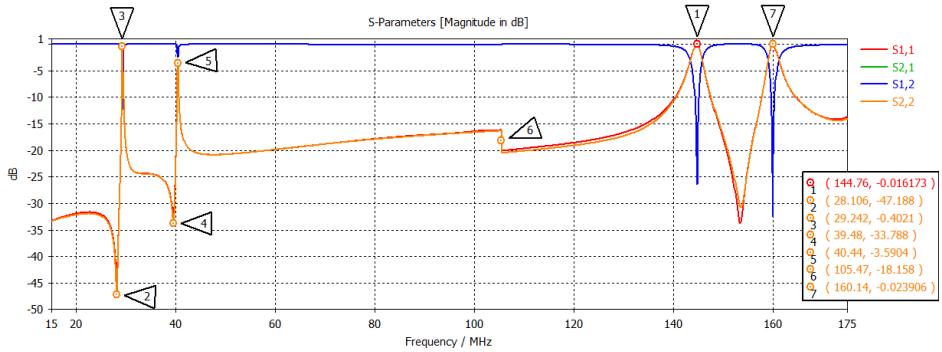

Figure 4.12: S-parameters obtained with the structure 1.

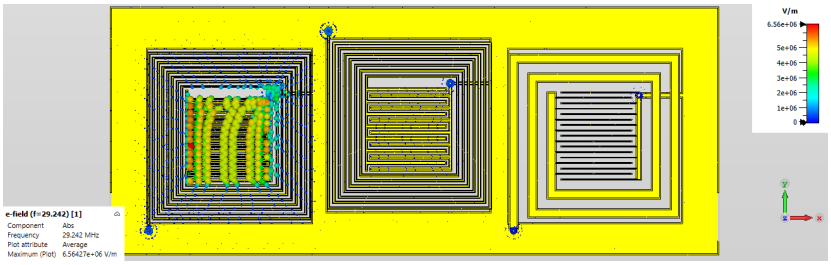

Figure 4.13: E-Field monitor applied to structure 1 at $29.242MHz$.

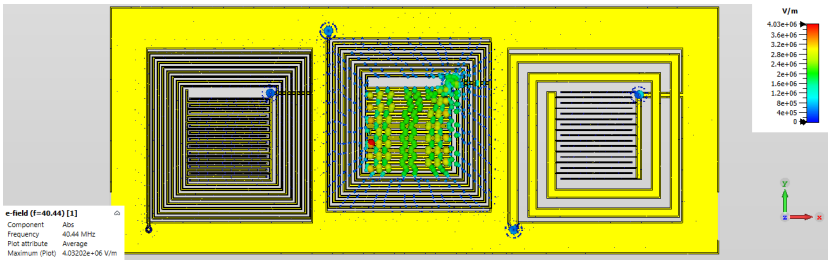

Figure 4.14: E-Field monitor applied to structure 1 at $40.44MHz$.

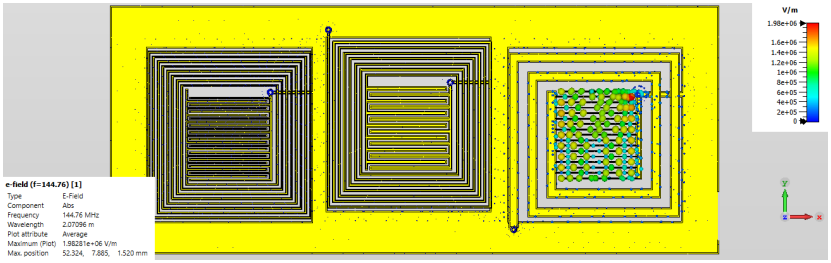

Figure 4.15: E-Field monitor applied to structure 1 at $144.76MHz$.

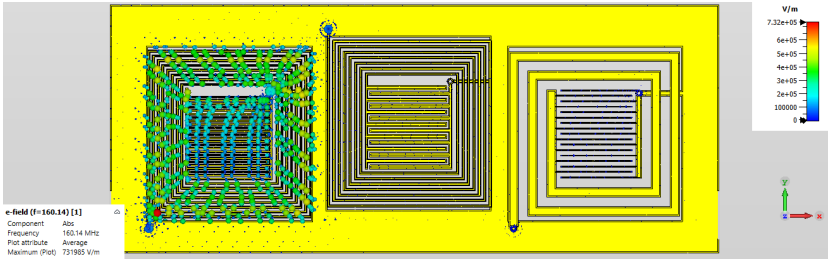

Figure 4.16: E-Field monitor applied to structure 1 at $160.14MHz$.

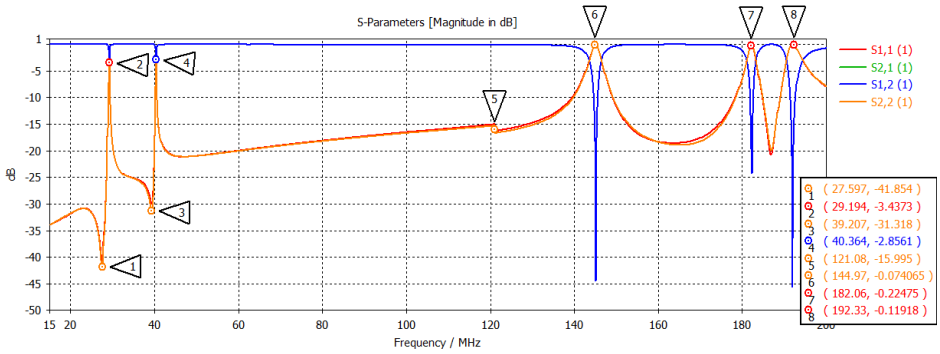

Figure 4.17: S-parameters obtained with the structure 2.

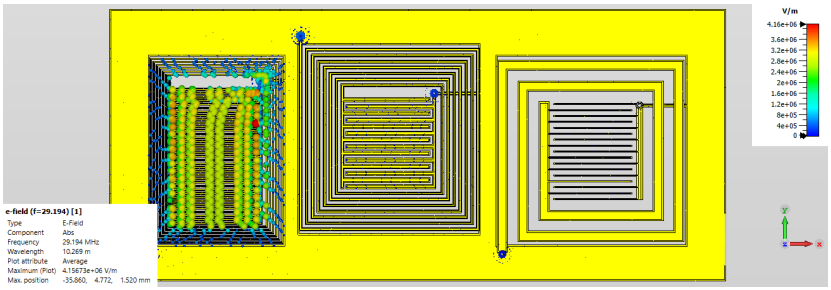

Figure 4.18: E-Field Monitor applied to structure 2 at 29.194MHz.

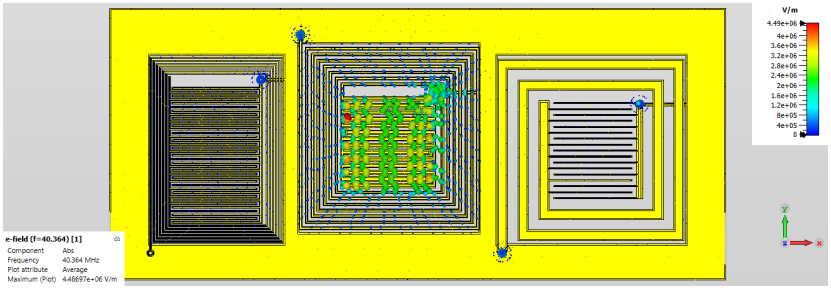

Figure 4.19: E-Field Monitor applied to structure 2 at 40.364MHz.

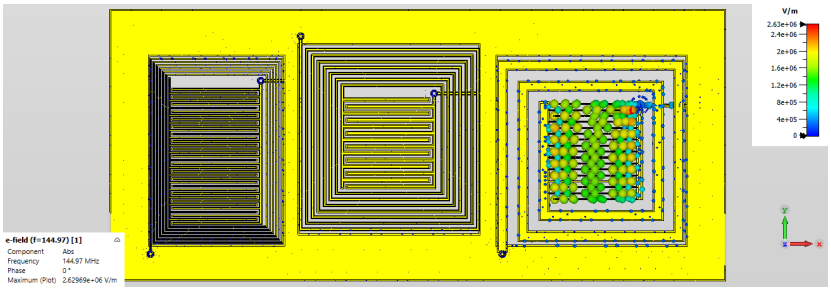

Figure 4.20: E-Field Monitor applied to structure 2 at 144.97MHz.

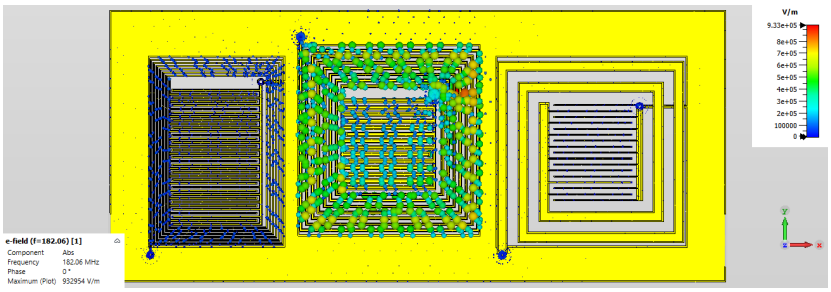

Figure 4.21: E-Field Monitor applied to structure 2 at $182.06 MHz$.

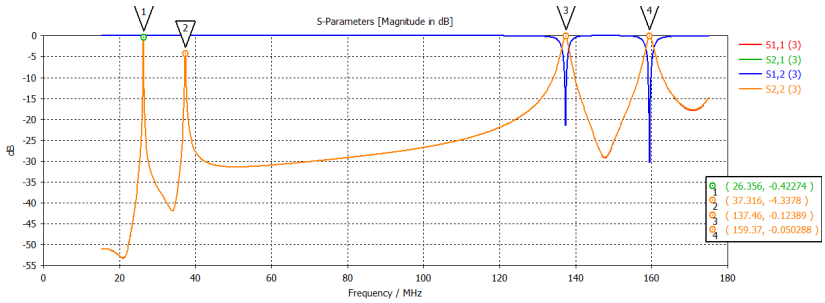

Figure 4.22: S-parameters obtained for structure 2 without the protective layer and finger, using FDS.

4.2.6 Simulation of Structure 2 using Frequency Domain solver

The S-parameters obtained just with the sensor structure (i.e. without human finger tissue or any other layers) and using the FDS are shown in Figure 4.22. This plot is shown to be able to compare it with the simulations of case with the protective layer, and with the protective layer plus the human finger placed on the sensor.

4.2.7 Simulation with protective layer

The S-parameters obtained with a protective layer made of PTFE, are shown in Figure 4.23. The obtained results are derived from structure 2.

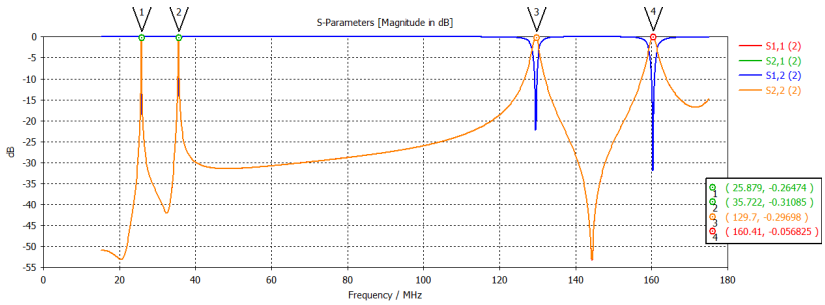

Figure 4.23: S-parameters obtained for structure 2 with a protective layer.

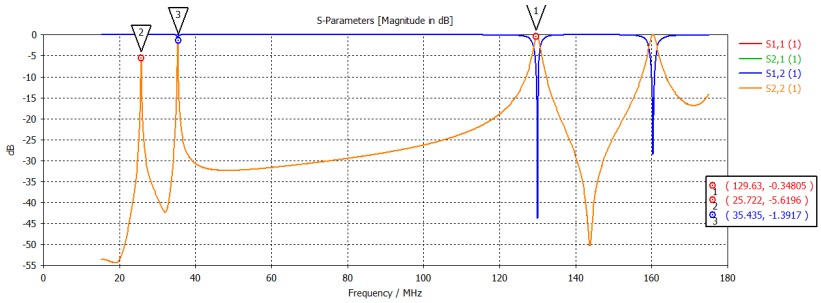

Figure 4.24: S-parameters obtained with a protective layer and a cylinder to simulate a finger.

4.2.8 Simulation with finger and protective layer

The S-parameters obtained with a protective layer made of PTFE and a dielectric cylinder to simulate a human finger are shown in Figure 4.24. The FDS was used in the simulation, because MLS can only model planar dielectric slabs. The obtained results are derived from structure 2. With all these results it is possible to do the analysis that is covered in detail in the next section.

4.3 Analysis and Discussion

The Analysis and Discussion section provides an analysis of the obtained results. This section is divided accordingly to the obtained results into the following sections:

- Analysis of the structure developed with macro file;
- Analysis of the simulations results for initial structure with FDS as compared to MLS;
- Analysis of the monitors results for the initial structure;
- Analysis of the structure 1 results and the respective monitors;
- Analysis of the structure 2 results and the respective monitors;
- Analysis of the structure 2 with the protective layer and finger using FDS;

4.3.1 Analysis of the structure developed with macro file

The structure of the developed macro is very relevant to the simulation process. Many simulations were done, and it was only possible to achieve because of the macro file. The finally obtained structure was exactly the desired structure. As was mentioned in section 4.1, in order to use MLS and copper modeled as PEC, the thickness of the metallization was set to zero. However, a problem was also found in the used version of CST Studio Suite software. To be able to run the macro file in this version of CST, the thickness of the layers had to be greater than 0 (however, we wanted it to be 0). To solve this, we need to run the macro first with a thickness greater than 0, and only then update the structure with the thickness set to 0. After following these steps it was possible to simulate with copper layers modeled as PEC of zero thickness, by using MLS. This simplification of the structure decreased the simulation time significantly. It is important to note that the macro file just works well with the parameters provided by the MATLAB® script, described in section 3.

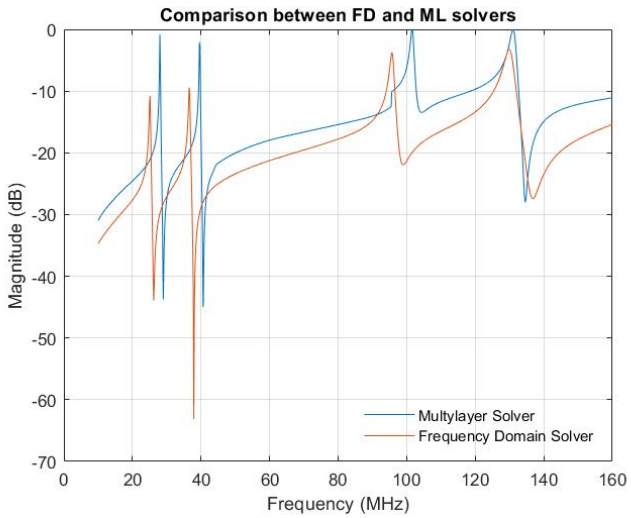

Figure 4.25: Comparison between the results with FDS and MLS.

4.3.2 Analysis of the simulations results for the initial structure comparing both solvers

The results with the FDS (Figure 4.6) and with the MLS (Figure 4.7) are similar, as shown on Figure 4.25 for the S-parameters. However, we chose the MLS, because with this method (thickness equal to zero) the simulator considers only one surface per a metallization layer. This doesn't happen with FDS, which considers multiple surfaces per same layer. This increases the simulation time. Because of that we chose the MLS technique. So with MLS the structure is simplified, the calculations are much faster, and for this reason the following results were almost all done using MLS. The results with MLS and FDS have some differences, but this is compensated by the time saved whilst using the MLS technique. To achieve better results with FDS and MLS two important steps were followed. We used mesh refinement during the simulations by selecting the "adaptive tetrahedral mesh refinement" option in the simulation setup. In addition, it was important to join all electrically connected objects for each structure, because the initial macro implementation created the structure by separate segments (for example, the microstrip was drawn using segments which were not directly connected and the simulator assumed they were separate structures). This caused the simulator to produce more tetrahedrons and taking longer to get the simulation results. To solve this we added the "add.bolean" command to the macro for each part of each structure.

4.3.3 Analysis of the monitors results for the initial structure

After analysing the differences between the solvers used in the simulations, it is important to analyse the results for the frequency response of the structures. The first analysis is for the initial structure. After applying the monitors at specific frequencies, 27.589, 39.70, 95.43, 101.65, and 131.20MHz, is was possible to reach to following conclusions:

- The frequencies 27.589, 39.7, and 101.65MHz were obtained for the sensor 1, 2 and 3, respectively. The first two frequencies are quite in range of the desired frequencies (28 to 29.7, and 40.66 to 40.7MHz). The realized frequency of 101.65MHz has a difference

of 42.35MHz between the desired and the obtained value.

- At 95.43MHz frequency we found an interesting feature in the simulated S-parameters when using MLS. At this frequency a peak appears and it only happens with this solver. In other simulations with this solver it occurs at other frequencies close to this one (for example, in the figure 4.14 occurs at 105.47MHz);

- The frequency 131.20MHz corresponds to the inductor resonating. This inductor corresponds to the sensor 1. It is necessary to decrease the number of loops in the sensor 1 to decrease this effect, because it may cause interference with the resonant frequency of sensor 3.

Based on this analysis we changed the structure. Sensor 1 was changed by decreasing the number of the loops to mitigate interference with the inductor self-resonance, and we also changed sensor 3 to increase the resonant frequency and achieve the desired range.

4.3.4 Analysis of the results for structure 1 and the respective monitors

With the changes made to obtain the desired ranges of resonant frequencies for each sensor and to decrease the interferences due to parasitic resonances, the structure 1 was created. After simulations, and analysed the S-parameters and found 4 resonant frequencies at 29.242, 40.44, 144.76, and 160.14MHz. It was possible to reach some conclusions after applying the monitors at these specific frequencies:

- The frequency of 29.242MHz corresponds to sensor 1, the frequency of 40.44MHz corresponds to sensor 2, and the 144.76MHz frequency corresponds to sensor 3.

- At 160.14MHz we detect another resonant frequency. With the help of the monitors at this frequency it was possible to conclude that this frequency corresponds to the self-resonance of the inductor of sensor 1. This means that this inductor can cause interference at 144.76MHz. With this in mind, we performed more simulations to reduce the effect caused by this inductor, while trying to maintain the resonant frequency of sensor 1 when reducing the number of loops of this inductor.

The final results for structure 1 became good in the full range of desired frequencies. It was only necessary to adjust the number of loops for sensor 1 so as not to cause interference with the resonance frequency of sensor 3. This change generated another structure described in the next section.

4.3.5 Analysis of the structure 2 results and the respective monitors

To decrease the parasitic effects of the inductor of sensor 1, the solution that we found was to change the size of sensor 1. The obtained new sensor has the size of 40mm by 30mm. This solution was named structure 2. This structure has 6 inductor loops, when the original structure had 8 loops. The parameters of the sensor 2, and sensor 3 are the same as in structure 1.

With the simulation of structure 2 it was possible to obtain the desired S-parameters. In S-parameters we found 4 resonant frequencies at 29.194, 40.464, 144.97, and 182.06MHz. After applying the monitors at these frequencies we concluded the following:

- The frequency of $29.194MHz$ corresponds to sensor 1, the frequency of $40.364MHz$ corresponds to sensor 2, and the frequency of $144.97MHz$ corresponds to sensor 3.

- The resonance at $182.06MHz$ corresponds to the inductor of sensor 2. This frequency does not cause interference to sensor 3, because the difference between the two frequencies is very large.

- Therefore, by decreasing the number of loops in sensor 1, the resonant frequency of the inductor increased without causing interference with the frequency of sensor 3.

Thus, the final results for structure 2 were very good results with the resonant frequencies in the desired range and without interferences.

4.3.6 Analysis of the structure 2 with the protective layer and finger, using the Frequency Domain Solver

As was mention before, here we must use FDS, because MLS cannot work with cylinders, it can only work with flat dielectric slabs. With the three results simulated with FDS for structure 2, structure 2 plus protective layer, and structure 2 plus protective layer and finger, it was possible to export the simulated S-parameters and by using the MATLAB® it was possible to obtain the three results in a same plot. The exported parameters were automatically re-normalized by CST Studio Suite to the characteristic impedance of 50Ω (in the simulations the waveguide port impedance was used as the reference and it was different from 50Ω). Figure 4.26 shows the obtained plot. From this figure it is possible to conclude that the results with just the protective layer and with the protective layer and finger have a large difference in frequencies, most significantly in sensors 2 and 3. This difference is due to the protective layer made by PTFE placed on top of the metallization. The impact of the finger was barely noticeable in the simulator. Only a small change in magnitude could be observed, but the resonant frequency did not change much. This is a problem, which may be possible to solve by using a better finger model (a bio-model) in the simulator. This finger bio-model is not freely available in the simulator, but we contacted the company and they provided us the bio-model. However, this bio-model required a license for a newer version of the software. The license available in IT Aveiro was for 2019 version, and due to this reason it was not possible to use and test this bio-model.

4.4 Final Remarks

The Simulations section provides a large set of results and conclusions relevant to the next chapter, the Experimental Measurements. The process and reason for making a macro file and the how the main results were obtained have been explained. The first obtained results and the two final structures were presented, as well as the analysis of the specific resonant frequencies by using monitors for each frequency. This way it was possible to see which sensors resonated at the obtained frequency. Furthermore, some problems encountered during the simulation process, and how we tried to solve them were explained. Therefore, with this chapter it was possible to develop and study the structures elaborated with the help of the macro and the MATLAB® script. The main outcome from this chapter was the validation of these two structures. After this validation it was possible to construct and implement

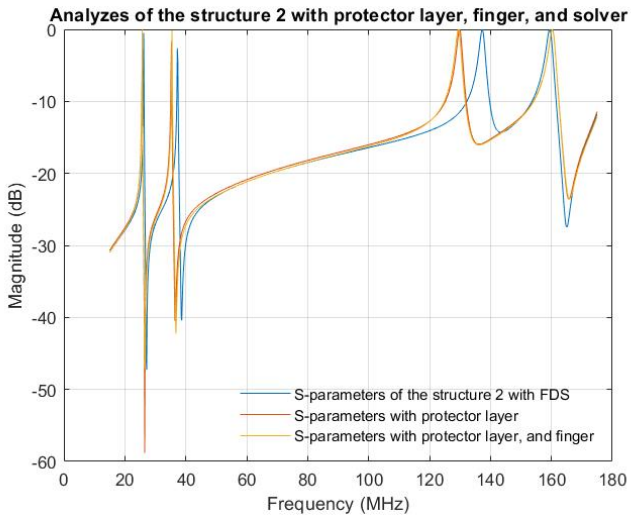

Figure 4.26: S-parameters comparison between the results with FDS, protective layer, and finger.

---

two PCBs. Measuremets of these structures and the respective analysis, discussions and conclusions are collected in chapter 5.

Chapter 5

Experimental Measurements

This chapter aims to explain the procedures to create and measure the final real prototypes. It also illustrates the obtained results, and performs analysis and discussion comparing the measured results with the results of simulations and calculations.

5.1 Implementations

After the simulations were completed we exported the final structure geometry form the 3D modeller of CST Studio Suite to Gerber files used in PCB production, layer by layer. With these files it was possible to build prototypes of structure 1 and 2 as two PCBs. The PCB 1 corresponds to structure 1, and the PCB 2 corresponds to structure 2.

The characteristics of both PCBs were:

- Isola Astra with thickness of $1.52mm$ and $35\mu m$ of metallization available in IT-Aveiro was used as a substrate 7.1;
- The sizes of each sensor were $40mm$ by $40mm$, except for the sensor 1 of PCB 2 with the dimensions $40mm$ by $30mm$;
- The total size of PCB 1 was $147.684mm$ by $60mm$ and the PCB 2 was $136.455mm$ by $60mm$;
- The width of the microstrip was $2.5mm$ for both PCBs;
- The PCBs were made in IT-Aveiro using a PCB milling machine.

Once the PCBs were ready it was possible to measure the S-parameters. To measure them we used the following apparatus:

- VNA (operates in the $30KHz$ to $26.5GHz$ range) - Keysight model N9918A;
- Calibration kit $3.5mm$ 50Ω - Keysight model 85521A;
- RF cables with SMA conectors;
- Torque wrench for SMA $3.5mm$(5/16") - model 01 201;
- Digital caliper;

- Binocular magnifier;

The process to measure the parameters was as follows:

- First the VNA power was connected;
- One RF cable was connected to port A and another to port B of the VNA — lightly hand-tightened, for which the torque wrench was used to apply the same force;
- Inside the VNA we selected the VNA mode;
- Selected the main parameters (Frequency Range, Power, Number of points) - These were $[30KHz, 200MHz]$, $-20dBm$, and 1001 points;
- Calibrated the RF cables — Calibration was selected in VNA mode, Mechanical configuration was selected, female, $3.5mm$, full 2-port calibration with the 85521A kit. The seven steps to calibrate the cables were followed. To verify that the cables were calibrated properly, the cable was connected to a known load and the Smith chart option was used to see if the load value matches the Smith chart;
- We selected the S-parameters. Several measurements were made with different setups and were saved in a $s2p$ file.

The setups for the measures were:

- Just with a PCB, starting with PCB 1;
- The PCB with one finger placed on each sensor at a time;
- A paper sheet was used to cover the top of the PCB and measure just with paper;
- A finger was placed on each sensor at a time, but now using the paper sheet as isolation;
- The process was repeated using PCB 2.

Figure 5.1 shows the setup with a PCB, the VNA, the RF cables, and the torque wrench. After the measurements were taken, the thickness of the paper was measured. To do this, five pieces of paper were cut and the thickness of these five pieces of paper stacked together was measured with a caliper. After that, the thickness was calculated by dividing this number by the number of pieces of paper. Another important step to take into account was to measure the dimensions of the metallizations and openings on the different parts of the PCB structure (the inductors, the capacitors and the microstrip) using a caliper to measure and a binocular magnifier to assist. The next section shows the results obtained for each PCBs, with and without a protective layer, with a finger placed on each sensor, and also the measured PCB dimensions.

5.2 Results

This section is divided into the following parts:

1. The PCBs manufactured;

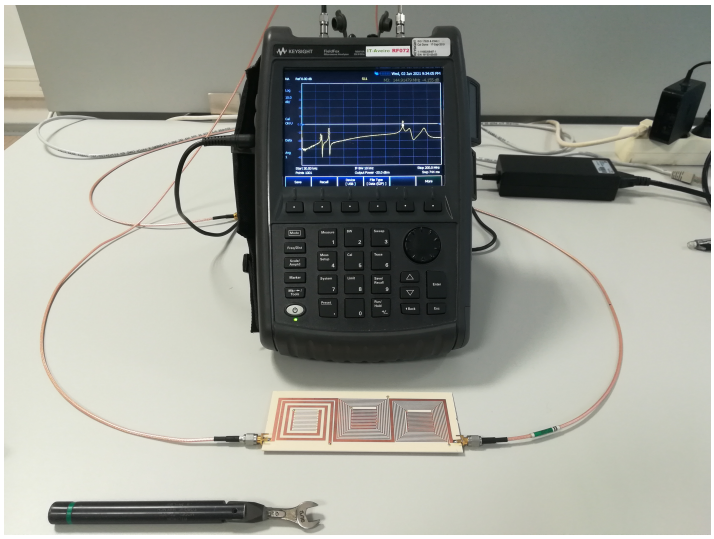

Figure 5.1: Experimental setup to measure the S-Parameters using the VNA.

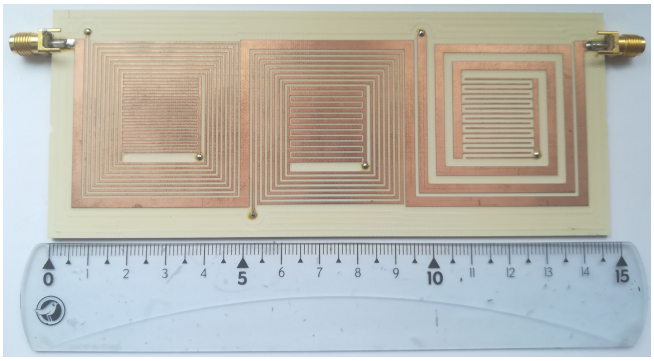

Figure 5.2: Top view of the manufactured PCB 1, to scale. Here, sensor 1 is on the left, sensor 2 is in the middle, and sensor 3 is on the right.

---

2. Measurements of the PCB 1, with and without the protective layer, and with and without a finger placed on each sensor;

3. Measurements of the PCB 2, with and without the protective layer, and with and without a finger placed on each sensor;

4. Measurements of the dimensions of each part, the metallization widths and gaps in the inductors, the capacitors and the microstrip, for each PCB.

5.2.1 PCBs manufactured

The first obtained result was the manufactured PCB 1 and 2. Figures 5.2 and 5.3 show the manufactured PCBs. Also, in Figure 5.4 the bottom views for both PCBs are shown.

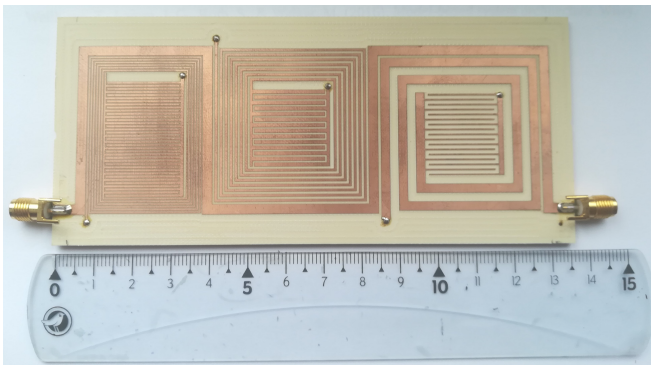

Figure 5.3: Top view of the manufactured PCB 2, to scale. Here, sensor 1 is on the left, sensor 2 in the middle, and sensor 3 is on the right.

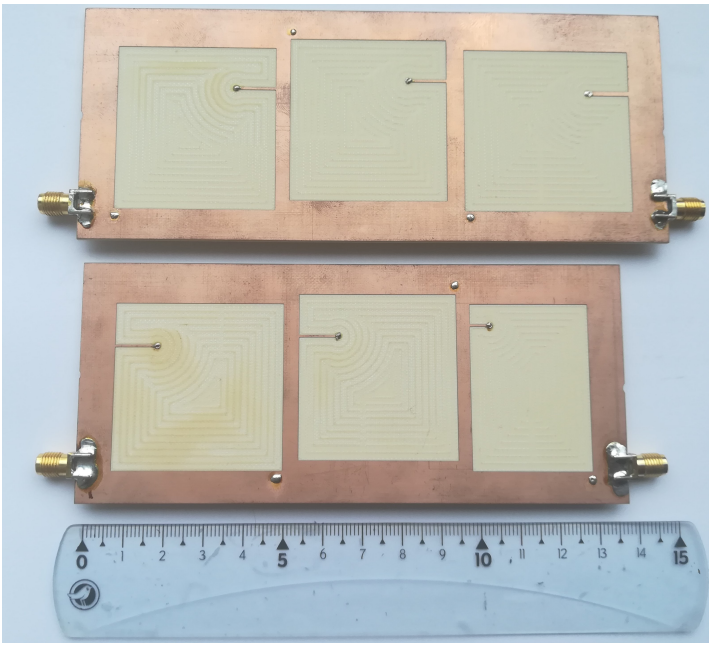

Figure 5.4: Bottom views of the manufactured PCBs 1 and 2, to scale.

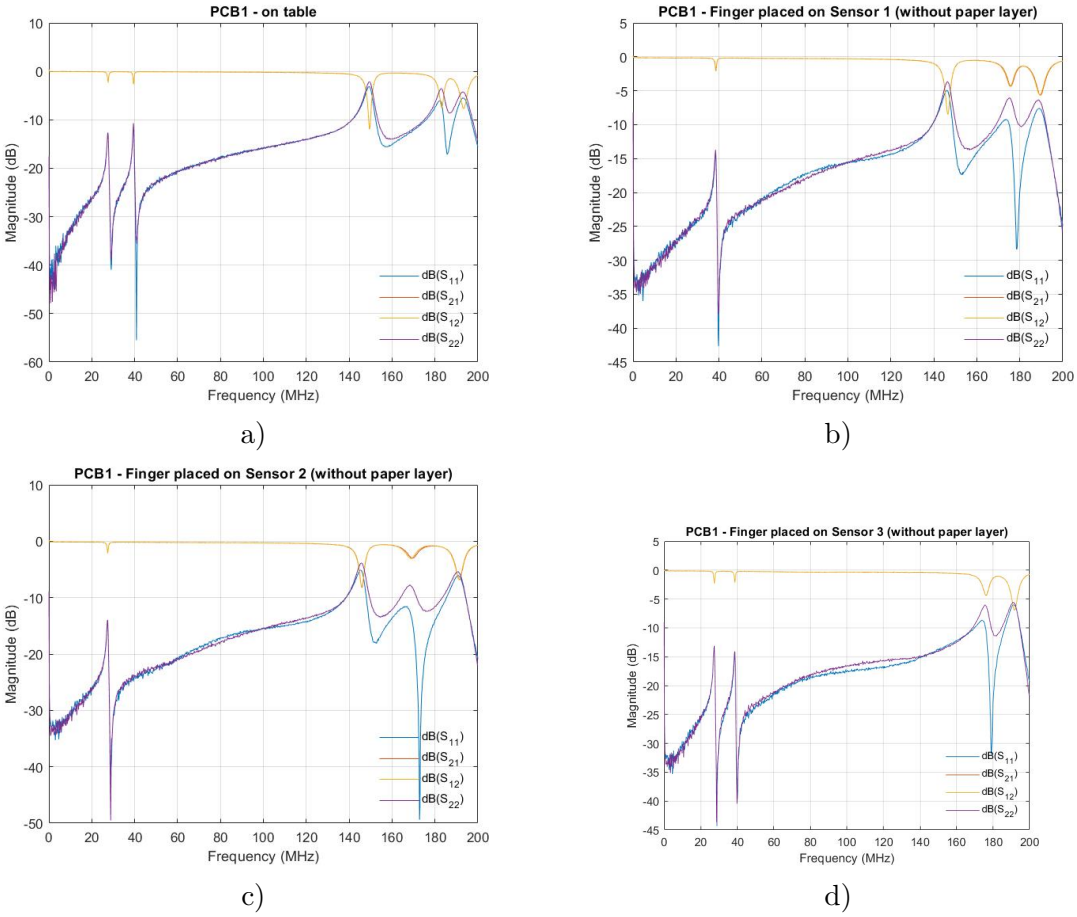

Figure 5.5: Measurements with the PCB 1, without protective layer. Figure a) shows the measurement only with PCB, b) is the measurement with the finger placed on sensor 1, c) is the measurement with the finger placed on sensor 2, and d) is the measurement with the finger on sensor 3.

5.2.2 Measurements of PCB 1

After the PCBs were manufactured a number of measurements were performed, as explained in Section 5.1. The first results were obtained for PCB 1, without the paper layer and with a finger placed on each sensor at a time. Figure 5.5 shows this results: After the results without the protective layer were obtained, the next measurements were made with the protective layer (made of paper), and a finger placed on each sensor at a time. Figure 5.6 shows these results.

5.2.3 Measurements of the PCB 2

After we concluded with the measurements of PCB 1, measurements with PCB 2 were performed. The first measurements were made without the protective layer and with finger placed on each sensor at a time. Figures 5.7 shows the obtained results. After the results without the protective layer, the next measurements were made with the protective layer (made of paper), and a finger placed on each sensor at a time. Figure 5.8 shows these results.

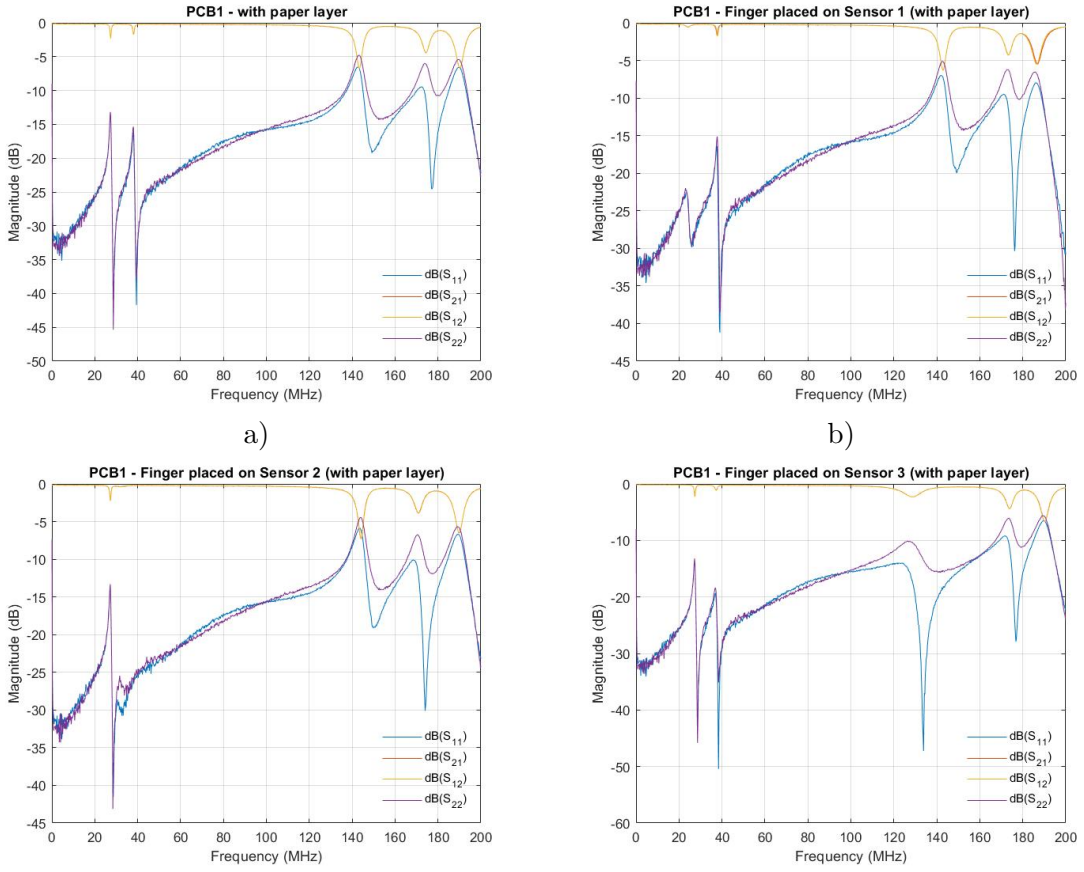

Figure 5.6: Measurements with PCB 1, but with paper layer. Figure a) shows the measurement just with PCB and the paper layer, b) is the measurement with the finger placed on sensor 1, c) is the measurement with the finger placed on sensor 2, and d) is the measurement with the finger placed on sensor 3.

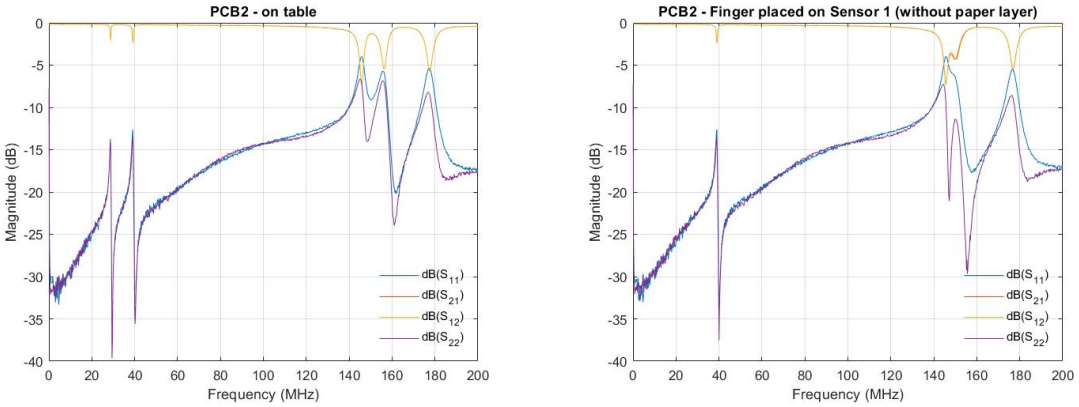

a)

b)

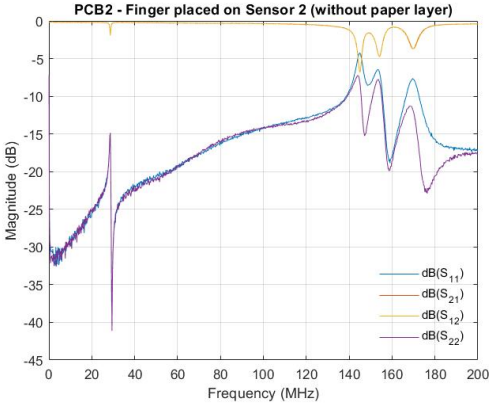

c)

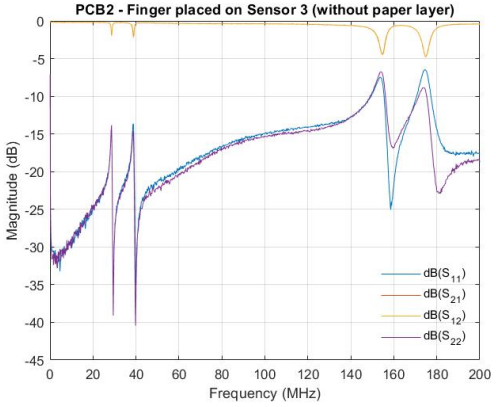

d)

Figure 5.7: Measurements with PCB 2, without protective layer. Figure a) shows the measurement just with PCB, b) is the measurement with the finger placed on sensor 1, c) is the measurement with the finger placed on sensor 2, and d) is the measurement with the finger placed on sensor 3.

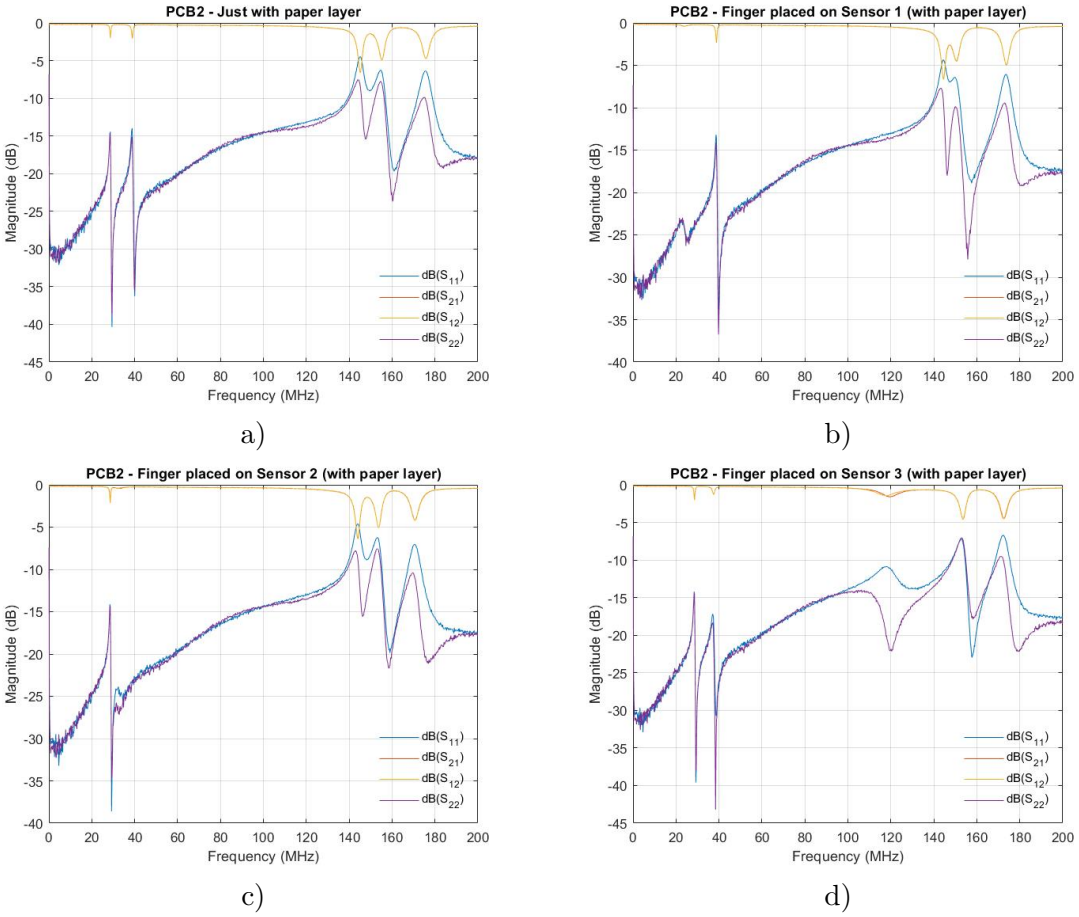

Figure 5.8: Measurements with PCB 2, but with paper layer. Figure a) shows the measurement just with PCB and the paper layer, b) is the measurement with the finger placed on sensor 1, c) is the measurement with the finger placed on sensor 2, and d) is the measurement with the finger placed on sensor 3.

5.2.4 Measurements of the dimensions

After the measurements were made using the VNA, we measured the dimensions of each PCB. Table 5.1 shows the dimensions obtained. The width was measured using a digital caliper. The gaps were not measured because it had a greater error margin with the used equipment and human vision. Indeed, to measure the gaps with the gauge it is necessary to observe the dimension, thus introducing human error. This is in contrast to the measurement of the track widths, because it is only necessary to apply force to the two sides of the track, thus not introducing human error to the measurement. Using a caliper, the measured thickness of five pieces of paper was $0.44mm$. Dividing this value by five we get the thickness of one piece of paper, which was $0.088mm$.

PCB dimensions measured						
	PCB 1			PCB 2		
Sensors / Parameters	S1	S2	S3	S1	S2	S3
Inductor width $*^1$	0.55	0.64	2.30	0.30	0.63	2.31
Capacitor width $*^1$	0.43	0.97	0.28	0.49	0.97	0.27
Microstrip width $*^1$	2.48	2.48	2.48	2.48	2.48	2.48

$*^1$ in mm.

Table 5.1: Dimensions measured on the PCBs 1 and 2.

5.3 Analysis and Discussion

From the obtained results it was possible to reach to some conclusions. This section is divided into the following subsections:

1. Analysis and comparison between the measured results and simulated results;
2. Analysis and comparison between the experimental results for PCB 1, with and without the protective layers, and with a finger placed on each sensor;
3. Analysis and comparison between the experimental results for PCB 2, with and without the protective layers, and with a finger placed on each sensor;
4. Analysis and comparison with and without fingers and with protective layer;
5. Analysis and comparison with and without fingers and without protective layer;
6. Comparison between the real dimensions and the theoretical dimensions of each part of each PCB;
7. Analysis and conclusions about the obtained results.

5.3.1 Analysis and comparison between the measured and simulated results

Having the measured results and the simulated results ready, it is now possible to analyze both comparing them with each other. Exporting the S-parameters from the simulation and importing the measured values to MATLAB® it was possible to plot the results of PCB 1 and PCB 2 in the same graph. When the S-parameters are exported from the CST Studio Suite simulator they are renormalized to 50Ω reference impedance, so that it is possible to compare both results. This was necessary because the simulator defines the S-parameters with respect to the waveguide port characteristic impedance, however, the measured values were obtained for the 50Ω characteristic impedance. Figure 5.9 shows a comparison of the results for the measurements without protective layer and finger. In both PCBs the obtained resonant frequencies occur in the desired ranges, as is shown in the figure. We can conclude that the simulations give a good approximation of the reality and can be used to design and simulate sensors and PCBs. Also we conclude that the MATLAB® script can generate reasonable values of parameters and dimensions to use in the simulations. Thus, we have

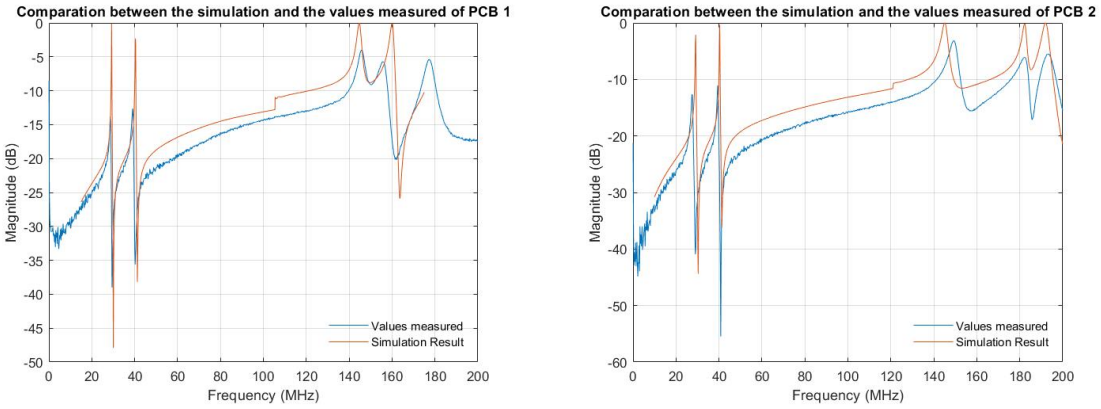

a) b)

Figure 5.9: Comparison of simulated and measured values in PCB 1 (Figure a)) and PCB 2 (Figure b)) without paper layer and finger.

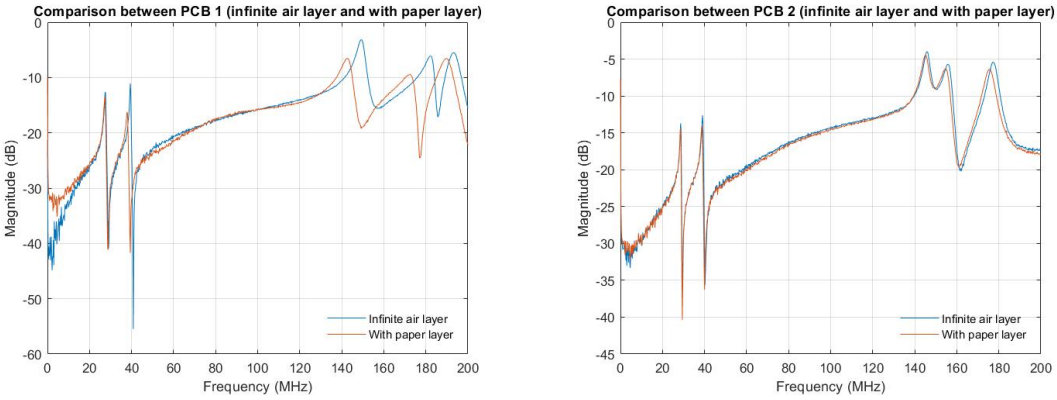

a) b)

Figure 5.10: Comparison between PCB 1 (Figure a) — infinite air layer) and PCB 2 (Figure b) — with paper).

---

obtained similar results in the simulation and the experimental measurements. In conclusion, the results presented are quite positive, for the reasons presented above.

5.3.2 Analysis and comparison between the experimental results for PCB 1

Next, to analyze the experimental results they were post-processed using MATLAB® in order to be able to compare the measured results obtained for both PCBs. Only the return loss S-parameter (S_{11}) was selected for comparison in order to be able to understand and compare each result in a simpler way.

The first analysis compares the structures with and without the protective layer. Figure shows 5.10 the results to be compared. This figure shows that the S-parameters are nearly the same with or without the protective layer made of paper, except on PCB 1, where there is a difference in the third resonant frequency. The difference is $-6.2\ MHz$ with the paper

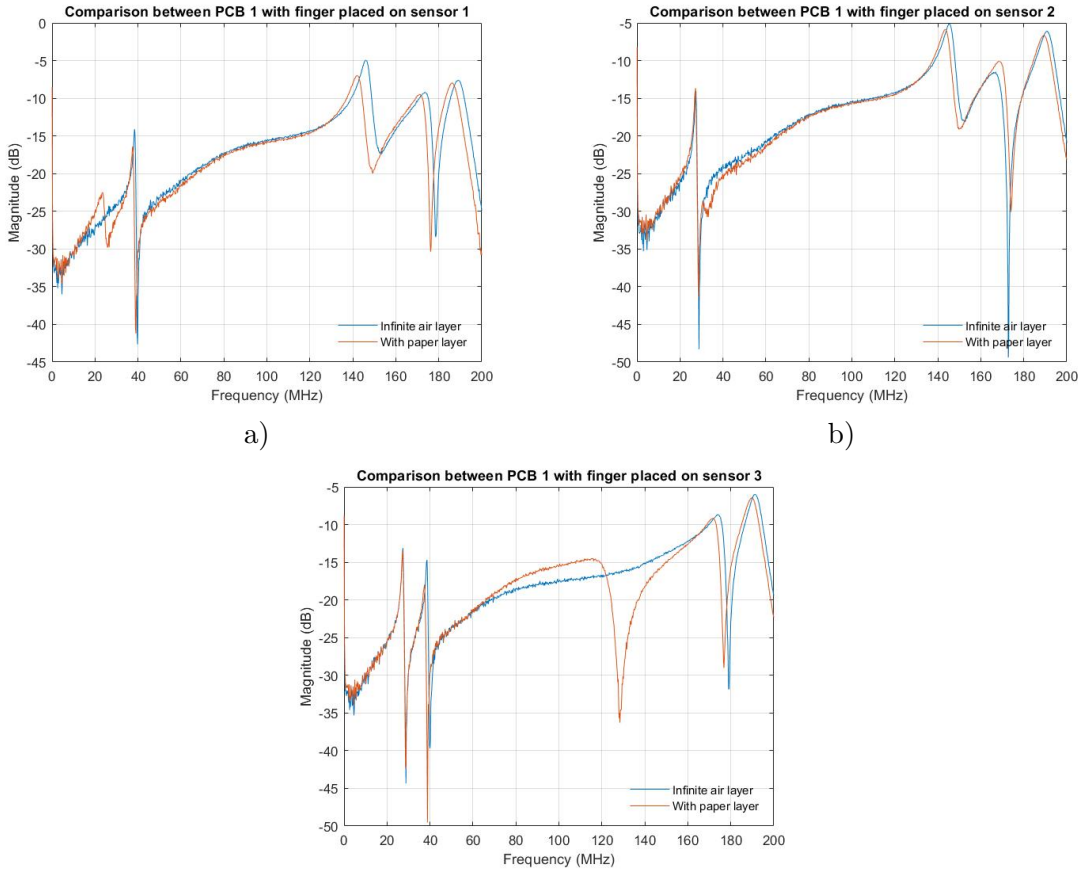

Figure 5.11: Comparison between measurements of PCB 1. Figure a) is for the finger placed on sensor 1, b) is for the finger placed on sensor 2, and c) is for the finger placed on sensor 3.

layer.

The second analysis compares the results with a finger placed on each sensor, with and without the paper layer. Figure 5.11 shows the obtained results. With this figure it is possible to observe the changes in frequencies. Moreover, the reflection magnitude decreases when the finger is placed on each sensor with the paper layer, and the resonance is fully damped when the finger is placed on the sensor without having the protective paper layer.

It is also possible to see the damping of the resonance when a finger is placed on the sensor in the results for the case without the paper layer (infinite air layer) at 27.43, 38.62, and $145.40 MHz$ of PCB 1.

5.3.3 Analysis and comparison between the experimental results for PCB 2

The first analysis compares the structures with and without the protective layer for the PCB 2. Figure 5.12 shows the results to be compared. This figure shows that the S-parameter resonant frequencies change and the reflection magnitude decreases when the finger is placed on each sensor with paper layer, and that the corresponding resonance is dumped on finger

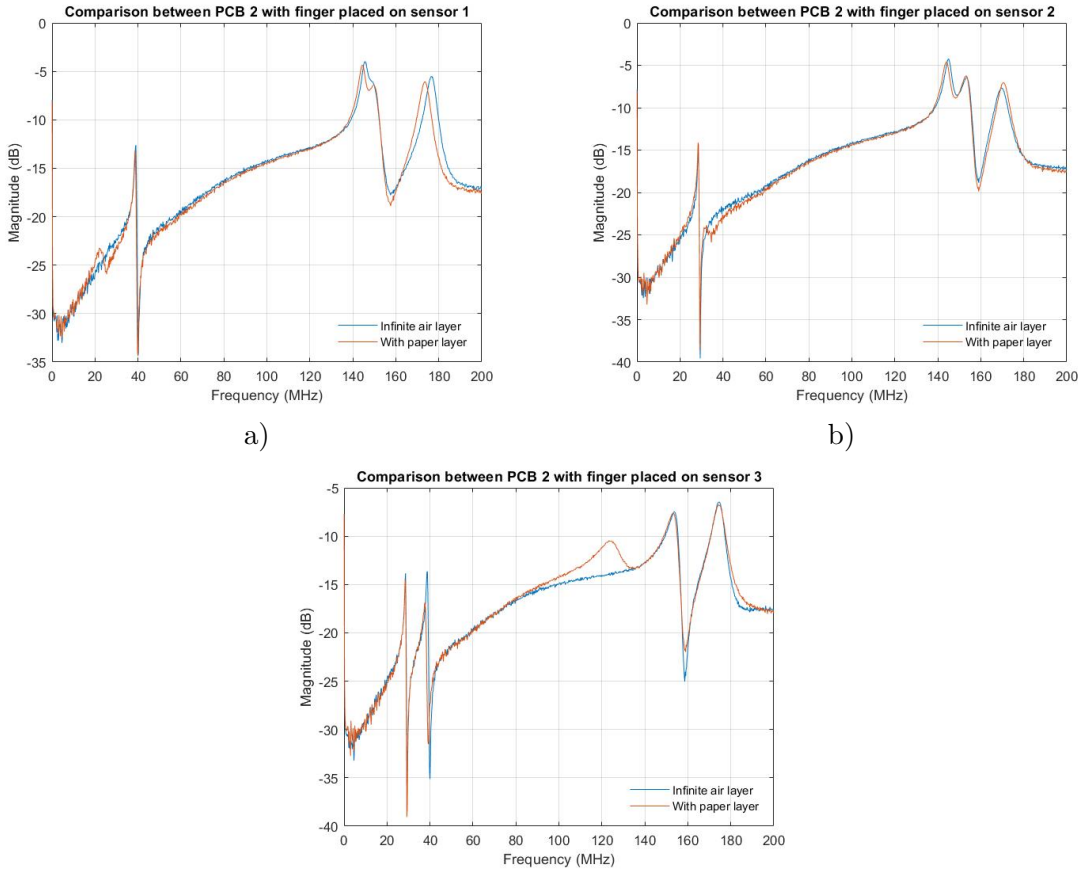

Figure 5.12: Comparison between different PCB 2 configurations. Figure a) is for the finger placed on sensor 1, b) is for the finger placed on sensor 2, and c) is for the finger placed on sensor 3.

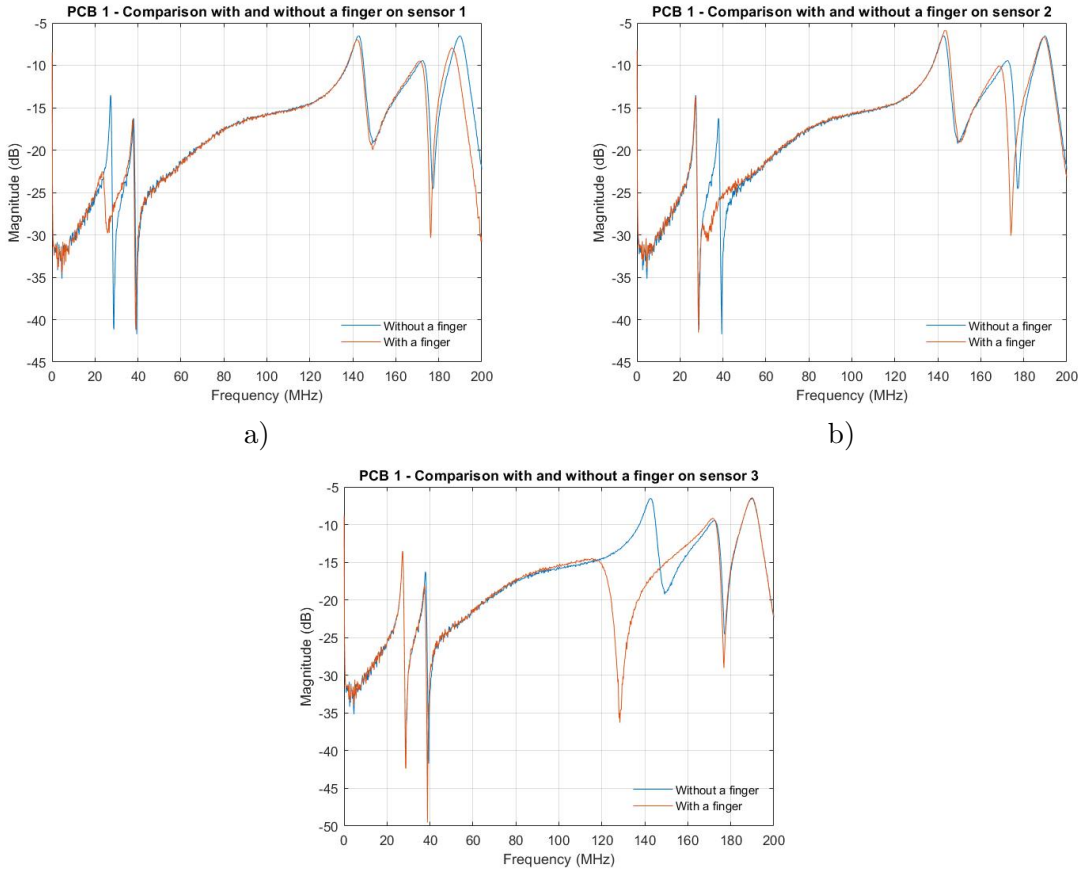

Figure 5.13: Comparison of the PCB 1 results with and without finger placed on each sensor. Figure a) is for the finger placed on sensor 1, b) is for the finger placed on sensor 2, and c) is for the finger placed on sensor 3.

touch, in the structures without protecting layer.

At 28.63, 39.02, and 145.06MHz it is also possible to see the damping of the resonance when a finger is placed on the sensor, for results without the paper layer on PCB 2.

5.3.4 Analysis with and without fingers and with protective layer

The following analysis is made to compare the PCBs without and with a finger placed on sensor, first with a paper layer. This is done to verify if the structure can be used for the final goal as a touch sensor. Figure 5.13 shows the results with PCB 1, and Figure 5.14 shows the results with PCB 2. Table 5.2 shows a summary comparison between the frequencies obtained with a paper layer and finger placed on each sensor, with the values obtained in Chapter 3.3 for PCB 1. Table 5.3 also shows the same, but for PCB 2. From these tables we can see that the resonant frequencies change when the finger is placed on each sensor. This proves that the developed structure works, and the prototype accomplishes the purpose for which it was made, i.e. to detect the finger touch by changing the resonant frequency. It can also be concluded that the MATLAB® script predicts a change in the resonance frequencies

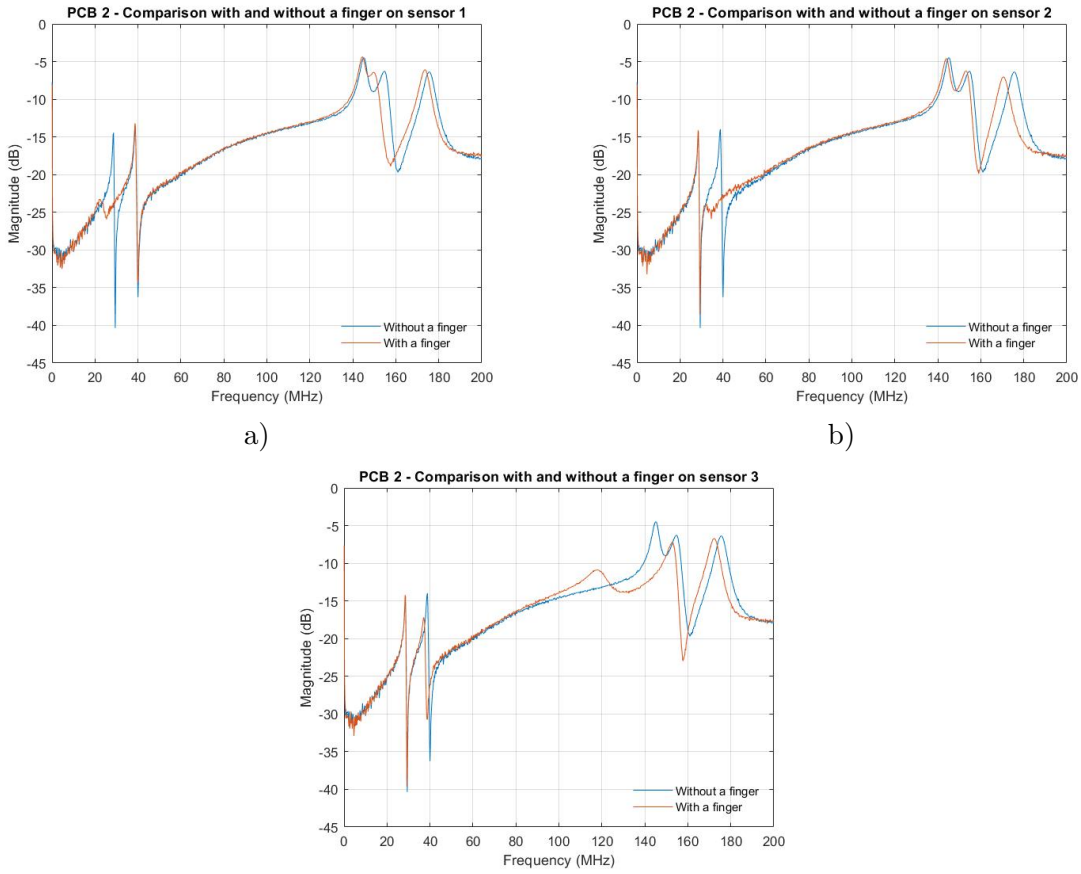

Figure 5.14: Comparison of the PCB 2 results with and without finger placed on each sensor. Figure a) is for the finger placed on sensor 1, b) is for the finger placed on sensor 2, and c) is for the finger placed on sensor 3.

Frequency comparison between the measured values and the calculated results			
Sensors / Frequencies	Sensor 1	Sensor 2	Sensor 3
Sensor frequency measured without finger $*^1$	$27.23MHz$	$37.62MHz$	$143.20MHz$
Frequency measured with finger $*^1$	$23.63MHz$	$30.63MHz$	$128.00MHz$
Calculations without finger	$28.32MHz$	$40.734MHz$	$166.85MHz$
Calculations with finger	$18.13MHz$	$26.10MHz$	$106.91MHz$

$*^1$ with paper layer.

Table 5.2: Frequencies with and without finger as compared with the results of calculations (Chapter 3.3) for PCB 1.

Frequency comparison with measured values and the calculated results			
Sensors / Frequencies	Sensor 1	Sensor 2	Sensor 3
Sensor frequency measured without a finger $*^1$	$28.43MHz$	$38.62MHz$	$144.4MHz$
Sensor frequency measured with a finger $*^1$	$22.03MHz$	$32.23MHz$	$124.4MHz$
Calculations without a finger	$27.912MHz$	$40.734MHz$	$166.85MHz$
Calculated frequency shift with a finger	$17.90MHz$	$26.10MHz$	$106.91MHz$

$*^1$ with paper layer.

Table 5.3: Frequencies with and without finger as compared with the results of calculations (Chapter 3.3) for the PCB 2.

when the finger is placed, however, these values have a difference when compared to the actually obtained values. Variations of parameters or different considerations realized in the code, such as the diameter and height of the finger, the thickness of the paper layer, etc., can cause these differences.

5.3.5 Analysis with and without fingers and without protective layer

The last analysis is made to compare the PCBs without and with a finger placed on each sensor, however, without a paper layer. Figure 5.15 shows the results for PCB 1, and figure 5.16 shows the results for PCB 2. From these figures it is possible to see the resonance damping at 27.43, 38.62 and $145.40MHz$ (PCB 1) and at 28.63, 39.02 and $145.06MHz$(PCB 2) when a finger is placed on sensor. This happens because the human body has high water content in its constitution, thus adding electric conductivity in parallel to the interdigital capacitor when the finger is placed on a sensor. This results in a dramatic decrease in the quality factor of the LC circuit and therefore the resonance is dumped.

5.3.6 Comparison between the real dimensions and the theoretical dimensions

Table 5.4 shows the theoretical dimensions, the dimensions of each part of each PCB in the simulator and as was sent to production, and the dimensions measured directly from the PCB. With this table it is possible to conclude about the production accuracy and estimate the margin of error that can influence the obtained results. The maximum margin of error was about a $0.07mm$, and the average was $0.0263mm$ for PCB 1, and $0.0224mm$ for PCB 2.

5.3.7 Analysis and conclusions about the obtained results

With these comparisons, with and without a paper layer, two methods for touch detection were identified. Initially, we intended to detect the changes of resonant frequency when the finger is placed on the sensor. However, with the experimental results another approach was found. Thus it is possible to detect touch in two different ways:

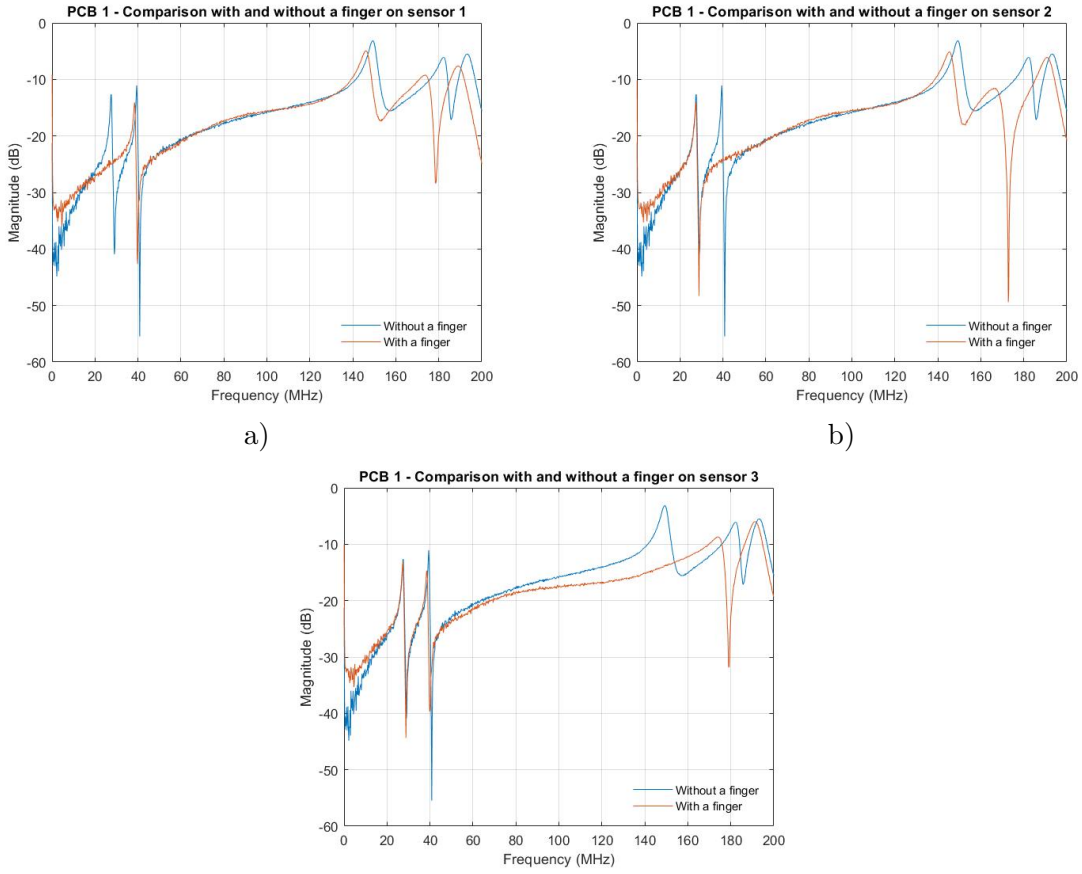

Figure 5.15: Comparison of the PCB 1 results with and without finger placed on each sensor. Figure a) is for the finger placed on sensor 1, b) is for the finger placed on sensor 2, and c) is for the finger placed on sensor 3.

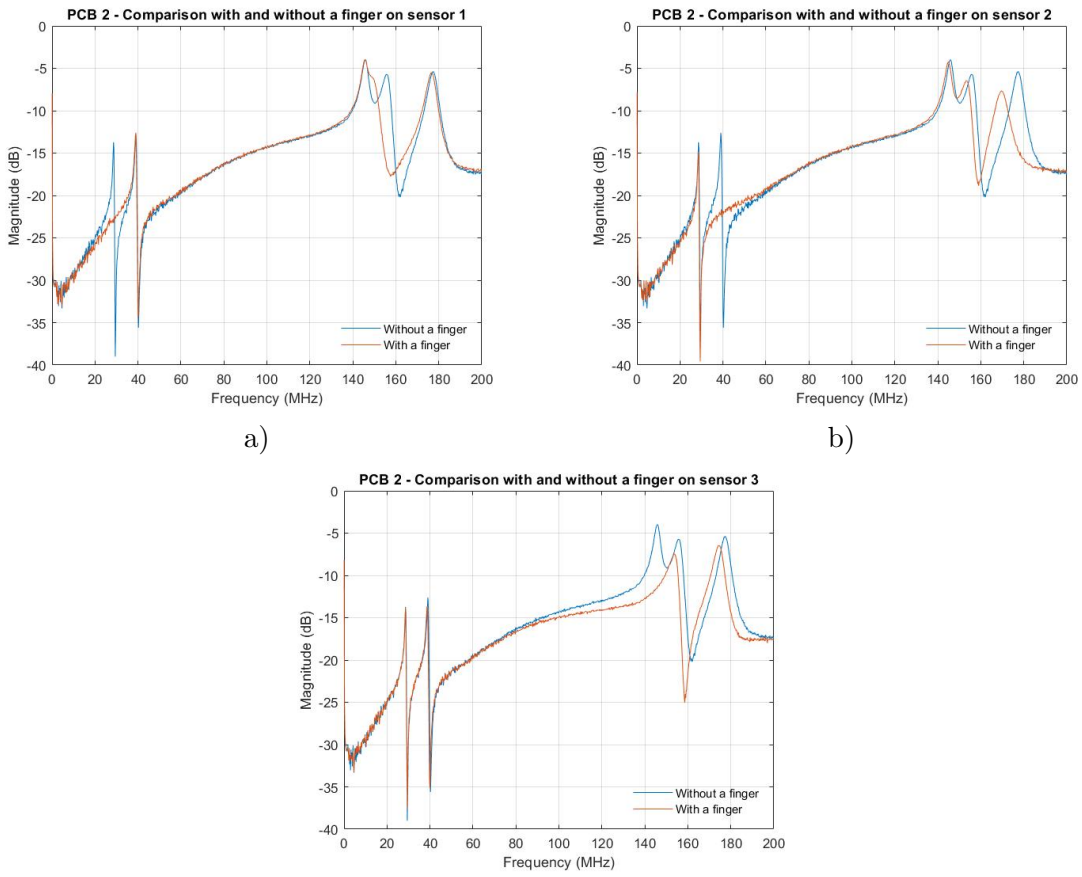

Figure 5.16: Comparison of the PCB 1 results with and without finger placed on each sensor. Figure a) is for the finger placed on sensor 1, b) is for the finger placed on sensor 2, and c) is for the finger placed on sensor 3.

Comparison of measured and theoretical dimensions						
	Theoretical S1	S1 Measured	Theoretical S2	S2 Measured	Theoretical S2	S3 Measured
PCB 1						
Inductor width $*^1$	0.575	0.55	0.6714	0.64	2.30	2.30
Capacitor width $*^1$	0.50	0.43	1.00	0.97	0.30	0.28
Microstrip width $*^1$	2.50	2.48	2.50	2.48	2.50	2.48
PCB 2						
Inductor width $*^1$	0.35	0.30	0.6714	0.63	2.30	2.31
Capacitor width $*^1$	0.50	0.49	1.00	0.97	0.30	0.27
Microstrip width $*^1$	2.50	2.48	2.50	2.48	2.50	2.48

$*^1$ in mm.

Table 5.4: Comparison of measured and theoretical dimensions.

- When the resonant frequency of the sensor change; applicable with protective layer;
- With the effect of resonance damping; applicable without protective layer;

The paper layer was used as a protective layer. Such layer can protect against degradation caused by humidity and dust, among other problems. So to achieve the second detection method it may be still necessary to use a protective layer to avoid such problems. This layer needs to be thinner than the paper layer. The resonance damping effect occurs due to the finger placed directly over the sensor. The fact that the finger has water in its constitution makes it a conductor of electricity. This causes damping of the resonance, as was explained earlier. The resonance damping effect may be better for detection because it forces one of the sensor frequencies to disappear from the reflected signal when the sensor is touched. Moreover, in the resonant frequency change method, the new frequency can sometimes interfere with other sensor frequencies, which can result in a detection failure. For this reason, the use of the damping effect can be more robust. However, it is necessary to use a protective layer to protect the sensors.

From the comparison between the real dimensions and the theoretical dimensions we can conclude that the margin of error is very small, and these errors do not have a large impact on the performance of the real prototype. However, the measured paper thickness was $0.088mm$, and the value used in the MATLAB® script was $0.1mm$, this small change can cause a few MHz difference from the values obtained by MATLAB®, when compared to the real cases with a finger and a layer of paper.

To conclude, both PCBs demonstrated good results:

- The resonant frequencies obtained in each sensor are placed in the expected frequency range;

- The resonant frequency decreases when a finger is placed on each sensor;

Thus, the developed structures accomplish the purpose for which they were made, namely, to detect the touch of a finger by using just a single microstrip line coupled to many sensors.

5.4 Final Remarks

The objective of this chapter is to verify the results obtained in Chapters 3 and 4. The procedures followed to measure the experimental values were explained in detail and each result for each PCB was analyzed.

It was possible to use the MATLAB® to post-process the results in order to show more easily the comparison between the two PCB results in the same plot. The obtained results show that the structures perform well and similar to what was expected in the Simulations. This demonstrates the reliability of the numerical simulations in CST Studio Suite and the analytical calculations done with MATLAB® scripts.

We gave also a discussion on how to detect the touch on a sensor. Initially, we intended to use the resonant frequency change as the detection method, but another way to detect tactile contact was found. This new method was discovered for the cases without the protective layer, i.e. a paper layer. It consists of damping the resonance when a finger is placed on the sensor.

With the obtained measurement results it was possible to validate the theoretical study, the produced structures, and the tools developed with the (MATLAB® script and the macro file. The final prototype can detect a finger touch on 3 sensors with just one connecting microstrip line.

Chapter 6

Conclusions

This chapter presents final remarks on the performed work. The obtained results are analysed, the limitations are presented and possible future work is discussed.

This Masters Degree Thesis began with a focus on understanding the 3D printing methods, the touch sensing approaches, and the EMC concepts, and it evolved into developing useful tools to facilitate more efficient testing and validation of different structures for touch sensors.

6.1 Summary of Developed Research

We started this thesis work by making a State of the Art research regarding the printed electronics using AM, which was followed by analysis of some common types of sensors (physical and chemical). A comparative study of types of materials, inks, and substrates was also done. The main focus of the State of the Art chapter was on the types of touch sensor measurements to understand which methods could be used to detect a touch. During this process, we selected a promising method for detecting a touch with a resonant frequency change, and we used MATLAB® and CST Studio Suite to test and validate this idea. We also discussed the best practices to design a capacitive touch sensor, and gave an explanation of the the issues and concerns related to the electromagnetic compatibility and interference.

Following this thorough State of the Art research, we implemented the analytical models of the sensor capacitance and inductance as functions in MATLAB®. Once we had the functions, we tried to develop a way to test many structural parameter combinations. The solution was a MATLAB® script that runs for all combinations of the structural parameters to find the desired resonant frequency (Chapter 3). With the use of this script a range of possibilities opens up, so that we can easily define the initial parameters and the desired resonant frequencies and a table with possible solutions is returned, with the resonant frequencies fit in the desired range.

After having obtained the structural parameters, it was necessary to test them in a simulator. To have the possibility to test for many parameter combinations (obtained from the MATLAB® script) without a need to manually change the simulated structure, a macro file was developed to use in the simulator. If the structure was assembled every time by hand it would be possible to test only for a small range of parameters, and if the parameters needed to be changed it would be necessary to rebuild the structure every time. Therefore, although to complete this macro a lot of time was invested, it paid off later because it allowed us to create new structures automatically each time the parameters needed to be changed. With

the structures done, it was necessary to excite the circuit and get the S-parameters results. By analyzing these parameters it was possible to detect reflection magnitude peaks at specific frequencies and thus discover the resonance frequencies for each sensor. However, to find out which sensor corresponded to which frequency it was necessary to use the simulator's "monitors" tool. Thus, with the monitors obtained at the resonance frequencies it was possible to see the electric and magnetic fields and the surface currents for each sensor. After testing different parameter settings it was possible to achieve the desired resonant frequencies so as not to interfere with the licensed RF spectrum. With the two structures completed and validated according to the desired resonant frequency, it was possible to export the CST Studio Suite designs layer by layer to make the Gerber files to produce the PCBs (Chapter 4).

With two developed prototype PCBs it was possible to validate the veracity of the MATLAB® script and the simulation macro. The procedures that were followed and the used equipment were detailed, and all the performed tests were analysed and a comparison between the obtained results were made. With the made comparison it was possible to reach to two conclusions about the sensor touch detection/measurement methodology (Chapter 5):

- With the initially proposed methodology, the resonant frequency shifts when the sensor is touched with a finger;
- With the discovered resonance damping methodology, the resonance of the sensor is dumped when it is touched with a finger.

6.2 Main Results

The main results achieved can be separated into two categories: tools and results. The main tools created in this thesis were:

1. **Capacitance and inductance functions:** For the IDE and spiral geometries, these functions allow you to get the sensor capacitance and the coil inductance by giving the structural parameters. These functions can be very useful because they make the code more flexible and automated. Also these functions can be reused;
2. **Script to obtain the structural parameters for the desired resonant frequencies:** It is very important to test different sets of initial parameters and after that confirm the results in the simulator. Providing the initial arguments to the developed functions allows one to get different structural parameters needed to obtain the desired resonant frequencies;
3. **Macro file:** creates a very complex 3D structure with different types of materials for each structure. It is very useful for changing structural parameters and recreating a new structure. It can be reused to test different structures.

Regarding the main results achieved:

1. **The results based on the change in frequency:** these were acceptable results for the case when a finger was placed on a sensor; the sensor "reacts" with the resonant frequency change. The simulations, and the performed measurements prove the reliability of this method;

2. **The results based on the resonance damping:** this gave very good results for the case when a finger is placed on the sensor; the resonance is attenuated. This method was discovered when the measurements were made. By using the simulations and the taken measurements we proved the reliability of this method as well. This method may perform better than the previous method because when a finger is placed on the sensor, this method does not cause any interference to the response of the surrounding sensors;

3. **The reliability of the tools developed:** this has been tested with significant results obtained. The capacitance function and the MATLAB® script were tested in simulator. The macro was tested in the simulator and with experimental measurements. The obtain results were very similar as was shown in Analysis and Discussion Chapters.

4. **Read 3 different frequencies with one just microstrip line.** From the obtained results it was possible to conclude that the developed structure can read 3 different resonant frequencies using only one microstrip. This has the advantage of resulting in a simpler and more robust sensor design.

6.3 Limitations

During the research and developments, some constraints occurred that were beyond our control, limiting the results of our work.

1. There was a problem with the software license for CST Studio Suite. The student license does not have many tools (for example the macro tool) and is not compatible with the academic license. With this it was necessary to redo the whole structure for a new license that has more tools such as the macro.

2. Limitations on simulations. Using FDS sometimes the simulator needed to calculate about 1 million tetrahedrons, and with the used laptop the simulations time was about 2 to 3 days per one simulation.

3. Frequencies overlap. The available frequency ranges in the RF spectrum can be insufficient for structures having many sensors. Since the available frequencies are close to each other, this causes a limitation to our method. In addition, care must be taken with the frequencies of other devices in order not to affect them, nor allowing them to affect our sensor.

6.4 Future Work

The work developed in this Masters Degree thesis proves the feasibility of the proposed structures and tools to develop touch sensors. This Master's thesis answers some important questions mentioned in 1.1 section, and it also allows to formulate new questions as follows:

- What types of materials are the best performing electrical conductors to be used in AM?

- Which are the best materials for printing the structures?

- Has the UX been improved?

- What interferences do these sensors have (can cause) in the automotive environment?

Thus, a number of possible future improvements for this work could be identified and proposed:

- Realizing these structures with different materials using AM. Taking measurements and drawing conclusions about the best methods and materials to use.
- Assembling a structure in a test car environment and performing reliability tests with real users.
- In this dissertation we have focused on designing tools and building the prototypes of the developed touch sensors, however, we did not study the behavior of these structures under surrounding interferences from other devices. Thus, future work is needed to study and perform measurements on these sensors subjected to electromagnetic interference for a better EMC assesment.

Currently, as the Master's Thesis is integrated in the AM4SP project, we are printing these sensors using the 3D printing technique to investigate the reliability of printing these sensors using additive manufacturing techniques.

Bibliography

[1] D. G. Bekas, Y. Hou, Y. Liu, and A. Panesar. 3D printing to enable multifunctionality in polymer-based composites: A review, dec 2019.

[2] Scopus - Document search . URL: `https://www.scopus.com/search/form.uri#basic`.

[3] McKinsey & Company Analysis. Automotive Electronics Architecture of the Future – Implications for semiconductor companies. 2018.

[4] Robert N. Charette. This Car Runs on Code - IEEE Spectrum. *Notes*, pages 1–8, 2010.

[5] Qiansu. Wan. *Life Cycle Assessment of Paper Based Printed Circuits*. 2017.

[6] ISO/ASTM. Additive Manufacturing - General Principles Terminology (ASTM52900). *Rapid Manufacturing Association*, page 2, 2013.

[7] Wai Houng Chou, Alexander Gamboa, and Javier O. Morales. Inkjet printing of small molecules, biologics, and nanoparticles. *International Journal of Pharmaceutics*, 600:3, may 2021.

[8] Rahul Patidar, Daniel Burkitt, Katherine Hooper, David Richards, and Trystan Watson. Slot-die coating of perovskite solar cells: An overview. *Materials Today Communications*, 22:2, mar 2020.

[9] Alaa Abdellah, Bernhard Fabel, Paolo Lugli, and Giuseppe Scarpa. Spray deposition of organic semiconducting thin-films: Towards the fabrication of arbitrary shaped organic electronic devices. *Organic Electronics*, 11(6):1033, jun 2010.

[10] Daniel Moldenhauer, Doan Chau Yen Nguyen, Lisa Jescheck, Franz Hack, Dagmar Fischer, and Achim Schneeberger. 3D screen printing – An innovative technology for large-scale manufacturing of pharmaceutical dosage forms. *International Journal of Pharmaceutics*, 592:120096, jan 2021.

[11] Rita Faddoul, Nadège Reverdy-Bruas, Anne Blayo, Thomas Haas, and Christian Zeilmann. Optimisation of silver paste for flexography printing on LTCC substrate. *Microelectronics Reliability*, 52(7):1483–1491, jul 2012.

[12] Giuliano Sico, Maria Montanino, Carmela Tania Prontera, Anna De Girolamo Del Mauro, and Carla Minarini. Gravure printing for thin film ceramics manufacturing from nanoparticles. *Ceramics International*, 44(16):19526–19534, nov 2018.

[13] Cleary, Feargal; Microchip Technology Inc. Capacitive touch sensor design guide. pages 1–39, 2019.

[14] Steffen O.P. Blume, Ridha Ben-Mrad, and Pierre E. Sullivan. Modelling the capacitance of multi-layer conductor-facing interdigitated electrode structures. *Sensors and Actuators, B: Chemical*, 213:423–433, jul 2015.

[15] Rui Igreja and C. J. Dias. Analytical evaluation of the interdigital electrodes capacitance for a multi-layered structure. *Sensors and Actuators, A: Physical*, 112(2-3), 2004.

[16] Xiaohui Hu and Wuqiang Yang. Planar capacitive sensors - Designs and applications. *Sensor Review*, 30(1):24–39, 2010.

[17] Atmel Corporation. Touch sensors, Design Guide. pages 1–72, 2008-2009.

[18] H. A. Aebischer. Inductance formula for rectangular planar spiral inductors with rectangular conductor cross section. *Advanced Electromagnetics*, 9(1):1–18, Feb. 2020.

[19] H. Kempa, U. Fügmann, U. Hahn, M. Bartzsch, K. Reuter, M. Hambsch, G. Schmidt, K. Weigelt, T. Fischer, B. Trnovec, M. Stanel, D. Sonntag, N. Wetzold, B. Meier, G. Schlegel, and A. C. Hübler. Progress in mass-printed electronics. *3rd International Symposium Technologies for Polymer Electronics - TPE 08*, page 146, 2008. Cited By :2.

[20] Helmut Kipphan. Fundamentals. In *Handbook of Print Media*, pages 1–202. Springer Berlin Heidelberg, Berlin, Heidelberg, 2001.

[21] Anne Blayo and Bernard Pineaux. Printing processes and their potential for RFID printing. In *ACM International Conference Proceeding Series*, volume 121, pages 27–30. Association for Computing Machinery (ACM), 2005.

[22] Mohammad Reza Khosravani and Tamara Reinicke. 3D-printed sensors: Current progress and future challenges, apr 2020.

[23] ANACOM. Quadro nacional de atribuição de frequências. pages 1–253, 2015. URL: `https://www.anacom.pt/streaming/qnaf20092010_07042010.pdf?contentId=1019281&field=ATTACHED_FILE`, visited on 2021-05-23.

[24] S.S. Mohan, M. del Mar Hershenson, S.P. Boyd, and T.H. Lee. Simple accurate expressions for planar spiral inductances. *IEEE Journal of Solid-State Circuits*, 34(10):1419–1424, 1999.

[25] P.s Hall and Yang Hao. Antennas and propagation for body centric communications. volume 626, pages 1 – 7, 12 2006.

[26] Ford Motor Company. [Online]. , note = URL: `https://corporate.ford.com/articles/history/the-model-t.html`, (visited on 2021-05-05).

[27] Fabrice Alizon, Steven B. Shooter, and Timothy W. Simpson. Henry Ford and the Model T: lessons for product platforming and mass customization. *Design Studies*, 30(5):588–605, sep 2009.

[28] Tanisha Pereira, John V. Kennedy, and Johan Potgieter. A comparison of traditional manufacturing vs additive manufacturing, the best method for the job. In *Procedia Manufacturing*, volume 30, page 12. Elsevier B.V., jan 2019.

[29] Antonio Jimeno-Morenilla, Philip Azariadis, Rafael Molina-Carmona, Sofia Kyratzi, and Vassilis Moulianitis. Technology enablers for the implementation of Industry 4.0 to traditional manufacturing sectors: A review. *Computers in Industry*, 125:103390, feb 2021.

[30] Mohsen Attaran. The rise of 3-D printing: The advantages of additive manufacturing over traditional manufacturing. *Business Horizons*, 60(5):677–688, sep 2017.

[31] Mohammad Reza Khosravani and Tamara Reinicke. On the environmental impacts of 3D printing technology. *Applied Materials Today*, 20:100689, sep 2020.

[32] Paula Vilarinho and Ana Alves Silva. AM4SP – Additive Manufacturing for Smart Plastics (Technical Annex). Technical report, Universidade de Aveiro, Simoldes Plásticos, 2020.

[33] The Mathworks, Inc., Natick, Massachusetts. *MATLAB version 9.3.0.713579 (R2019b)*, 2019.

[34] 3D Experience Company. *CST Studio Suite version 2020.07 (July 10 2020), version Academic*, 2020.

[35] Zhou Ping Yin, Yong An Huang, Ning Bin Bu, Xiao Mei Wang, and You Lun Xiong. Inkjet printing for flexible electronics: Materials, processes and equipments, oct 2010.

[36] Almudena Rivadeneyra and Juan Antonio López-Villanueva. Recent advances in printed capacitive sensors, 2020.

[37] Al-Chami. H. Inkjet Printing of Transducers, University of British Columbia: Vancouver, BC, Canada. 2010.

[38] J. Karthikeyan. The advantages and disadvantages of the cold spray coating process. In *The Cold Spray Materials Deposition Process: Fundamentals and Applications*. Elsevier Ltd., jan 2007.

[39] Eerik Halonen, Kimmo Kaija, Matti Mantysalo, Antti Kemppainen, Ronald Osterbacka, and Niklas Bjorklund. Evaluation of printed electronics manufacturing line with sensor platform application. In *2009 European Microelectronics and Packaging Conference*, pages 1–8, 2009.

[40] Gianni Stano, Attilio Di Nisio, Annamaria Lanzolla, and Gianluca Percoco. Additive manufacturing and characterization of a load cell with embedded strain gauges. *Precision Engineering*, 62:113–120, mar 2020.

[41] James Britton, Katarzyna Krukiewicz, Malu Chandran, Jorge Fernandez, Anup Poudel, Jose-Ramon Sarasua, Una Fitzgerald, and Manus J.P. Biggs. A flexible strain-responsive sensor fabricated from a biocompatible electronic ink via an additive-manufacturing process. *Materials & Design*, 206:109700, apr 2021.

[42] Joseph T. Muth, Daniel M. Vogt, Ryan L. Truby, Yiğit Mengüç, David B. Kolesky, Robert J. Wood, and Jennifer A. Lewis. Embedded 3D printing of strain sensors within highly stretchable elastomers. *Advanced Materials*, 26(36):6307–6312, sep 2014.

[43] Md Taibur Rahman, Arya Rahimi, Subhanshu Gupta, and Rahul Panat. Microscale additive manufacturing and modeling of interdigitated capacitive touch sensors. *Sensors and Actuators, A: Physical*, 248:94–103, sep 2016.

[44] Yeonju Kim, Yepu Cui, Manos M. Tentzeris, and Sungjoon Lim. Additively manufactured electromagnetic based planar pressure sensor using substrate integrated waveguide technology. *Additive Manufacturing*, 34:101225, aug 2020.

[45] Pengyu Zhou, Wuxiong Cao, Yaozhong Liao, Kai Wang, Xiongbin Yang, Jianwei Yang, Yiyin Su, Lei Xu, Li min Zhou, Zhong Zhang, and Zhongqing Su. Temperature effect on all-inkjet-printed nanocomposite piezoresistive sensors for ultrasonics-based health monitoring. *Composites Science and Technology*, 197:108273, sep 2020.

[46] Ahmed Salim and Sungjoon Lim. Review of recent inkjet-printed capacitive tactile sensors, nov 2017.

[47] Capacitive Sensing Basics — CapTIvate ™ Technology Guide 1.83.00.08 documentation.

[48] C. L. W. Sonntag, E. A. Lomonova, and J. L. Duarte. Implementation of the neumann formula for calculating the mutual inductance between planar pcb inductors. In *2008 18th International Conference on Electrical Machines*, pages 1–6, 2008.

[49] Ruinan Chang, Jie Wang, Wenjun Zhang, and Zhiping Yu. An analytical method for the calculation of self and mutual inductance on rf circuit. In *2007 7th International Conference on ASIC*, pages 1129–1132, 2007.

[50] a. Eroglu. Progress In Electromagnetics Research B, Vol. 35, 53–67, 2011. *Progress In Electromagnetics Research B*, 35(August):53–67, 2011.

[51] E. B. Rosa and F. W. Grover. Formulas and tables for the calculation of mutual and self-inductance (Revised). *Bulletin of the Bureau of Standards*, 8(1):1, jan 1912.

[52] Ashraf B. Islam, Syed K. Islam, and Fahmida S. Tulip. Design and Optimization of Printed Circuit Board Inductors for Wireless Power Transfer System. *Circuits and Systems*, 04(02):237–244, apr 2013.

[53] H Nagaoka. The Inductance Coefficients of Solenoids, 1909.

[54] Samuel Zuk, Alena Pietrikova, and Igor Vehec. Capacitive touch sensor. *Microelectronics International*, 35(3):153–157, jan 2018.

[55] C G Xie, A L Stott, A Plaskowski, and M S Beck. Design of capacitance electrodes for concentration measurement of two-phase flow. *Measurement Science and Technology*, 1(1):65–78, jan 1990.

[56] Almudena Rivadeneyra, José Fernández-Salmerón, Manuel Agudo-Acemel, Juan A. López-Villanueva, Luis Fermín Capitan-Vallvey, and Alberto J. Palma. Printed electrodes structures as capacitive humidity sensors: A comparison. *Sensors and Actuators, A: Physical*, 244:56–65, jun 2016.

[57] Cheng P. Wen. Coplanar Waveguide: A Surface Strip Transmission Line Suitable for Nonreciprocal Gyromagnetic Device Applications. *IEEE Transactions on Microwave Theory and Techniques*, 17(12):1087–1090, 1969.

[58] The European Parliament and 26 February 2014. Directive 2014/30/EU on the harmonisation of the laws of the Member States relating to electromagnetic compatibility the Council.

[59] *EMC Fundamentals*, chapter 1, pages 1–21. John Wiley & Sons, Ltd, 1998.

[60] Mandeep Kaur, Shikha Kakar, and Danvir Mandal. Electromagnetic interference. In *2011 3rd International Conference on Electronics Computer Technology*, volume 4, pages 1–5, 2011.

[61] Yunfeng Xi, Javier A Salcedo, Yuanzhong Zhou, Juin J Liou, and Jean-Jacques Hajjar. Introductory Invited Paper Design and characterization of ESD solutions with EMC robustness for automotive applications. 2015.

[62] [Online] ANACOM - Frequencies. URL: `https://www.anacom.pt/render.jsp?categoryId=334998&languageId=1`, visited on 2021-05-23.

[63] Milton Abramowitz, Irene A. Stegun, and Robert H. Romer. Handbook of Mathematical Functions with Formulas, Graphs, and Mathematical Tables . *American Journal of Physics*, 56(10):958–958, oct 1988.

[64] Milton Abramowitz. *Handbook of Mathematical Functions, With Formulas, Graphs, and Mathematical Tables*. Dover Publications, Inc., USA, 1974.

[65] Tobin A. Driscoll and Lloyd N. Trefethen. *Schwarz-Christoffel Mapping*. Cambridge Monographs on Applied and Computational Mathematics. Cambridge University Press, 2002.

[66] milan batista. elfun18 - MATLAB Central File Exchange. URL: https://www.mathworks.com/matlabcentral/fileexchange/65915-elfun18.

[67] G.D. Alley. Interdigital capacitors and their application to lumped-element microwave integrated circuits. *IEEE Transactions on Microwave Theory and Techniques*, 18(12):1028–1033, 1970.

[68] Agilent Technologies Inc. Agilent AN 154 S-Parameter Design. *Agilent Tehnologies, Inc., Application Note*, pages 1–44, 2006.

[69] H.A. Wheeler. Transmission-line properties of parallel strips separated by a dielectric sheet. *IEEE Transactions on Microwave Theory and Techniques*, 13(2):172–185, 1965.

Chapter 7

Appendices

7.1 Appendix A: Substrates Available

Table 7.1 shows the substrates available on Aveiro IT that can be used.

7.2 Appendix B: Auxiliary Equations to obtain Resonant Frequency

7.2.1 Auxiliary Equations to Calculate Capacitance

The Jacobi theta functions [63, 64] are given by the following equations:

$$\partial_1(u,q) = 2q^{\frac{1}{4}} \sum_{n=0}^{\infty} -1^n q^{n(n+1)} \sin{(2n+1)u} \tag{7.1}$$

$$\partial_2(u,q) = 2q^{\frac{1}{4}} \sum_{n=0}^{\infty} (q^{n(n+1)} \cos{(2n+1)u} \tag{7.2}$$

$$\partial_2(u,q) = 1 + 2\sum_{n=1}^{\infty} q^{n^2} \cos{(2nu)} \tag{7.3}$$

$$\partial_2(u,q) = 1 + 2\sum_{n=1}^{\infty} (-1)^n q^{n^2} \cos{(2nu)} \tag{7.4}$$

7.2.2 Auxiliary Equations to Calculate Inductance

The following equations and approximations are made to be more accessible to achieve the ultimate goal, to calculate the total inductance. The approximations for the mean distances are [18]:

$$GMD_1 \approx 0.2235(s+h) \tag{7.5}$$

$$\log GMD_1 \approx \log(s+h) - \frac{3}{2} \tag{7.6}$$

Available substrates			
Substrate	Thickness	Cladding	DK*
FR4	$0.8mm$	35μm	4.3 - 4-7
FR4	$1mm$	17.5μm	4.3 - 4-7
FR4	$1mm$	35μm	4.3 - 4-7
FR4	$1.6mm$	17.5μm	4.3 - 4-7
FR4	$1.6mm$	35μm	4.3 - 4-7
FR4 (single layer)	$1.6mm$	35μm	4.3 - 4-7
Rogers RO4725JXR	$0.78mm$	17.5μm	2.55
Rogers RO4725JXR	$1.54mm$	17.5μm	2.55
Rogers RO4360G2	$1.524mm$	17.5μm	6.15
Rogers RO4360G2	$0.81mm$	17.5μm	6.15
Isola IS680	$0.76mm$	35μm	3.38
Isola IS680	$1.52mm$	35μm	3.38
Isola Astra	$0.76mm$	35μm	3
Isola Astra	$1.52mm$	35μm	3
Rogers RO4350B	$0.76mm$	17.5μm	3.48

* The DK corresponds to the dielectric constant of the substrate.

Table 7.1: Overview of substrates available in Aveiro IT.

Where s is the width, and h is height of a single rectangle. AMD_1 can be calculated as:

$$AMD_1 \approx \frac{\sqrt{s^2 + h^2 + 0.46sh}}{3} \tag{7.7}$$

The formula 7.7 gives a precision of about 2 %. In the literature, AMD can be approximated by GMD.

$$AMD_1 \approx GMD_1 AMD_2 \approx GMD_2 \tag{7.8}$$

$$\log GMD_2 \approx \log(s+h) - \frac{k}{2} - \frac{-1.46\gamma + 1.45}{2.14\gamma + 1} \tag{7.9}$$

$$AMSD_1^2 = \frac{1}{6}(s^2 + h^2) \tag{7.10}$$

7.2.3 Relative Permittivity of Body Tissue

The following table gives the values of the relative permittivity of the body tissue (ϵ_r), used to calculate the resonant frequency when touching the sensor with the finger.

Relative Permittivity of Body Tissue	
	ϵ_1
Muscle	50.00
Skin(dry)	32.00
Skin(wet)	39.00

Table 7.2: Relative Permittivity of Body Tissue at any frequency. Adapted: [25].

7.3 Appendix C: Equations to calculate the impedance of microstrip

The following equations are used to calculate the characteristic impedance of the microstrip [69].

$$Z_0 = \frac{\eta_0}{2.0\sqrt{2.0}\pi(\epsilon_r + 1)^{\frac{1}{2}}} \left[\ln 1.0 + \frac{4.0h}{w_{eff}}(A + B)^{\frac{1}{2}}\right] \tag{7.11}$$

where A is given by:

$$A = \frac{14.0 + \frac{8.0}{\epsilon_r}}{11.0}\frac{4.0h}{w_{eff}} \tag{7.12}$$

and B is given by:

$$B = \left(A^2 + \frac{1.0 + \frac{1.0}{\epsilon_r}}{2.0}\pi^{\frac{1}{2}}\right)^{\frac{1}{2}} \tag{7.13}$$

with w_{eff} being:

$$w_{eff} = W + \left(\frac{t}{\pi}\right)\ln\frac{4e}{\sqrt{(\frac{T}{H})^2 + (\frac{T}{W_\pi + 1.1T_\pi})^2}}\frac{\epsilon_r + 1}{2\epsilon_r} \tag{7.14}$$

7.4 Appendix D: Capacitance function code

The accompanying function shows the code used to help calculate the capacitance using PCT for different configurations, with or without a finger and with or without a protective layer.

```
1   function [C, eta, r_s] = capacitance_epsilon_effect(h_s, W_C, G_C, ...
        Nfingers, epsilon1_r, epsilonS_r, L,option)
2   epsilon0 = 8.8541878128e-12;          % epsilon0 - vacuum
3   h_1 = 0.03;                           % finger tissue height
4   h_2 = 0.0001;                         % paper layer height
5
6   filling_factor = 0.12566;             % percentage of sensor cover by ...
        the finger
7   epsilon2_r = 2.31;
8   if option == 1 && epsilon1_r == 50    % with finger placed and paper layer
9       eps_eff = (h_1+h_2)/((h_1/epsilon1_r) + (h_2/epsilon2_r));  % use ...
            epsilon effective
10      eps_eff = filling_factor*eps_eff + (1-filling_factor)*1;
```

```
11      elseif option == 2 && epsilon1_r == 50 % with finger placed and ...
            without protective layer
12          eps_eff = epsilon1_r;              % use epsilon effective
13          eps_eff = filling_factor*eps_eff + (1-filling_factor)*1;
14      elseif option == 3 || epsilon1_r ≠ 50
15          epsilon2_r = epsilon1_r;            % just with protective layer
16          eps_eff = (h_1+h_2)/((h_1/epsilon1_r) + (h_2/epsilon2_r));  % use ...
                epsilon effective
17      elseif option == 0
18          eps_eff = 1;                       % without finger and without ...
                protective layer (infinite air layer)
19                                             % to cancel the second addend
20                                             % in Ci and Ce formula
21      end
22      lambda = 2*(W_C+G_C);                  % spatial wavelength
23      eta = (2*W_C)/lambda;                  % metallization
24
25      u = 0;
26      % initial parameters for interior, substrate term
27      r_s = h_s /lambda;
28      q_s = exp(-4*pi*r_s);
29      v2_int_s = jtheta2(u,q_s);
30      v3_int_s = jtheta3(u,q_s);
31
32      % initial parameters for interior, 1st term
33      r_1 = (h_2+h_1) /lambda;
34      q_1 = exp(-4*pi*r_1);
35      v2_int_1 = jtheta2(u,q_1);
36      v3_int_1 = jtheta3(u,q_1);
37
38      % arrays
39      v2_array = [v2_int_1 v2_int_s];
40      v3_array = [v3_int_1 v3_int_s];
41      r_array = [r_1 r_s];
42
43      % to confirm if function theta give great results
44      confirme = 0;
45      v2_aux = 0;
46      v3_aux = 0;
47      if confirme == 1
48          for n = 0:200000-1
49              v2_aux = v2_aux + q_int^(n*(n+1)) * cos((2*n+1)*u);
50              v3_aux = v3_aux + q_int^(n+1)^2 * cos(2*(n+1)*u);
51          end
52          v2_aux = v2_aux*2*q_int^(1/4)
53          v3_aux = 1+2*v3_aux
54      end
55
56      %---- Interior ----  ( below )
57
58      for i = 1:length(v2_array)
59          k(i) = (v2_array(i)/v3_array(i))^2;
60          K(i) = ellipke(k(i));
61          z2(i) = K(i) * eta;
62          t2(i) = ellipj(z2(i),k(i));        % ellipj return SN
63          t4(i) = 1/k(i);
64
```

```
65          k_i(i) = t2(i)*sqrt(((t4(i)^2)-1)/((t4(i)^2)-(t2(i)^2)));  ...
                %((v2)/(v3))^2;          % modulus
66          k_c_i(i) = sqrt(1-(k_i(i)^2));     % modulus complementary
67          K_i(i) = ellipke(k_i(i));          % k big
68          K_c_i(i) = ellipke(k_c_i(i));      % k big complementary
69      end
70
71      % for infinite term
72      k_i_inf = sin((pi/2)*eta);
73      k_c_i_inf = sqrt(1-(k_i_inf^2));
74      K_i_inf = ellipke(k_i_inf);
75      K_c_i_inf = ellipke(k_c_i_inf);
76
77      % -- Capacitante interior
78
79      Ci = epsilon0 * L * [(K_i_inf/K_c_i_inf) + (eps_eff-1) * ...
            (K_i(1)/K_c_i(1)) ...
80                           + epsilonS_r * (K_i(2)/K_c_i(2))];
81         %addend1=(K_i_inf/K_c_i_inf)
82         %addend2=(eps_eff-1) * (K_i(1)/K_c_i(1))
83         %addend3=epsilonS_r * (K_i(2)/K_c_i(2))
84
85      %---- Exterior ----
86      for i = 1:length(v2_array)
87          t3(i) = cosh((pi * (1-eta))/(8*r_array(i)));
88          t4(i) = cosh((pi * (eta+1))/(8*r_array(i)));
89          k_e(i) = (1/t3(i)) * sqrt((t4(i)^2 - t3(i)^2)/((t4(i)^2)-1));
90          k_c_e(i) = sqrt(1-(k_e(i)^2));     % modulus complementary
91          K_e(i) = ellipke(k_e(i));          % k big
92          K_c_e(i) = ellipke(k_c_e(i));      % k big complementary
93      end
94
95      % for infinite
96      k_e_inf = (2*sqrt(eta))/(1+eta);
97      k_c_e_inf = sqrt(1-(k_e_inf)^2);
98      K_e_inf = ellipke(k_e_inf);
99      K_c_e_inf = ellipke(k_c_e_inf);
100
101     % -- Capacitante exterior
102
103     Ce = epsilon0 * L * [(K_e_inf/K_c_e_inf) + (eps_eff-1) * ...
            (K_e(1)/K_c_e(1)) ...
104                          + epsilonS_r * (K_e(2)/K_c_e(2))];
105 %       addend1 =(K_e_inf/K_c_e_inf)
106 %       addend2 = (eps_eff-1) * (K_e(1)/K_c_e(1))
107 %       addend3 = epsilonS_r * (K_e(2)/K_c_e(2))
108
109     % --- Total capacitance
110     C = (Nfingers-3)*(Ci/2) + 2*((Ci*Ce)/(Ci+Ce));
111     %fprintf('-- Total capacitance: %4.6d\n\n',C)
```

7.5 Appendix E: MATLAB script

The following script is used to obtain the parameters for the resonant frequencies in desired range. It provides three tables with the parameters, and the corresponding resonant

frequencies of each sensor.

```
%% Script used to obtain the parameters at the desired frequencies
clear all
close all
clc

format shortE
            % initial parameters
h_s = 1.52e-3;                      % Substrate thickness
h_L = 0.035e-3;
epsilon1_r = [50 1];                % epsilon1 relative
epsilonS_r = 3;                     % epsilon substrate relative
Strip_length = 2e-2;                % length of the electrodes strips

W_M = 0.0025;                       % width of microstrip
vias_out = 0.0008;                  % radius of external vias

B = 0.04;                           % sensor size
A = 0.04;                           % sensor size

aux3 = 1;
aux2 = 1;
aux1 = 1;

Nfingers =5:1:19;                    % Number of electrodes of interdigital ...
    capacitor
auxN = Nfingers(length(Nfingers)) - Nfingers(1);
auxN = auxN +3;
Nloops = 2:1:10;                       % Number of loops
W_C = 0.3e-3:0.1e-3:4.2e-3;       % ftingers have a width

lines = ones(length(W_C),1);       % this part is to increment the lines
for i = 1 :length(W_C)             % into the excel
    lines(i) = lines(i)*(i-1)*length(Nfingers);
end
min_and_max = [inf 0 inf 0]';      % min and max of resonant frequency (two ...
    first row
                                   % - with human finger finger and two ...
                                       last without)

freq_selected = [28e6 40e6 144.8e6]';     % obtain the parameters from the ...
    frequency selected

CST_result_sensor3 = 122.9e6;
%shift_S1 = freq_selected(1) - CST_result_sensor1;
%shift_S2 = freq_selected(2) - CST_result_sensor2;
shift_S3 = freq_selected(3) - CST_result_sensor3;
%freq_shifted(1) = freq_selected(1)+ shift_S1;
%freq_shifted(2) = freq_selected(2) + shift_S2;
%freq_shifted(3) = freq_selected(3) + shift_S3;
%shift_S3_v2 = freq_selected(3) - CST_result_sensor3v2;
%freq_selected(3) = freq_shifted(3);

margin1 = 0.5e6;              % margin for desired resonant frequency of ...
    sensor 1
```

```
margin2 = 0.5e6;                % margin for desired resonant frequency of ...
    sensor 2
margin3 = 2e6;                % margin for desired resonant frequency of ...
    sensor 3


cap_option = 1;                % with 0 - without finger and without ...
    protective layer
                               % with 1 - with finger placed and protective layer
                               % with 2 - with finger placed and without ...
                                   protective layer
                               % with 3 - just with protective layer
if cap_option == 0
    label0 = {'Frequency inf ...
        air','Nloops','Nfingers','W_C','G_C','W_L','G_L'};
elseif cap_option == 1
    label1 = {'Frequency','Freq. w/ finger and paper ...
        layer','Nloops','Nfingers','W_C','G_C','W_L','G_L'};
elseif cap_option == 2
    label2 = {'Frequency','Freq. w/ finger and without paper ...
        layer','Nloops','Nfingers','W_C','G_C','W_L','G_L'};
elseif cap_option == 3
    label3 = {'Freq. w/ protective ...
        layer','Nloops','Nfingers','W_C','G_C','W_L','G_L'};
end

for j = 1:length(epsilon1_r)
    for k = 1:length(W_C)
        for i = 1:length(Nfingers)
            for aux = 1:length(Nloops)
                W_L(aux,i) = ((B - (Strip_length ...
                    +(vias_out*2)))/Nloops(aux))/4;       % divide by 4 ...
                    because exists 2 loops and G_L and W_L
                G_L(aux,i) = W_L(aux,i);
                Winding_dis = 2*W_L(aux,i);          % winding distance
                %auxiliar_A(aux,i)= Strip_length +vias_out*2+ ...
                    Nloops(aux)*( W_L(aux,i)*2*2);
                total_filled = Nfingers(i)*W_C(k) + 2*Nloops(aux)* ...
                                (W_L(aux,i)+G_L(aux,i))-W_L(aux,i)+ ...
                                    2*vias_out;     % longer side length ...
                                    (mid-conductor)
                free_space(aux,i) = A - total_filled;
                G_C(aux,i) = free_space(aux,i) / (Nfingers(i));

                if free_space(aux,i) ≥ 0 && W_L(aux,i)>0.3e-3 && ...
                    G_C(aux,i) >0.3e-3 && G_L(aux,i) > 0.3e-3
                    C(aux,i) = capacitance_epsilon_effect(h_s, W_C(k), ...
                        G_C(aux,i), Nfingers(i),...
                        epsilon1_r(j), epsilonS_r, Strip_length, ...
                            cap_option);       % without permittivity of finger
                    L(aux,i) = L_RectPlanarSpiral(Nloops(aux), A, B, ...
                        Winding_dis, W_L(aux,i), h_L);
                         % Calculate resonante freq
                    omega(aux,i) = 1/sqrt(L(aux,i)*C(aux,i));
                    if j == 1       % with human tissue
                        fr(aux+lines(k),i) = omega(aux,i)/(2*pi);

```

```
90                          if min_and_max(1,1) > fr(aux+lines(k),i)        % ...
                                min with human tissue
91                              min_and_max(1,1) = fr(aux+lines(k),i);      % ...
                                    to obtain the min and max of fr and its ...
                                    parameters
92                              paramet_min_max(1,:) = [aux+1 i+4 k G_C(aux,i) ...
                                    W_L(aux,i) ];  % [Nloops Nfingers W_C] or ...
                                    [aux i k]: i-column; k: lines(k) + aux ...
                                    obtain the line
93                          end
94                          if min_and_max(2,1) < fr(aux+lines(k),i) ...
                                            % max with human tissue
95                              min_and_max(2,1)  = fr(aux+lines(k),i);
96                              paramet_min_max(2,:) = [aux+1 i+4 k G_C(aux,i) ...
                                    W_L(aux,i)];    % [Nloops Nfingers W_C]
97                          end
98                      else           % without human tissue
99                          fr(aux+lines(k),i+auxN) = omega(aux,i)/(2*pi);
100                         if min_and_max(3,1) > fr(aux+lines(k),i+auxN) ...
                                            % min without human tissue
101                             min_and_max(3,1)   = fr(aux+lines(k),i+auxN);
102                             paramet_min_max(3,:) = [aux+1 i+4 k G_C(aux,i) ...
                                    W_L(aux,i)]; % [Nloops Nfingers W_C]
103                         end
104                         if min_and_max(4,1) < fr(aux+lines(k),i+auxN) ...
                                            % max without human tissue
105                             min_and_max(4,1)  = fr(aux+lines(k),i+auxN);
106                             paramet_min_max(4,:) = [aux+1 i+4 k G_C(aux,i) ...
                                    W_L(aux,i)]; % [Nloops Nfingers W_C]
107                         end
108
109                         if freq_selected(1,1)< ...
                                fr(aux+lines(k),i+auxN)+margin1 && ...
                                freq_selected(1,1)> ...
                                fr(aux+lines(k),i+auxN)-margin1         % max ...
                                with human tissue
110                             paramet_freq_1(aux1,:) = [aux+1 i+4 W_C(k) ...
                                    G_C(aux,i) W_L(aux,i) G_L(aux,i)];
111                             check_freq_1(aux1,:) = fr(aux+lines(k),i+auxN);
112                             check_freq_1_wfinger(aux1,:) = fr(aux+lines(k),i);
113                             row_column_freq_1(aux1,:) = [lines(k)+aux i+auxN];
114                             sensibility1(aux1,:) = (check_freq_1(aux1,:) - ...
                                    check_freq_1_wfinger(aux1,:))/...
115                                         (check_freq_1_wfinger(aux1,:));
116                             aux1=aux1+1;
117                         elseif freq_selected(2,1)< ...
                                fr(aux+lines(k),i+auxN)+margin2 && ...
                                freq_selected(2,1)> fr(aux+lines(k),i+auxN)-margin2
118                             paramet_freq_2(aux2,:) = [aux+1 i+4 W_C(k) ...
                                    G_C(aux,i) W_L(aux,i) G_L(aux,i)];
119                             check_freq_2(aux2,:) = fr(aux+lines(k),i+auxN);
120                             check_freq_2_wfinger(aux2,:) = fr(aux+lines(k),i);
121                             row_column_freq_2(aux2,:) = [lines(k)+aux i+auxN];
122                             sensibility2(aux2,:) = (check_freq_2(aux2,:) - ...
                                    check_freq_2_wfinger(aux2,:))/...
123                                         (check_freq_2_wfinger(aux2,:));
124                             aux2=aux2+1;
```

```
125                         elseif freq_selected(3,1)< ...
                                fr(aux+lines(k),i+auxN)+margin3 && ...
                                freq_selected(3,1)> fr(aux+lines(k),i+auxN)-margin3
126                             paramet_freq_3(aux3,:) = [aux+1 i+4 W_C(k) ...
                                    G_C(aux,i) W_L(aux,i) G_L(aux,i)];
127                             check_freq_3(aux3,:) = fr(aux+lines(k),i+auxN);
128                             check_freq_3_wfinger(aux3,:) = fr(aux+lines(k),i);
129                             row_column_freq_3(aux3,:) = [lines(k)+aux i+auxN];
130                             sensibility3(aux3,:) = (check_freq_3(aux3,:) - ...
                                    check_freq_3_wfinger(aux3,:))/...
131                                         (check_freq_3_wfinger(aux3,:));
132                             aux3=aux3+1;
133                         end
134                     end
135                     %fprintf('-- resonante freq. %5g \n    ... with L %5g ...
                            \n    ...C %5g \n\n',fr(aux),L(aux),C(aux))
136                 end
137             end
138         end
139     end
140 end
141
142 if cap_option == 0
143     T1 = table(check_freq_1,paramet_freq_1(:,1),...
144             paramet_freq_1(:,2),paramet_freq_1(:,3),paramet_freq_1(:,4),...
145             paramet_freq_1(:,5),paramet_freq_1(:,6),'VariableNames',label0);
146     T2 = table(check_freq_2,paramet_freq_2(:,1),paramet_freq_2(:,2),...
147             paramet_freq_2(:,3),paramet_freq_2(:,4),paramet_freq_2(:,5),...
148             paramet_freq_2(:,6),'VariableNames',label0);
149     T3 = table(check_freq_3,paramet_freq_3(:,1),paramet_freq_3(:,2),...
150             paramet_freq_3(:,3),paramet_freq_3(:,4),paramet_freq_3(:,5),...
151             paramet_freq_3(:,6),'VariableNames',label0);
152 elseif cap_option == 1
153     T1 = table(check_freq_1,check_freq_1_wfinger,paramet_freq_1(:,1),...
154             paramet_freq_1(:,2),paramet_freq_1(:,3),paramet_freq_1(:,4),...
155             paramet_freq_1(:,5),paramet_freq_1(:,6),'VariableNames',label1);
156     T2 = table(check_freq_2,check_freq_2_wfinger,paramet_freq_2(:,1),...
157             paramet_freq_2(:,2),paramet_freq_2(:,3),paramet_freq_2(:,4),...
158             paramet_freq_2(:,5),paramet_freq_2(:,6),'VariableNames',label1);
159     T3 = table(check_freq_3,check_freq_3_wfinger,paramet_freq_3(:,1),...
160             paramet_freq_3(:,2),paramet_freq_3(:,3),paramet_freq_3(:,4),...
161             paramet_freq_3(:,5),paramet_freq_3(:,6),'VariableNames',label1);
162 elseif cap_option == 2
163     T1 = table(check_freq_1,check_freq_1_wfinger,paramet_freq_1(:,1),...
164             paramet_freq_1(:,2),paramet_freq_1(:,3),paramet_freq_1(:,4),...
165             paramet_freq_1(:,5),paramet_freq_1(:,6),'VariableNames',label2);
166     T2 = table(check_freq_2,check_freq_2_wfinger,paramet_freq_2(:,1),...
167             paramet_freq_2(:,2),paramet_freq_2(:,3),paramet_freq_2(:,4),...
168             paramet_freq_2(:,5),paramet_freq_2(:,6),'VariableNames',label2);
169     T3 = table(check_freq_3,check_freq_3_wfinger,paramet_freq_3(:,1),...
170             paramet_freq_3(:,2),paramet_freq_3(:,3),paramet_freq_3(:,4),...
171             paramet_freq_3(:,5),paramet_freq_3(:,6),'VariableNames',label2);
172 elseif cap_option == 3
173     T1 = table(check_freq_1,paramet_freq_1(:,1),paramet_freq_1(:,2),...
174             paramet_freq_1(:,3),paramet_freq_1(:,4),...
175             paramet_freq_1(:,5),paramet_freq_1(:,6),'VariableNames',label3);
176     T2 = table(check_freq_2,paramet_freq_2(:,1),...
```

```
177             paramet_freq_2(:,2),paramet_freq_2(:,3),paramet_freq_2(:,4),...
178             paramet_freq_2(:,5),paramet_freq_2(:,6),'VariableNames',label3);
179     T3 = table(check_freq_3,paramet_freq_3(:,1),...
180             paramet_freq_3(:,2),paramet_freq_3(:,3),paramet_freq_3(:,4),...
181             paramet_freq_3(:,5),paramet_freq_3(:,6),'VariableNames',label3);
182 end
183
184 final_range(1,1) = min_and_max(3,1) - min_and_max(1,1);        % with ...
        human finger
185 final_range(1,2) = min_and_max(4,1) - min_and_max(2,1);        % without ...
        human finger
186
187 xlswrite('Results.xls',fr,'Resonant Frequency');
188 xlswrite('Results.xls',sensibility1,'sensitivity_sensor1');
189 xlswrite('Results.xls',sensibility2,'sensitivity_sensor2');
190 xlswrite('Results.xls',sensibility3,'sensitivity_sensor3');
```

7.6 Appendix F: CST Studio Suite macro

The following macro shows the code to obtain a 3D model for the three sensors, microstrip, vias, substrate, amongst others. When the parameters are changed, the macro provides another 3D model that corresponds to the chosen parameters.

```
1  ' Macro file to create each structure
2
3  Global y_init, ys
4
5  Sub Main ()
6      ' variables declaration
7      Dim I,Iy,Ix,Nfingers, NLoops,Nsensors As Integer
8      Dim Nfingers_S2, NLoops_S2 As Integer
9      Dim Nfingers_S3, NLoops_S3 As Integer
10     Dim aux,aux1,y0,x0,G_C,W_M,G_M,st,G_L,W_L,aux_y,aux_x,vias_in As Double
11     Dim vias_out,y_via1,A_stru_S1, auxiliarAs,b_space_vias As Double
12     Dim M_leng,G_M_y,G_M_x,A,B,G_C0,W_C,W_C_y,xs,b_space,B_stru_S1 As Double
13     Dim G_C_S2,G_M_S2,G_L_S2,W_L_S2,aux_y_S2,aux_x_S2,G_M_y_S2 As Double
14     Dim G_M_x_S2,G_C0_S2,W_C_S2,G_M_x_S3,G_C0_S3,W_C_S3 As Double
15     Dim G_C_S3,G_M_S3,G_L_S3,W_L_S3,aux_y_S3,aux_x_S3,G_M_y_S3 As Double
16     Dim W_C_y_S3,B_stru_S3,A_stru_S3,W_C_y_S2,B_stru_S2,A_stru_S2 As Double
17
18     ' global parameters
19     A = 40                  ' A is the length of the longer loop, from the ...
           middle of the conductors
20     B = 40                  ' B is the width of the longer loop, from the ...
           middle of the conductors
21
22     Nsensors = 3            ' Number of sensors
23
24     vias_in = 0.4           ' dimension of inner vias
25     vias_out = 0.8          ' dimension of outer vias
26     b_space_vias = 2        ' the space between the tracks and the ...
           extremity of board
27
28     W_M = 2.5               ' Width of microstrip
```

```
29      M_leng = 6              ' length of microstrip at start and end
30
31      ' -- -- parameters of sensor 1 -- -- '
32      G_C0 = 0.32300                      ' Gap of capacitance (mm)
33      W_C = 0.5                           ' Gap of capacitor (mm)
34      W_C_y = 0.8
35      G_C = W_C + G_C0
36
37      Nfingers = 25
38      NLoops = 8
39      W_L = 0.575                         ' Width of inductor (mm)
40      G_L = 0.575                         ' Gap of inductor (mm)
41
42      G_M_y = G_L
43      G_M_x = G_L
44
45      aux_y = 2*(NLoops)*(G_L+W_L) + 2*G_M_y
46      aux_x = 2*(NLoops)*(G_L+W_L) + 2*G_M_x
47
48      A_stru_S1 = A+2*G_M_y+W_L
49      B_stru_S1 = aux_x+ls+vias_out+W_L
50
51      ' -- -- parameters of sensor 2 -- -- '
52      G_C0_S2 = 0.47551                   ' Gap of capacitor (mm)
53      W_C_S2 = 1                          ' Width of capacitor(mm)
54      W_C_y_S2 = 0.8
55      G_C_S2 = W_C_S2 + G_C0_S2
56
57      Nfingers_S2 = 14
58      NLoops_S2 = 7
59      W_L_S2 = 0.65714                    ' Width of inductor (mm)
60      G_L_S2 = 0.65714                    ' Gap of inductor (mm)
61
62      G_M_y_S2 = G_L_S2
63      G_M_x_S2 = G_L_S2
64
65      aux_y_S2 = 2*(NLoops_S2)*(G_L_S2+W_L_S2) + 2*G_M_y_S2
66      aux_x_S2 = 2*(NLoops_S2)*(G_L_S2+W_L_S2) + 2*G_M_x_S2
67
68      A_stru_S2 = A+2*G_M_y_S2+W_L_S2
69      B_stru_S2 = aux_x_S2+ls+vias_out+W_L_S2
70
71      ' -- -- parameters of sensor 3 -- -- '
72
73      G_C0_S3 = 1.0118                ' Gap of capacitance (mm)
74      W_C_S3 = 0.3                    ' Width of capacitance (mm)
75      W_C_y_S3 = 1.3
76      G_C_S3 = W_C_S3 + G_C0_S3
77
78      Nfingers_S3 = 17
79      NLoops_S3 = 2
80
81      W_L_S3 = 2.3                    ' Width of inductor (mm)
82      G_L_S3 = 2.3                    ' Gap of inductor (mm)
83
84      G_M_y_S3 = G_L_S3/2.2
85      G_M_x_S3 = G_L_S3/2.2
```

```
86
87      aux_y_S3 = 2*(NLoops_S3)*(G_L_S3+W_L_S3) + 2*G_M_y_S3
88      aux_x_S3 = 2*(NLoops_S3)*(G_L_S3+W_L_S3) + 2*G_M_x_S3
89
90      A_stru_S3 = A+2*G_M_y_S3+W_L_S3
91      B_stru_S3 = aux_x_S3+ls+vias_out+W_L_S3
92
93
94      '@ define material: Isola
95      With Material
96           .Reset
97           .Name "Isola"
98           .Folder ""
99           .Rho "0.0"
100          .ThermalType "Normal"
101          .ThermalConductivity "0"
102          .SpecificHeat "0", "J/K/kg"
103          .DynamicViscosity "0"
104          .Emissivity "0"
105          .MetabolicRate "0.0"
106          .VoxelConvection "0.0"
107          .BloodFlow "0"
108          .MechanicsType "Unused"
109          .FrqType "all"
110          .Type "Normal"
111          .MaterialUnit "Frequency", "MHz"
112          .MaterialUnit "Geometry", "mm"
113          .MaterialUnit "Time", "ns"
114          .MaterialUnit "Temperature", "Celsius"
115          .Epsilon "3.0"
116          .Mu "1"
117          .Sigma "0"
118          .TanD "0.0"
119          .TanDFreq "0.0"
120          .TanDGiven "False"
121          .TanDModel "ConstTanD"
122          .EnableUserConstTanDModelOrderEps "False"
123          .ConstTanDModelOrderEps "1"
124          .SetElParametricConductivity "False"
125          .ReferenceCoordSystem "Global"
126          .CoordSystemType "Cartesian"
127          .SigmaM "0"
128          .TanDM "0.0"
129          .TanDMFreq "0.0"
130          .TanDMGiven "False"
131          .TanDMModel "ConstTanD"
132          .EnableUserConstTanDModelOrderMu "False"
133          .ConstTanDModelOrderMu "1"
134          .SetMagParametricConductivity "False"
135          .DispModelEps  "None"
136          .DispModelMu "None"
137          .DispersiveFittingSchemeEps "Nth Order"
138          .MaximalOrderNthModelFitEps "10"
139          .ErrorLimitNthModelFitEps "0.1"
140          .UseOnlyDataInSimFreqRangeNthModelEps "False"
141          .DispersiveFittingSchemeMu "Nth Order"
142          .MaximalOrderNthModelFitMu "10"
```

```
143           .ErrorLimitNthModelFitMu "0.1"
144           .UseOnlyDataInSimFreqRangeNthModelMu "False"
145           .UseGeneralDispersionEps "False"
146           .UseGeneralDispersionMu "False"
147           .NLAnisotropy "False"
148           .NLAStackingFactor "1"
149           .NLADirectionX "1"
150           .NLADirectionY "0"
151           .NLADirectionZ "0"
152           .Colour "0", "1", "1"
153           .Wireframe "False"
154           .Reflection "False"
155           .Allowoutline "True"
156           .Transparentoutline "False"
157           .Transparency "0"
158           .Create
159      End With
160
161      '@ define material: finger
162      With Material
163           .Reset
164           .Name "finger"
165           .Folder ""
166           .Rho "0.0"
167           .ThermalType "Normal"
168           .ThermalConductivity "0"
169           .SpecificHeat "0", "J/K/kg"
170           .DynamicViscosity "0"
171           .Emissivity "0"
172           .MetabolicRate "0.0"
173           .VoxelConvection "0.0"
174           .BloodFlow "0"
175           .MechanicsType "Unused"
176           .FrqType "all"
177           .Type "Normal"
178           .MaterialUnit "Frequency", "MHz"
179           .MaterialUnit "Geometry", "mm"
180           .MaterialUnit "Time", "ns"
181           .MaterialUnit "Temperature", "Celsius"
182           .Epsilon "50"
183           .Mu "1"
184           .Sigma "0"
185           .TanD "0.0"
186           .TanDFreq "0.0"
187           .TanDGiven "False"
188           .TanDModel "ConstTanD"
189           .EnableUserConstTanDModelOrderEps "False"
190           .ConstTanDModelOrderEps "1"
191           .SetElParametricConductivity "False"
192           .ReferenceCoordSystem "Global"
193           .CoordSystemType "Cartesian"
194           .SigmaM "0"
195           .TanDM "0.0"
196           .TanDMFreq "0.0"
197           .TanDMGiven "False"
198           .TanDMModel "ConstTanD"
199           .EnableUserConstTanDModelOrderMu "False"
```

```
200           .ConstTanDModelOrderMu "1"
201           .SetMagParametricConductivity "False"
202           .DispModelEps  "None"
203           .DispModelMu "None"
204           .DispersiveFittingSchemeEps "Nth Order"
205           .MaximalOrderNthModelFitEps "10"
206           .ErrorLimitNthModelFitEps "0.1"
207           .UseOnlyDataInSimFreqRangeNthModelEps "False"
208           .DispersiveFittingSchemeMu "Nth Order"
209           .MaximalOrderNthModelFitMu "10"
210           .ErrorLimitNthModelFitMu "0.1"
211           .UseOnlyDataInSimFreqRangeNthModelMu "False"
212           .UseGeneralDispersionEps "False"
213           .UseGeneralDispersionMu "False"
214           .NLAnisotropy "False"
215           .NLAStackingFactor "1"
216           .NLADirectionX "1"
217           .NLADirectionY "0"
218           .NLADirectionZ "0"
219           .Colour "1", "0.501961", "0.501961"
220           .Wireframe "False"
221           .Reflection "False"
222           .Allowoutline "True"
223           .Transparentoutline "False"
224           .Transparency "35"
225           .Create
226      End With
227
228      '@ define material: Paper
229      With Material
230           .Reset
231           .Name "Paper"
232           .Folder ""
233          .FrqType "all"
234          .Type "Normal"
235          .SetMaterialUnit "GHz", "mm"
236          .Epsilon "2.31"
237          .Mu "1"
238          .Kappa "0"
239          .TanD "0.0"
240          .TanDFreq "0.0"
241          .TanDGiven "False"
242          .TanDModel "ConstTanD"
243          .KappaM "0"
244          .TanDM "0.0"
245          .TanDMFreq "0.0"
246          .TanDMGiven "False"
247          .TanDMModel "ConstTanD"
248          .DispModelEps "None"
249          .DispModelMu "None"
250          .DispersiveFittingSchemeEps "General 1st"
251          .DispersiveFittingSchemeMu "General 1st"
252          .UseGeneralDispersionEps "False"
253          .UseGeneralDispersionMu "False"
254          .Rho "800"
255          .ThermalType "Normal"
256          .ThermalConductivity "0.05"
```

```
257         .SpecificHeat "1400", "J/K/kg"
258         .Colour "1", "0", "0"
259         .Wireframe "False"
260         .Transparency "0"
261         .Create
262     End With
263 
264         ' -- -- Important general parameters  -- -- '
265     ' -- -- -- --- -------- --- --  -- -- '
266     b_space = ( ys - (A_stru_S1+W_M))/2     ' for the space in vertical of ...
            the extermite
267     y_via1 = -ys/2+b_space -b_space_vias    ' y center of two vias in botton
268 
269     xs = B_stru_S1+B_stru_S2+B_stru_S3 + W_M*4+ M_leng*2
270 
271     ' ------------------------- code start ---------------------- '
272    '-------------------------------------------------------------------'
273 
274       '-------------------------Ground plane-------------------'
275 
276     With Brick       ' top
277          .Reset
278          .Name "top"
279          .Component "Ground"
280          .Material "Copper (annealed)"
281          .Xrange -xs/2,xs/2
282          .Yrange -ys/2,-ys/2+b_space
283          .Zrange 0, "G_t"
284          .Create
285     End With
286 
287     With Brick       ' top2
288          .Reset
289          .Name "top2"
290          .Component "Ground"
291          .Material "Copper (annealed)"
292          .Xrange -xs/2+M_leng+2*W_M+aux_x+ls+vias_out+W_L+G_M_x_S2, _
293          xs/2-M_leng-2*W_M-aux_x_S3-ls-vias_out-W_L_S3-G_M_x_S3
294          .Yrange -ys/2,-ys/2+b_space+W_M
295          .Zrange 0, "G_t"
296          .Create
297     End With
298     Solid.Add "Ground:top", "Ground:top2"
299     With Brick       ' x1
300          .Reset
301          .Name "x1"
302          .Component "Ground"
303          .Material "Copper (annealed)"
304          .Xrange -xs/2+M_leng+2*W_M+aux_x+ls+vias_out+W_L+G_M_x_S2, _
305          -xs/2+M_leng+2*W_M+aux_x+ls+vias_out+W_L+G_M_x_S2-W_M-G_M_x-G_M_x_S2
306          .Yrange -ys/2,ys/2
307          .Zrange 0, "G_t"
308          .Create
309     End With
310     Solid.Add "Ground:top", "Ground:x1"
311     With Brick       ' x2
312          .Reset
```

```
313           .Name "x2"
314           .Component "Ground"
315           .Material "Copper (annealed)"
316           .Xrange xs/2-M_leng-2*W_M-aux_x_S3-ls-vias_out-W_L_S3-G_M_x_S3, _
317           xs/2-M_leng-W_M-aux_x_S3-ls-vias_out-W_L_S3+G_M_S2+G_M_x_S3
318           .Yrange -ys/2,ys/2
319           .Zrange 0, "G_t"
320           .Create
321      End With
322      Solid.Add "Ground:top", "Ground:x2"
323
324      With Brick       ' bottom
325           .Reset
326           .Name "bottom"
327           .Component "Ground"
328           .Material "Copper (annealed)"
329           .Xrange -xs/2,xs/2
330           .Yrange ys/2,ys/2-b_space
331           .Zrange 0, "G_t"
332           .Create
333      End With
334      Solid.Add "Ground:top", "Ground:bottom"
335
336      With Brick       ' bottom 2
337           .Reset
338           .Name "bottom2"
339           .Component "Ground"
340           .Material "Copper (annealed)"
341           .Xrange -xs/2,-xs/2+M_leng+2*W_M+aux_x+ls+vias_out+W_L+G_M_x_S2
342           .Yrange ys/2,ys/2-b_space-W_M
343           .Zrange 0, "G_t"
344           .Create
345      End With
346      Solid.Add "Ground:top", "Ground:bottom2"
347
348      With Brick       ' bottom 3
349           .Reset
350           .Name "bottom3"
351           .Component "Ground"
352           .Material "Copper (annealed)"
353           .Xrange xs/2,xs/2-M_leng-2*W_M-aux_x_S3-ls-vias_out-W_L_S3-G_M_x_S3
354           .Yrange ys/2,ys/2-b_space-W_M
355           .Zrange 0, "G_t"
356           .Create
357      End With
358      Solid.Add "Ground:top", "Ground:bottom3"
359
360      With Brick       ' rigth
361           .Reset
362           .Name "rigth"
363           .Component "Ground"
364           .Material "Copper (annealed)"
365           .Xrange -xs/2,-xs/2+M_leng+W_M+G_M_x
366           .Yrange "-ys/2","ys/2"
367           .Zrange 0, "G_t"
368           .Create
369      End With
```

```
370      Solid.Add "Ground:top", "Ground:rigth"
371
372      With Brick       ' left
373           .Reset
374           .Name "left"
375           .Component "Ground"
376           .Material "Copper (annealed)"
377           .Xrange xs/2,xs/2-M_leng-W_M-G_M_x
378           .Yrange "-ys/2","ys/2"
379           .Zrange 0, "G_t"
380           .Create
381      End With
382      Solid.Add "Ground:top", "Ground:left"
383
384
385      'if necessary, cover the ground plane below each sensor
386      'With Brick       ' for sensor 1
387      '     .Reset
388      '     .Name "sensorS1"
389      '     .Component "Ground"
390      '     .Material "Isola"
391      '     .Xrange -xs/2+M_leng+W_M+G_M_x,-xs/2+M_leng+aux_x+ls+W_M+ _
392      '      W_L-G_M_x+vias_out
393      '     .Yrange ys/2+b_space, -(ys/2)-b_space-W_M
394      '     .Zrange 0, "G_t"
395      '     .Create
396      'End With
397
398  '   With Brick       ' for sensor 2
399  '        .Reset
400  '        .Name "sensorS2"
401  '        .Component "Ground"
402  '        .Material "Isola"
403  '        .Xrange -xs/2+M_leng+aux_x+ls+2*W_M+W_L+vias_out+G_M_x_S2, _
404  '       xs/2-M_leng-aux_x_S3-ls-2*W_M-W_L_S3-vias_out-G_M_x_S2
405  '        .Yrange ys/2+b_space+W_M, -(ys/2)-b_space
406  '        .Zrange 0, "G_t"
407  '        .Create
408  '   End With
409
410  '   With Brick       ' for sensor 3
411  '        .Reset
412  '        .Name "sensorS3"
413  '        .Component "Ground"
414  '        .Material "Isola"
415  '        .Xrange xs/2-M_leng-W_M-G_M_x_S3,xs/2-M_leng-aux_x_S3-ls _
416  '           -W_M-W_L_S3+G_M_x_S3-vias_out
417  '        .Yrange ys/2+b_space, -(ys/2)-b_space-W_M
418  '        .Zrange 0, "G_t"
419  '        .Create
420  '   End With
421
422      With Brick       ' line for sensor 1
423           .Reset
424           .Name "line_sensorS1"
425           .Component "Ground"
426           .Material "Copper (annealed)"
```

```
427           .Xrange -xs/2+M_leng+2*W_M+aux_x+ls+vias_out+W_L+G_M_x_S2- _
428              W_M-G_M_x-G_M_x_S2,-xs/2+M_leng + W_M + aux_x/2 + ls+ W_L+vias_in
429           .Yrange ys/2-b_space-W_M- aux_y/2-vias_out-W_C_y/2, _
430              ys/2-b_space-W_M- aux_y/2-vias_out+W_C_y/2
431           .Zrange 0, "G_t"
432           .Create
433      End With
434      Solid.Add "Ground:top", "Ground:line_sensorS1"
435
436      With Brick       ' line for sensor 2
437           .Reset
438           .Name "line_sensorS2"
439           .Component "Ground"
440           .Material "Copper (annealed)"
441           .Xrange xs/2-M_leng - 2*W_M - aux_x_S3-ls-W_L_S3 -vias_out -  _
442              aux_x_S2/2-(vias_out-vias_in) ,  xs/2-M_leng - 2*W_M - ...
                     aux_x_S3 _
443              -ls -vias_out- G_M_x_S2-W_L_S3
444           .Yrange ys/2-b_space- aux_y_S2/2-vias_out-W_C_y_S2/2, ys/2- _
445              b_space- aux_y_S2/2-vias_out+W_C_y_S2/2
446           .Zrange 0, "G_t"
447           .Create
448      End With
449      Solid.Add "Ground:top", "Ground:line_sensorS2"
450
451      With Brick       ' line for sensor 3
452           .Reset
453           .Name "line_sensorS3"
454           .Component "Ground"
455           .Material "Copper (annealed)"
456           .Xrange xs/2-M_leng - W_M - aux_x_S3/2 -(vias_out-vias_in), _
457              xs/2-M_leng-W_M
458           .Yrange ys/2-b_space-W_M- aux_y_S3/2-vias_out-W_C_y_S3/2, _
459              ys/2-b_space-W_M- aux_y_S3/2-vias_out+W_C_y_S3/2
460           .Zrange 0, "G_t"
461           .Create
462      End With
463      Solid.Add "Ground:top", "Ground:line_sensorS3"
464
465
466        '------------------------ Microstrip ----------------------'
467      With Brick      ' Microstrip_line1 ( left side)
468           .Reset
469           .Name "line1"
470           .Component "Microstrip"
471           .Material "Copper (annealed)"
472           .Xrange -xs/2, -xs/2+M_leng
473           .Yrange -(ys/2)+b_space, -(ys/2)+(W_M)+b_space
474           .Zrange "G_t+h", "G_t+h+t"
475           .Create
476      End With
477
478      With Brick       ' first Vertical microstrip line
479           .Reset
480           .Name "line_y1"
481           .Component "Microstrip"
482           .Material "Copper (annealed)"
```

```
483           .Xrange -xs/2+M_leng ,-xs/2+M_leng+ W_M
484           .Yrange -ys/2+b_space, (ys/2)-b_space
485           .Zrange "G_t+h", "G_t+h+t"
486           .Create
487       End With
488
489       With Brick       ' second Vertical microstrip line
490           .Reset
491           .Name "line_y2"
492           .Component "Microstrip"
493           .Material "Copper (annealed)"
494           .Xrange -xs/2+M_leng+W_M + aux_x+ls+vias_out +W_L  ,-xs/2+M_leng _
495              + 2*W_M + aux_x+ls+vias_out +W_L
496           .Yrange -ys/2+b_space, (ys/2)-b_space
497           .Zrange "G_t+h", "G_t+h+t"
498           .Create
499       End With
500       Solid.Add "Microstrip:line_y1", "Microstrip:line_y2"
501
502       With Brick       ' third Vertical microstrip line
503           .Reset
504           .Name "line_y3"
505           .Component "Microstrip"
506           .Material "Copper (annealed)"
507           .Xrange xs/2 - M_leng - aux_x_S3 -ls -W_L_S3 - vias_out - 2*W_M, _
508              xs/2 - M_leng - aux_x_S3 -ls -W_L_S3 - W_M - vias_out
509           .Yrange -ys/2+b_space, (ys/2)-b_space
510           .Zrange "G_t+h", "G_t+h+t"
511           .Create
512       End With
513       Solid.Add "Microstrip:line_y1", "Microstrip:line_y3"
514
515       With Brick      ' Last Veritcal Microstrip line
516           .Reset
517           .Name "line_y4"
518           .Component "Microstrip"
519           .Material "Copper (annealed)"
520           .Xrange xs/2-M_leng,xs/2-M_leng-W_M
521           .Yrange -ys/2+b_space, (ys/2)-b_space
522           .Zrange "G_t+h", "G_t+h+t"
523           .Create
524       End With
525       Solid.Add "Microstrip:line_y1", "Microstrip:line_y4"
526
527       For I = 0 To Nsensors   'Horizontal microstrip line
528           If I Mod 2 Then         'bottom microstrip
529               If I = 1 Then
530                   With Brick
531                     .Reset
532                     .Name "line_x_" + Str(I)
533                     .Component "Microstrip"
534                     .Material "Copper (annealed)"
535                     .Xrange -xs/2+M_leng+ W_M*(I+1) + I*(ls+aux_x)+W_L*(I)+ _
536                       vias_out*I,-xs/2+M_leng+ W_M*(I+1) + ...
                              (I)*(ls+aux_x)+(I)* _
537                       (ls+aux_x_S2)+W_L +W_L_S2 +vias_out*(I+1)
538                     .Yrange -(ys/2)+b_space, -(ys/2)+(W_M)+b_space
```

```
                    .Zrange "G_t+h", "G_t+h+t"
                    .Create
                End With
                Solid.Add "Microstrip:line_y1", "Microstrip:line_x_"+ Str(I)
            ElseIf I = 3 Then
                With Brick      'Last microstrip line
                    .Reset
                    .Name "line9"
                    .Component "Microstrip"
                    .Material "Copper (annealed)"
                    .Xrange xs/2-M_leng,xs/2
                    .Yrange -(ys/2)+b_space, -(ys/2)+(W_M)+b_space
                    .Zrange "G_t+h", "G_t+h+t"
                    .Create
                End With
            End If
        End If

    Next
    With Brick              'first top microstrip
        .Reset
        .Name "top_xx" + Str(I)
        .Component "Microstrip"
        .Material "Copper (annealed)"
        .Xrange -xs/2+M_leng+W_M, -xs/2+M_leng+ls +aux_x+W_M +W_L+vias_out
        .Yrange ys/2-b_space, (ys/2)-b_space-W_M
        .Zrange "G_t+h", "G_t+h+t"
        .Create
    End With
    Solid.Add "Microstrip:line_y1", "Microstrip:top_xx"+ Str(I)

    With Brick              'last top microstrip
        .Reset
        .Name "top_x" + Str(I)
        .Component "Microstrip"
        .Material "Copper (annealed)"
        .Xrange xs/2-M_leng-W_M, xs/2-M_leng-ls-aux_x_S3-W_M-W_L_S3-vias_out
        .Yrange ys/2-b_space, (ys/2)-b_space-W_M
        .Zrange "G_t+h", "G_t+h+t"
        .Create
    End With
    Solid.Add "Microstrip:line_y1", "Microstrip:top_x"+ Str(I)


    '------------------------ sensor Number 1--------------------'

    For I = 0 To Nfingers-1
        y0 = I*G_C0 - (ys/2) + b_space + NLoops*W_L + NLoops*G_L
    '   If I = Nfingers-1 Then
    '       If I Mod 2 Then   'last
    '           With Brick
    '                .Reset
    '                .Name "strip_last"
    ''               .Component "sensor_S1"
    '                .Material "Copper (annealed)"
    '                .Xrange -xs/2+M_leng + W_M +aux_x/2 + W_L+G_C0, _
    '                      -xs/2+M_leng + W_M + aux_x/2 + ls+ W_L ...
```

```
        -W_C_y/2+G_C0
'                .Yrange y0+W_C*(Nfingers-1)+G_M_y, ...
        y0+W_C*(Nfingers)+G_M_y
'                .Zrange "G_t+h", "G_t+h+t"
'                .Create
'            End With
'        Else
'            With Brick
'                .Reset
'                .Name "strip_last"
'                .Component "sensor_S1"
'                .Material "Copper (annealed)"
'                .Xrange -xs/2+M_leng + W_M +aux_x/2 + W_L+G_C0,    _
'                  -xs/2+M_leng + W_M + aux_x/2+ls+ W_L -W_C_y+ ...
        vias_out-vias_in
'                .Yrange y0+W_C*(Nfingers-1)+G_M_y, ...
        y0+W_C*(Nfingers)+G_M_y
'                .Zrange "G_t+h", "G_t+h+t"
'                .Create
'            End With
'        End If
'        Solid.Add "sensor_S1:strip 0", "sensor_S1:strip_last"
        If I Mod 2 Then       'bottom
            If I = Nfingers-1 Then        'last
                With Brick          ' sensor:strip with contact in left side
                    .Reset
                    .Name "strip_last"
                    .Component "sensor_S1"
                    .Material "Copper (annealed)"
                    .Xrange -xs/2+M_leng + W_M +aux_x/2 + W_L, -xs/2+ _
                       M_leng + W_M + aux_x/2 + ls+ W_L - G_C0-2*W_C_y
                    .Yrange y0+W_C*(Nfingers-1)+G_M_y, ...
                        y0+W_C*(Nfingers)+G_M_y
                    .Zrange "G_t+h", "G_t+h+t"
                    .Create
                End With
            Else
                With Brick          ' sensor:strip with contact in left side
                    .Reset
                    .Name "strip"+Str(I)
                    .Component "sensor_S1"
                    .Material "Copper (annealed)"
                    .Xrange -xs/2+M_leng + W_M +aux_x/2 + ...
                        W_L,-xs/2+M_leng + _
                       W_M + aux_x/2 + ls+ W_L -  G_C0-W_C_y/2
                    .Yrange y0+W_C*I+G_M_y, y0+W_C*(I+1)+G_M_y
                    .Zrange "G_t+h", "G_t+h+t"
                    .Create
                End With
            End If
            Solid.Add "sensor_S1:strip 0", "sensor_S1:strip"+ Str(I)
        ElseIf I = Nfingers Then          'last
            If I Mod 3 Then       'bottom
                With Brick          ' sensor:strip with contact in left side
                    .Reset
                    .Name "strip_last"
                    .Component "sensor_S1"
```

```
                    .Material "Copper (annealed)"
                    .Xrange -xs/2+M_leng + W_M +aux_x/2 + W_L, -xs/2+ _
                       M_leng + W_M + aux_x/2 + ls+ W_L - G_C0-2*W_C_y
                    .Yrange y0+W_C*(Nfingers-1)+G_M_y, ...
                        y0+W_C*(Nfingers)+G_M_y
                    .Zrange "G_t+h", "G_t+h+t"
                    .Create
                End With
            End If
        Else
            With Brick          ' sensor:strip with contact in right side
                 .Reset
                 .Name "strip"+Str(I)
                 .Component "sensor_S1"
                 .Material "Copper (annealed)"
                 .Xrange -xs/2+M_leng + W_M +aux_x/2 + W_L + G_C0,  _
                   -xs/2+M_leng + W_M +aux_x/2 + W_L + G_C0+ls
                 .Yrange  y0+W_C*I+G_M_y, y0+W_C*(I+1)+G_M_y
                 .Zrange "G_t+h", "G_t+h+t"
                 .Create
            End With
            Solid.Add "sensor_S1:strip 0", "sensor_S1:strip"+ Str(I)
        End If

        With Brick         ' sensor: capacitance line
             .Reset
             .Name "line"+Str(I)
             .Component "sensor_S1"
             .Material "Copper (annealed)"
             .Xrange -xs/2+M_leng + W_M + aux_x/2 + ls+ W_L -W_C_y/2, _
                -xs/2+M_leng + W_M + aux_x/2 + ls+ W_L+W_C_y/2
             .Yrange  y0+G_M_y, (ys/2)-b_space-W_M-aux_y/2-2*vias_out+ _
                (vias_out-vias_in)
             .Zrange "G_t+h", "G_t+h+t"
             .Create
        End With
        Solid.Add "sensor_S1:strip 0", "sensor_S1:line"+ Str(I)
    Next

    With Cylinder             ' Vias:via2
         .Reset
         .Name "Via2_S1"
         .Component "Vias"
         .Material "Copper (annealed)"
         .OuterRadius vias_out
         .InnerRadius vias_in
         .Axis "z"
         .Zrange 0, "G_t+h+t"
         .Xcenter -xs/2+M_leng + W_M + aux_x/2 + ls+ W_L
         .Ycenter ys/2-b_space-W_M- aux_y/2-vias_out
         .Segments "0"
         .Create
    End With
    Solid.Add "sensor_S1:strip 0", "Vias:Via2_S1"
    '------------------------ Coil of Sensor 1 --------------------'

    For I = 1 To NLoops+1     ' Coil left part
```

```
703         With Brick
704              .Reset
705              .Name "line_left_" +Str(I)
706              .Component "Coil_S1"
707              .Material "Copper (annealed)"
708              .Xrange -xs/2+M_leng + W_M + G_M_x + G_L * (I-1)+ W_L * ...
                     (I-1), _
709                 -xs/2+M_leng + W_M + G_M_x + G_L * (I-1) + W_L * I
710              .Yrange -(ys/2)+b_space+G_L*(I-2)+W_L*(I-1)+G_M_y, (ys/2)- _
711                 b_space-W_M-G_M_y-G_L*(I-1)-W_L*(I-1)
712              .Zrange "G_t+h", "G_t+h+t"
713              .Create
714         End With
715         Solid.Add "sensor_S1:strip 0", "Coil_S1:line_left_"+ Str(I)
716     Next
717
718     For I = 1 To NLoops       ' Coil top part
719         With Brick
720              .Reset
721              .Name "line_top_" +Str(I)
722              .Component "Coil_S1"
723              .Material "Copper (annealed)"
724              .Xrange -xs/2+M_leng + W_M + G_M_x + G_L * (I-1)+ W_L * ...
                     (I-1), _
725                 - xs/2+M_leng + W_M + aux_x + ls  -G_L*(I-1)-W_L*(I-2) _
726                 +vias_out - G_M_x
727              .Yrange  ys/2-b_space-W_M-G_M_y-G_L*(I-1)-W_L*(I-1), (ys/2)- _
728                 b_space-W_M-G_M_y-G_L*(I-1)-W_L*(I)
729              .Zrange "G_t+h", "G_t+h+t"
730              .Create
731         End With
732         Solid.Add "sensor_S1:strip 0", "Coil_S1:line_top_"+ Str(I)
733     Next
734
735     For I = 1 To NLoops       ' Coil right part
736         With Brick
737              .Reset
738              .Name "line_right_" +Str(I)
739              .Component "Coil_S1"
740              .Material "Copper (annealed)"
741              .Xrange -xs/2+M_leng + W_M + aux_x/2 + ls  +G_L*(I)+W_L*(I)+ _
742               vias_out, -xs/2+M_leng + W_M + aux_x/2 + ls  ...
                      +G_L*(I)+W_L*(I+1) +vias_out
743              .Yrange -ys/2+b_space+G_M_y-G_L*(I)-W_L*(I)+(NLoops) ...
                     *(G_L+W_L ), _
744                 ys/2-b_space-W_M-G_M_y+G_L*(I)+W_L*(I)-(NLoops) *(G_L+W_L )
745              .Zrange "G_t+h", "G_t+h+t"
746              .Create
747         End With
748         Solid.Add "sensor_S1:strip 0", "Coil_S1:line_right_"+ Str(I)
749     Next
750
751     For I = 1 To NLoops       ' Coil bottom part
752         With Brick
753              .Reset
754              .Name "line_bottom_" +Str(I)
755              .Component "Coil_S1"
```

```
756             .Material "Copper (annealed)"
757             .Xrange -xs/2+M_leng + W_M + G_M_x+G_L *(I) + W_L * (I), _
758                -xs/2+M_leng+ W_M + aux_x + ls ...
                       -G_L*(I-1)-W_L*(I-2)-G_M_x+vias_out
759             .Yrange -(ys/2)+b_space+G_L*(I-1)+W_L*(I)+G_M_y,  -(ys/2)+ _
760                b_space+G_L*(I-1)+W_L*(I-1)+G_M_y
761             .Zrange "G_t+h", "G_t+h+t"
762             .Create
763         End With
764         Solid.Add "sensor_S1:strip 0", "Coil_S1:line_bottom_"+ Str(I)
765     Next
766
767     With Brick                ' loop_line0
768          .Reset
769          .Name "line0"
770          .Component "Coil_S1"
771          .Material "Copper (annealed)"
772          .Xrange -xs/2+M_leng + W_M + G_M_x , -xs/2+M_leng + W_M + G_M_x +W_L
773          .Yrange y_via1+vias_in, y_via1+vias_in+aux_y
774          .Zrange "G_t+h", "G_t+h+t"
775          .Create
776     End With
777     Solid.Add "sensor_S1:strip 0", "Coil_S1:line0"
778
779     With Cylinder             ' Vias:via1
780          .Reset
781          .Name "Via1_S1"
782          .Component "Vias"
783          .Material "Copper (annealed)"
784          .OuterRadius vias_out
785          .InnerRadius vias_in
786          .Axis "z"
787          .Zrange 0, "G_t+h+t"
788          .Xcenter -xs/2+M_leng + W_M + G_M_x  +W_L/2
789          .Ycenter y_via1
790          .Segments "0"
791          .Create
792     End With
793     Solid.Add "sensor_S1:strip 0", "Vias:Via1_S1"
794
795     '------------------------ Coil of sensor 3 ---------------------'
796     For I = 1 To NLoops_S3    ' Coil right part
797         With Brick
798              .Reset
799              .Name "line_right_S3_" +Str(I)
800              .Component "Coil_S3"
801              .Material "Copper (annealed)"
802              .Xrange xs/2-M_leng - W_M -G_M_x_S3 - G_L_S3 * (I-1)- W_L_S3 ...
                      * _
803                 (I-1),xs/2-M_leng - W_M -G_M_x_S3 - G_L_S3 * (I-1)- W_L_S3 ...
                         * (I)
804              .Yrange   -(ys/2)+b_space+G_L_S3*(I-1)+W_L_S3*(I-1)+G_M_y_S3, _
805                 (ys/2)-b_space-W_M-G_M_y_S3-G_L_S3*(I-1)-W_L_S3*(I-1)
806              .Zrange "G_t+h", "G_t+h+t"
807              .Create
808         End With
809         Solid.Add "Coil_S3:line_right_S3_ 1", "Coil_S3:line_right_S3_"+Str(I)
```

```
    Next

    For I = 1 To NLoops_S3        ' Coil top part
        With Brick
             .Reset
             .Name "line_top_S3_" +Str(I)
             .Component "Coil_S3"
             .Material "Copper (annealed)"
             .Xrange xs/2-M_leng-W_M-G_M_x_S3-G_L_S3*(I-1)-W_L_S3 *(I-1), _
               xs/2-M_leng-W_M-aux_x_S3-ls+G_L_S3*(I-1)+W_L_S3*(I-2)- _
               vias_out + G_M_x_S3
             .Yrange  ys/2-b_space-W_M-G_M_y_S3-G_L_S3*(I-1)-W_L_S3*(I-1), _
                (ys/2)-b_space-W_M-G_M_y_S3-G_L_S3*(I-1)-W_L_S3*(I)
             .Zrange "G_t+h", "G_t+h+t"
             .Create
        End With
        Solid.Add "Coil_S3:line_right_S3_ 1", "Coil_S3:line_top_S3_"+Str(I)
    Next

    For I = 0 To NLoops_S3        ' Coil left part
        With Brick
             .Reset
             .Name "line_left_S3_" +Str(I)
             .Component "Coil_S3"
             .Material "Copper (annealed)"
             .Xrange xs/2-M_leng- W_M -aux_x_S3/2 - ls  -G_L_S3*(I)- _
                W_L_S3*(I)-vias_out,xs/2-M_leng- W_M -aux_x_S3/2 - ls _
                -G_L_S3*(I)-W_L_S3*(I+1)-vias_out
             .Yrange ...
                 -ys/2+b_space+G_M_y_S3-G_L_S3*(I+1)-W_L_S3*(I)+(NLoops_S3) _
                *(G_L_S3+W_L_S3 ), ys/2-b_space-W_M-G_M_y_S3+G_L_S3*(I)+ _
                W_L_S3*(I) -(NLoops_S3) *(G_L_S3+W_L_S3 )
             .Zrange "G_t+h", "G_t+h+t"
             .Create
        End With
        Solid.Add "Coil_S3:line_right_S3_ 1", "Coil_S3:line_left_S3_"+Str(I)
    Next

    For I = 1 To NLoops_S3        ' Coil bottom part
        With Brick
             .Reset
             .Name "line_bottom_S3_" +Str(I)
             .Component "Coil_S3"
             .Material "Copper (annealed)"
             .Xrange xs/2-M_leng - W_M - G_M_x_S3-G_L_S3 *(I-1) - W_L_S3 * ...
                 (I), _
                xs/2-M_leng- W_M - aux_x_S3 -ls ...
                    +G_L_S3*(I)+W_L_S3*(I-1)+G_M_x_S3-vias_out
             .Yrange -(ys/2)+b_space+G_L_S3*(I-1)+W_L_S3*(I)+G_M_y_S3, _
                -(ys/2)+b_space+G_L_S3*(I-1)+W_L_S3*(I-1)+G_M_y_S3
             .Zrange "G_t+h", "G_t+h+t"
             .Create
        End With
        Solid.Add "Coil_S3:line_right_S3_ 1", "Coil_S3:line_bottom_S3_"+Str(I)
    Next

    With Brick                ' loop_line S3
```

```
        .Reset
        .Name "lineS3"
        .Component "Coil_S3"
        .Material "Copper (annealed)"
        .Xrange xs/2-M_leng - W_M - aux_x_S3 -ls + G_M_x_S3- vias_out, _
           xs/2-M_leng -W_M  - aux_x_S3-W_L_S3-ls+ G_M_x_S3- vias_out
        .Yrange y_via1+vias_in, y_via1+vias_in+aux_y_S3
        .Zrange "G_t+h", "G_t+h+t"
        .Create
    End With
    Solid.Add "Coil_S3:line_right_S3_ 1", "Coil_S3:lineS3"

    With Cylinder             ' Vias:via 5
        .Reset
        .Name "Via5_S3"
        .Component "Vias"
        .Material "Copper (annealed)"
        .OuterRadius vias_out
        .InnerRadius vias_in
        .Axis "z"
        .Zrange 0, "G_t+h+t"
        .Xcenter  xs/2-M_leng-W_M-aux_x_S3-ls+G_M_x_S3- vias_out-W_L_S3/2
        .Ycenter y_via1
        .Segments "0"
        .Create
    End With
    Solid.Add "Coil_S3:line_right_S3_ 1", "Vias:Via5_S3"

    '------------------------ sensor Number 3 ---------------------'

    For I = 0 To Nfingers_S3-1
        y0 = I*G_C0_S3 - (ys/2) + b_space + NLoops_S3*W_L_S3 + ...
            NLoops_S3*G_L_S3
        If I Mod 2 Then       'bottom
            With Brick          ' sensor:strip with contact in left side
                .Reset
                .Name "strip_S3"+Str(I)
                .Component "sensor_S3"
                .Material "Copper (annealed)"
                .Xrange xs/2-M_leng-W_M-aux_x_S3/2-vias_out-W_C_y_S3/2 - _
                   G_C0_S3 ,xs/2-M_leng-W_M-aux_x_S3/2-vias_out -ls
                .Yrange y0+W_C_S3*I+G_M_y_S3, y0+W_C_S3*(I+1)+G_M_y_S3
                .Zrange "G_t+h", "G_t+h+t"
                .Create
            End With
            Solid.Add "Coil_S3:line_right_S3_ 1", "sensor_S3:strip_S3"+Str(I)
        Else
            With Brick          ' sensor:strip with contact in right side
                .Reset
                .Name "strip_S3"+Str(I)
                .Component "sensor_S3"
                .Material "Copper (annealed)"
                .Xrange xs/2-M_leng-W_M-aux_x_S3/2-vias_out,xs/2-M_leng- _
                   W_M-aux_x_S3/2-vias_out -ls + G_C0_S3
                .Yrange y0+W_C_S3*I+G_M_y_S3, y0+W_C_S3*(I+1)+G_M_y_S3
                .Zrange "G_t+h", "G_t+h+t"
                .Create
```

```
920             End With
921             Solid.Add "Coil_S3:line_right_S3_ 1", "sensor_S3:strip_S3"+Str(I)
922         End If
923
924         With Brick          ' sensor: capacitance line
925              .Reset
926              .Name "line_S3"+Str(I)
927              .Component "sensor_S3"
928              .Material "Copper (annealed)"
929              .Xrange xs/2-M_leng -W_M -aux_x_S3/2 -W_C_y_S3/2 -vias_out, _
930                 xs/2-M_leng -W_M -aux_x_S3/2 +W_C_y_S3/2-vias_out
931              .Yrange  y0+G_M_y_S3, (ys/2)-b_space-W_M-aux_y_S3/2-2* _
932                 vias_out+(vias_out-vias_in)
933              .Zrange "G_t+h", "G_t+h+t"
934              .Create
935         End With
936         Solid.Add "Coil_S3:line_right_S3_ 1", "sensor_S3:line_S3"+Str(I)
937     Next
938
939     With Cylinder             ' Vias:via6
940          .Reset
941          .Name "Via6_S3"
942          .Component "Vias"
943          .Material "Copper (annealed)"
944          .OuterRadius vias_out
945          .InnerRadius vias_in
946          .Axis "z"
947          .Zrange 0, "G_t+h+t"
948          .Xcenter xs/2-M_leng -W_M -aux_x_S3/2-vias_out
949          .Ycenter ys/2-b_space-W_M- aux_y_S3/2-vias_out
950          .Segments "0"
951          .Create
952     End With
953     Solid.Add "Coil_S3:line_right_S3_ 1", "Vias:Via6_S3"
954
955               '------------------------ ---------------------'
956      '------------------------ Coil of sensor 2 ---------------------'
957               '------------------------  ---------------------'
958
959    For I = 1 To NLoops_S2          ' Coil right part
960         With Brick
961              .Reset
962              .Name "line_right_S2_" +Str(I)
963              .Component "Coil_S2"
964              .Material "Copper (annealed)"
965              .Xrange xs/2-M_leng-2*W_M-aux_x_S3-W_L_S3-ls-G_M_x_S2- _
966                G_L_S2*(I-1)- W_L_S2*(I-1)- vias_out,xs/2-M_leng-2*W_M _
967                -aux_x_S3-W_L_S3-ls-G_M_x_S2-G_L_S2*(I-1)-W_L_S2*(I)-vias_out
968              .Yrange ...
                    -(ys/2)+b_space+G_L_S2*(I-1)+W_L_S2*(I-1)+G_M_y_S2+W_M, _
969             (ys/2)-b_space-G_M_y_S2-G_L_S2*(I-1)-W_L_S2*(I-1)
970              .Zrange "G_t+h", "G_t+h+t"
971              .Create
972         End With
973         Solid.Add "Coil_S2:line_right_S2_ 1", "Coil_S2:line_right_S2_"+Str(I)
974     Next
975
```

```
976     For I = 1 To NLoops_S2          ' Coil top part
977         With Brick
978              .Reset
979              .Name "line_top_S2_" +Str(I)
980              .Component "Coil_S2"
981              .Material "Copper (annealed)"
982              .Xrange xs/2-M_leng- 2*W_M - aux_x_S3-W_L_S3-ls +G_M_x_S2- _
983                 aux_x_S2-ls+G_L_S2*(I)+W_L_S2*(I-1)-2*vias_out,xs/2- _
984                 M_leng-2*W_M-aux_x_S3-W_L_S3-ls-G_M_x_S2-G_L_S2*(I-1)- _
985                 W_L_S2*(I-1)-vias_out
986              .Yrange  ys/2-b_space-G_M_y_S2-G_L_S2*(I-1)-W_L_S2*(I-1), _
987              (ys/2)-b_space-W_M-G_M_y_S2-G_L_S2*(I-1)-W_L_S2*(I)+W_M
988              .Zrange "G_t+h", "G_t+h+t"
989              .Create
990         End With
991         Solid.Add "Coil_S2:line_right_S2_ 1", "Coil_S2:line_top_S2_"+Str(I)
992     Next
993
994     For I = 0 To NLoops_S2          ' Coil left part
995         With Brick
996              .Reset
997              .Name "line_left_S2_" + Str(I)
998              .Component "Coil_S2"
999              .Material "Copper (annealed)"
1000             .Xrange ...
                     xs/2-M_leng-2*W_M-aux_x_S3-W_L_S3-ls-aux_x_S2/2-ls-G_L_S2* _
1001                 (I)-W_L_S2*(I)-2*vias_out,xs/2-M_leng- 2*W_M ...
                         -aux_x_S3-W_L_S3-ls _
1002                 -aux_x_S2/2-ls-G_L_S2*(I)-W_L_S2*(I+1)-2*vias_out
1003             .Yrange ...
                     -ys/2+b_space+G_M_y_S2-G_L_S2*(I)-W_L_S2*(I)+(NLoops_S2)* _
1004                (G_L_S2+W_L_S2 )+W_M,  ys/2-b_space-G_M_y_S2+G_L_S2*(I+1)+ _
1005                 W_L_S2*(I)-(NLoops_S2) *(G_L_S2+W_L_S2 )
1006             .Zrange "G_t+h", "G_t+h+t"
1007             .Create
1008        End With
1009        Solid.Add "Coil_S2:line_right_S2_ 1", "Coil_S2:line_left_S2_"+Str(I)
1010    Next
1011
1012    For I = 1 To NLoops_S2          ' Coil bottom part
1013        With Brick
1014             .Reset
1015             .Name "line_bottom_S2_" +Str(I)
1016             .Component "Coil_S2"
1017             .Material "Copper (annealed)"
1018             .Xrange xs/2-M_leng- 2*W_M -aux_x_S3-W_L_S3 - ls ...
                     +G_M_x_S2-aux_x_S2-ls _
1019                +G_L_S2*(I-1)+W_L_S2*(I-1)-2*vias_out, xs/2-M_leng - 2*W_M _
1020                -aux_x_S3-W_L_S3-ls-G_M_x_S2 -G_L_S2 * ...
                        (I-1)-W_L_S2*(I)-vias_out
1021             .Yrange -(ys/2)+b_space+G_L_S2*(I-1)+W_L_S2*(I)+G_M_y_S2+W_M, _
1022                -(ys/2)+b_space+G_L_S2*(I-1)+W_L_S2*(I-1)+G_M_y_S2+W_M
1023             .Zrange "G_t+h", "G_t+h+t"
1024             .Create
1025        End With
1026        Solid.Add "Coil_S2:line_right_S2_ 1", "Coil_S2:line_bottom_S2_"+Str(I)
1027    Next
```

```
1028
1029      With Brick                ' loop_line S2
1030           .Reset
1031           .Name "lineS2"
1032           .Component "Coil_S2"
1033           .Material "Copper (annealed)"
1034           .Xrange xs/2-M_leng - 2*W_M - aux_x_S3 -W_L_S3 -2*ls -aux_x_S2+ _
1035              G_M_x_S2- 2*vias_out-W_L_S2, xs/2-M_leng - 2*W_M - aux_x_S3 _
1036              -W_L_S3 -2*ls -aux_x_S2+ G_M_x_S2- 2*vias_out
1037           .Yrange -y_via1-vias_in, -y_via1-vias_in-aux_y_S2
1038           .Zrange "G_t+h", "G_t+h+t"
1039           .Create
1040      End With
1041      Solid.Add "Coil_S2:line_right_S2_ 1", "Coil_S2:lineS2"
1042
1043       '------------------------ sensor Number 2 ---------------------'
1044
1045      For I = 0 To Nfingers_S2-1
1046          y0 = I*G_C0_S2 - (ys/2) + b_space + NLoops_S2*W_L_S2 + ...
                 NLoops_S2*G_L_S2
1047          If I Mod 2 Then       'bottom
1048              With Brick          ' sensor:strip with contact in left side
1049                   .Reset
1050                   .Name "strip_S2"+Str(I)
1051                   .Component "sensor_S2"
1052                   .Material "Copper (annealed)"
1053                   .Xrange xs/2-M_leng-2*W_M-aux_x_S3-ls-W_L_S3 ...
                           -aux_x_S2/2-2*vias_out _
1054                       -W_C_y_S2/2 - ...
                               G_C0_S2,xs/2-M_leng-2*W_M-aux_x_S3-ls-W_L_S3- _
1055                        aux_x_S2/2-2*vias_out -ls
1056                   .Yrange y0+W_C_S2*I+G_M_y_S2+W_M, ...
                           y0+W_C_S2*(I+1)+G_M_y_S2+W_M
1057                   .Zrange "G_t+h", "G_t+h+t"
1058                   .Create
1059              End With
1060              Solid.Add "Coil_S2:line_right_S2_ 1", "sensor_S2:strip_S2"+Str(I)
1061          Else
1062              With Brick          ' sensor:strip with contact in right side
1063                   .Reset
1064                   .Name "strip_S2"+Str(I)
1065                   .Component "sensor_S2"
1066                   .Material "Copper (annealed)"
1067                   .Xrange xs/2-M_leng-2*W_M-aux_x_S3-ls-W_L_S3-aux_x_S2/2- _
1068                      2*vias_out,xs/2-M_leng-2*W_M-aux_x_S3-ls-W_L_S3- _
1069                      aux_x_S2/2-2*vias_out-ls+G_C0_S2
1070                   .Yrange y0+W_C_S2*I+G_M_y_S2+W_M, ...
                           y0+W_C_S2*(I+1)+G_M_y_S2+W_M
1071                   .Zrange "G_t+h", "G_t+h+t"
1072                   .Create
1073              End With
1074              Solid.Add "Coil_S2:line_right_S2_ 1", "sensor_S2:strip_S2"+Str(I)
1075          End If
1076
1077          With Brick          ' sensor: capacitance line
1078               .Reset
1079               .Name "line_S2"+Str(I)
```

```
            .Component "sensor_S2"
            .Material "Copper (annealed)"
            .Xrange xs/2-M_leng-2*W_M-aux_x_S3-ls-W_L_S3 ...
                -aux_x_S2/2-2*vias_out+ _
               W_C_y_S2/2, xs/2-M_leng-2*W_M-aux_x_S3-ls-W_L_S3 ...
                   -aux_x_S2/2 _
               -2*vias_out-W_C_y_S2/2
            .Yrange y0+G_M_y_S2+W_M,(ys/2)-b_space-W_M-aux_y_S2/2- _
               2*vias_out+(vias_out-vias_in)+W_M
            .Zrange "G_t+h", "G_t+h+t"
            .Create
        End With
        Solid.Add "Coil_S2:line_right_S2_ 1", "sensor_S2:line_S2"+Str(I)
    Next

    With Cylinder          ' Vias:via4
         .Reset
         .Name "Via4_S3"
         .Component "Vias"
         .Material "Copper (annealed)"
         .OuterRadius vias_out
         .InnerRadius vias_in
         .Axis "z"
         .Zrange 0, "G_t+h+t"
         .Xcenter xs/2-M_leng-2*W_M-aux_x_S3-ls-W_L_S3-aux_x_S2/2-2*vias_out
         .Ycenter ys/2-b_space- aux_y_S2/2-vias_out
         .Segments "0"
         .Create
    End With
    Solid.Add "Coil_S2:line_right_S2_ 1", "Vias:Via4_S3"

    With Cylinder          ' Vias:via3
         .Reset
         .Name "Via3_S3"
         .Component "Vias"
         .Material "Copper (annealed)"
         .OuterRadius vias_out
         .InnerRadius vias_in
         .Axis "z"
         .Zrange 0, "G_t+h+t"
         .Xcenter xs/2-M_leng-2*W_M-aux_x_S3-2*ls-W_L_S3-aux_x_S2- _
            vias_out*2+G_M_x_S2-W_L_S2/2
         .Ycenter -y_via1-vias_in+vias_in
         .Segments "0"
         .Create
    End With
    Solid.Add "Coil_S2:line_right_S2_ 1", "Vias:Via3_S3"

    With Brick          'brick: pcb:substrate
         .Reset
         .Name "substrate"
         .Component "pcb"
         .Material "Isola"
         .Xrange -xs/2, xs/2
         .Yrange "-ys/2", "ys/2"
         .Zrange "G_t", "h+G_t"
         .Create
```

```
1135      End With
1136
1137       '------------------------ Ports to excite the circuit ...
              ---------------------'
1138      With Port
1139           .Reset
1140           .PortNumber "1"
1141           .Label ""
1142           .Folder ""
1143           .NumberOfModes "1"
1144           .AdjustPolarization "False"
1145           .PolarizationAngle "0.0"
1146           .ReferencePlaneDistance "0"
1147           .TextSize "50"
1148           .TextMaxLimit "1"
1149           .Coordinates "Free"
1150           .Orientation "xmin"
1151           .PortOnBound "False"
1152           .ClipPickedPortToBound "False"
1153           .Xrange -xs/2, -xs/2
1154           .Yrange -ys/2+b_space-3*h, -ys/2+b_space+W_M+3*h
1155           .Zrange "G_t", "4*h"
1156           .XrangeAdd "0.0", "0.0"
1157           .YrangeAdd "0.0", "0.0"
1158           .ZrangeAdd "0.0", "0.0"
1159           .SingleEnded "False"
1160           .AddPotentialEdgePicked "1", "positive", "Microstrip:line1", "3"
1161           .Shield "none"
1162           .WaveguideMonitor "False"
1163           .Create
1164      End With
1165
1166      With Port
1167           .Reset
1168           .PortNumber "2"
1169           .Label ""
1170           .Folder ""
1171           .NumberOfModes "1"
1172           .AdjustPolarization "False"
1173           .PolarizationAngle "0.0"
1174           .ReferencePlaneDistance "0"
1175           .TextSize "50"
1176           .TextMaxLimit "1"
1177           .Coordinates "Free"
1178           .Orientation "xmax"
1179           .PortOnBound "False"
1180           .ClipPickedPortToBound "False"
1181           .Xrange xs/2, xs/2
1182           .Yrange -ys/2+b_space-3*h, -ys/2+b_space+W_M+3*h
1183           .Zrange "G_t", "4*h"
1184           .XrangeAdd "0.0", "0.0"
1185           .YrangeAdd "0.0", "0.0"
1186           .ZrangeAdd "0.0", "0.0"
1187           .SingleEnded "False"
1188           .AddPotentialEdgePicked "1", "positive", "Microstrip:line9", "1"
1189           .Shield "none"
1190           .WaveguideMonitor "False"
```

```
1191          .Create
1192      End With
1193
1194  '   With Brick          'brick: pcb:protective layer
1195          '.Reset
1196          '.Name "shield"
1197          '.Component "pcb"
1198          '.Material "Paper"
1199          '.Xrange -xs/2, xs/2
1200          '.Yrange "-ys/2", "ys/2"
1201          '.Zrange "G_t+h+t", "G_t+t+h+t_S"
1202          '.Create
1203  '   End With
1204
1205  '     basic version
1206      With Cylinder
1207          .Reset
1208          .Name "finger"
1209          .Component "pcb"
1210          .Material "finger"
1211          .OuterRadius 7.5
1212          .InnerRadius "0"
1213          .Axis "z"
1214          .Zrange "G_t+t+h+t_S", "G_t+t+h+t_S+finger"
1215          .Xcenter 0
1216          .Ycenter 0
1217          .Segments "0"
1218          .Create
1219      End With
1220
1221      'version more complex (multiple cylinders)
1222  '   For Iy = 0 To 5
1223  '       For Ix = 0 To 5
1224  '           With Cylinder'
1225  '               .Reset
1226  '               .Name "finger"+Str(Ix)+Str(Iy)
1227  '               .Component "pcb"
1228  '               .Material "finger"
1229  '               .OuterRadius 0.47
1230  '               .InnerRadius "0"
1231  '               .Axis "z"
1232  '               .Zrange "G_t+t+h+t_S", "G_t+t+h+t_S+finger"
1233  '               .Xcenter 0+Ix
1234  '               .Ycenter 0+Iy
1235  '               .Segments "0"
1236  '               .Create
1237  '           End With
1238  '           Solid.Add "pcb:finger 0 0", "pcb:finger"+Str(Ix)+Str(Iy)
1239  '       Next
1240  '   Next
1241
1242      ' merge the final componentes
1243      Solid.Add "Microstrip:line_y1", "Microstrip:line1"
1244      Solid.Add "Microstrip:line_y1", "Microstrip:line9"
1245      Solid.Add "Ground:top", "Coil_S3:line_right_S3_ 1"
1246      Solid.Add "Ground:top", "Coil_S2:line_right_S2_ 1"
1247      Solid.Add "Ground:top", "sensor_S1:strip 0"
```

```
1248
1249  End Sub
```